



RETURNING MATERIALS:
Place in book drop to
remove this checkout from
your record. FINES will
be charged if book is
returned after the date
stamped below.

--	--	--

SYNTHESIS AND CHARACTERIZATION OF NEW
ALKALIDES AND ELECTRIDES
VIA THE TERTIARY AMINE COMPLEXING AGENTS:
STEPS TOWARDS THERMAL STABILITY

by

Mark E. Kuchenmeister

A Dissertation

Submitted to
Michigan State University
in partial fulfillment of the requirements
for the degree of

DOCTOR OF PHILOSOPHY

Department of Chemistry

1989

ABSTRACT

SYNTHESIS AND CHARACTERIZATION OF NEW ALKALIDES AND
ELECTRIDES VIA THE TERTIARY AMINE COMPLEXING
AGENTS: STEPS TOWARDS THERMAL STABILITY

By

Mark E. Kuchenmeister

Although a number of salts with the alkali metal anions (alkalides) or trapped electrons (electrides) are known, previously all were thermally unstable to irreversible decomposition of the cation complexant (crown ether or cryptand). By using the fully methylated nitrogen analogs of the crown ethers, five crystalline sodides and one crystalline electride have been synthesized. The remarkable feature of the aza-crowns is their extreme resistance to reductive decomposition. Differential scanning calorimetry (DSC) of the three sodides that contain HMHCY (hexamethyl hexacyclen) shows that each compound melts without decomposition at temperatures ranging from 7 to 40 °C and decomplexes to yield liquid HMHCY and the alkali metals at temperatures about 30 degrees above the melting point. For all three compounds, irreversible decomposition does not occur until ~140 °C.

The crystal structures for the three sodides with HMHCY have

been determined, and they are isostructural in the orthorhombic space group $P2_12_12_1$. In each case, the structure shows that Na^- is very nearly in contact with one alkali metal cation. The solid may be viewed as containing closest-packed contact ion-pairs in which the cation is embedded in the complexant but is exposed on one face to the sodide anion. The optical spectra of thin films and the ^{23}Na MAS-NMR spectrum confirmed the presence of Na^- .

Two additional compounds have been synthesized with PMPCY (pentamethyl pentacyclen), one sodide and one electride. Both compounds are remarkably stable at room temperature for over 10 days, but eventually decomplex into PMPCY and the alkali metals. The DSC spectrum of each compound indicates a phase transition at ~ -54 and ~ -74 °C for the sodide and electride respectively. This transition is also detected for the electride in magnetic susceptibility and conductivity measurements with very different behaviors above and below the transition.

All of these compounds with the aza-crowns are very soluble in dimethyl ether and somewhat soluble in diethyl ether and trimethylamine. Solutions in dimethyl ether are remarkably stable. These studies point to a strategy for synthesizing thermally stable alkalides and electrides in which tertiary amine cyclic or bicyclic complexants are used to enhance stability. The limiting factor is weak complexation that tends to yield the free amine and alkali metals at elevated temperatures.

to

my Parents

and Claudia

ACKNOWLEDGEMENTS

I would like to express my gratitude to Professor Dye for his constant support and guidance throughout this work. I would also like to thank Lauren Hill and Jineun Kim for helping with the NMR spectra, and Ahmed Ellaboudy for helping with the EPR spectra. Special thanks goes to Dr. Ward and Rui Huang for their assistance in obtaining the crystal structures and for the informative discussions I had with Dr. Ward. I would also like to thank Professor Farnum and his group for the aza-complexants they provided.

The technical and clerical staff deserve thanks also, especially the glassblowers Keki Mistry, Manfred Langer, and Scott Bancroft for their outstanding service.

Research support from NSF Grants DMR 87-14751 is gratefully acknowledged.

TABLE OF CONTENTS

	Page
List of Tables	ix
List of Figures	x
I. INTRODUCTION	1
I. A. History of Complexing Agents	1
I. B. Alkalides and Electrides	4
I. C. Current Work	8
II. SYNTHESIS AND ANALYSIS	10
II. A. Vacuum Lines and Inert Atmosphere Techniques	10
II. B. Reagents	11
II. B. 1. Complexing Agents	11
II. B. 2. Metals	13
II. C. Synthesis	13
II. D. Analysis	15
II. D. 1. Hydrogen Evolution	16
II. D. 2. pH Titration	17
II. D. 3. Plasma Emission	18
II. D. 4. ^1H NMR	18
II. E. Results	19
II. E. 1. HM CY Compounds	19
II. E. 2. PM CY Compounds	20

II. E. 3.	TRIMCY Compounds	20
II. E. 4.	TETMCM Compounds	21
II. F.	Summary	21
III	OPTICAL SPECTROSCOPY	23
III. A.	Introduction	23
III. B.	Experimental	25
III. B. 1.	Compounds with HMHCY	27
III. B. 2.	Compounds with PMPCY	32
III. B. 3.	$\text{Li}^+(\text{TRIMCY})_2 \cdot \text{Na}^-$	36
III. C.	Summary	36
IV.	THERMODYNAMIC PROPERTIES	39
IV. A.	Introduction	39
IV. B.	Experimental Methods	40
IV. C.	Thermodynamic Properties	42
IV. C. 1.	HMHCY Compounds	42
IV. C. 2.	PMPCY Compounds	56
IV. C. 2.	$\text{Li}^+(\text{TRIMCY})_2 \cdot \text{Na}^-$	60
IV. D.	Summary	60
V.	MAGNETIC PROPERTIES	62
V. A.	MAS-NMR	62
V. A. 1.	HMHCY Compounds	63
V. A. 2.	PMPCY Compounds	64
V. B.	EPR	64
V. B. 1.	Alkalides and Electrides	66
V. B. 2.	Results	67
V. C.	Magnetic Susceptibility	70

V. C. 1. $\text{Li}^+(\text{PMPCY})\cdot\text{e}^-$	72
V. C. Summary	76
VI. X-RAY STRUCTURES	78
VI. A. Introduction	78
VI. B. Experimental	79
VI. C. X-Ray Data Collections	80
VI. C. 1. $\text{K}^+(\text{HMHCY})\cdot\text{Na}^-$	80
VI. C. 2. $\text{Cs}^+(\text{HMHCY})\cdot\text{Na}^-$	83
VI. C. 3. $\text{Rb}^+(\text{HMHCY})\cdot\text{Na}^-$	89
VI. D. Discussion	86
VI. E. Compounds with PMPCY	93
VII. CONCLUSIONS	95
VII. A. Designing new Complexants	96
APPENDIX A	98
REFERENCES	107

LIST OF TABLES

TABLE	Page
1. Summary of Purification Conditions For the Various Aza-Crowns.....	12
2. Summary of Alkalides and Electrides Synthesized and Characterized in This Study.....	22
3. Absorption Maxima Position For Na^- in Various Sodide Films	24
4. Summary of Optical Absorption Peak Positions	38
5. Values Used to Obtain the Enthalpy of Formation of the Metal Alloys	49
6. Summary of Enthalpy Changes for Various Steps in the Thermodynamic Cycle Shown in Figure 14	50
7. Summary of the Thermal Processes That Occur in the DSC Traces With a Heating Rate of 5 deg/min in $^{\circ}\text{C}$	61
8. Summary of Cell Constants for $\text{K}^+(\text{HMHCY})\cdot\text{Na}^-$ (I), $\text{Rb}^+(\text{HMHCY})\cdot\text{Na}^-$ (II), and $\text{Cs}^+(\text{HMHCY})\cdot\text{Na}^-$ (III)	88
9. Summary of Atomic Distances With Respect to the Plane in Figure 26	90
A1. Positional Parameters and Their Estimated Standard Deviations for $\text{K}^+(\text{HMHCY})\cdot\text{Na}^-$ (I)	99
A2. Positional Parameters and Their Estimated Standard Deviations for $\text{Rb}^+(\text{HMHCY})\cdot\text{Na}^-$ (II)	100
A3. Positional Parameters and Their Estimated Standard Deviations for $\text{Cs}^+(\text{HMHCY})\cdot\text{Na}^-$ (III)	101
A4. Bond Distances (in Angstroms) for $\text{K}^+(\text{HMHCY})\cdot\text{Na}^-$ (I), $\text{Rb}^+(\text{HMHCY})\cdot\text{Na}^-$ (II), and $\text{Cs}^+(\text{HMHCY})\cdot\text{Na}^-$ (III)	102
A5. Bond Angles (in Degrees) for $\text{K}^+(\text{HMHCY})\cdot\text{Na}^-$ (I), $\text{Rb}^+(\text{HMHCY})\cdot\text{Na}^-$ (II), and $\text{Cs}^+(\text{HMHCY})\cdot\text{Na}^-$ (III)	104

LIST OF FIGURES

FIGURE	Page
1. A) 1,4,7,10,13,16,-Hexaoxacyclooctadecane [18-Crown-6]; B) 1,4,13,16,21,24-Hexaoxa-1,10-Diazabicyclo [8.8.8] Hexacosane [Cryptand 2,2,2]; C) 1,4,7,10,13,16-Hexaaza- 1,4,7,10,13,16-Hexamethylcyclooctadecane [HMHCY]	2
2. Mechanism for Crown Ether Decomposition. A) By hydrogen atom removal. B) By proton removal	6
3. Vacuum apparatus used in the synthesis of alkalides and electrides [K-Cell]	14
4. Apparatus used to obtain optical spectra	26
5. Absorption Spectrum of $K^+(HMHCY) \cdot Na^-$ at $-120^\circ C$	28
6. Absorption Spectrum of $Rb^+(HMHCY) \cdot Na^-$ at $-100^\circ C$	29
7. Absorption Spectrum of $Cs^+(HMHCY) \cdot Na^-$ at $-107^\circ C$	30
8. Absorption Spectrum of $Ba^{2+}(HMHCY) \cdot (Na_x e_{2-x})^{2-}$ at $-117^\circ C$	33
9. Absorption Spectra of A) $Li^+(FMPCY) \cdot Na^-$ at $-80^\circ C$; and B) $Li^+(FMPCY) \cdot e^-$ at $-90^\circ C$	34
10. Absorption Spectrum of $Li^+(TRIMCY)_2 \cdot Na^-$ at $-114^\circ C$	37
11. Differential scanning calorimetry trace for a 3.3 mg sample of $K^+(HMHCY) \cdot Na^-$ at 10 deg/min. Endothermic values are negative	43
12. Differential scanning calorimetry trace for a 2.5 mg sample of $Cs^+(HMHCY) \cdot Na^-$ at 5 deg/min. Endothermic values are negative	46
13. Differential scanning calorimetry trace for a 2.2 mg sample of $Rb^+(HMHCY) \cdot Na^-$ at 5 deg/min. Endothermic values are negative	47

14.	Thermodynamic cycle used to calculate enthalpies of formation of $K^+(HMHCY) \cdot Na^-$, $Rb^+(HMHCY) \cdot Na^-$, and $Cs^+(HMHCY) \cdot Na^-$ from the metals and complexant at 225 K from the DSC measurements	50
15.	Thermodynamic Cycles for $Rb^+(HMHCY) \cdot Na^-$; A) Processes occurring during decomplexation over a large temperature range. B) Decomplexation process at 300 K. Enthalpy values are in $kJ mol^{-1}$	53
16.	Thermodynamic Cycles for $Cs^+(HMHCY) \cdot Na^-$; A) Processes occurring during decomplexation over a large temperature range. B) Decomplexation process at 300 K. Enthalpy values are in $kJ mol^{-1}$	54
17.	DSC spectrum for A) $Li^+(PMPCY) \cdot Na^-$; and B) $Li^+(PMPCY) \cdot e^-$; at 5 deg/min. Endothermic values are negative	57
18.	DSC trace over the phase transition in $Li^+(PMPCY) \cdot Na^-$. A) Heating; B) Cooling	59
19.	DSC spectrum of $Li^+(TRIMCY)_2 \cdot Na^-$ at 5 deg/min. Endothermic values are negative	59
20.	EPR spectra for the three sodides $K^+(HMHCY) \cdot Na^-$; $Rb^+(HMHCY) \cdot Na^-$; C) $Cs^+(HMHCY) \cdot Na^-$. Taken with an X-band spectrometer	68
21.	Plot of the molar susceptibility of $Li^+(PMPCY) \cdot e^-$ as a function of temperature in a 3 kG magnetic field	73
22.	Plot of $1/\chi$ as a function of temperature. There are two noticeably different behaviors above and below the transition temperature at ~ 190 K	75
23.	The molecular structure and the numbering of the atoms; and B) stereopacking diagram of $K^+(HMHCY) \cdot Na^-$	82
24.	The molecular structure and the numbering of the atoms; and B) stereopacking diagram of $Cs^+(HMHCY) \cdot Na^-$	85
25.	The molecular structure and the numbering of the atoms; and B) stereopacking diagram of $Rb^+(HMHCY) \cdot Na^-$	87
26.	Diagram of plane through the Nitrogens 1,7,10,16. The axis are only approximate	90
27.	Computer simulation of one "molecule" of $Cs^+(HMHCY) \cdot Na^-$. Generated on an Evans and Sutherland PS350 system with the program FRODO. [$K^+(HMHCY) \cdot Na^-$ and $Rb^+(HMHCY) \cdot Na^-$ would appear similar	91

28. Two cutaway views of the cation-anion packing in $K^+(HMHCY) \cdot Na^-$. A) View down the y-axis; B) View down the x-axis. Distances are in Angstroms. The Na^- is not drawn to scale. The structures of $Rb^+(HMHCY) \cdot Na^-$ and $Cs^+(HMHCY) \cdot Na^-$ are similar 94

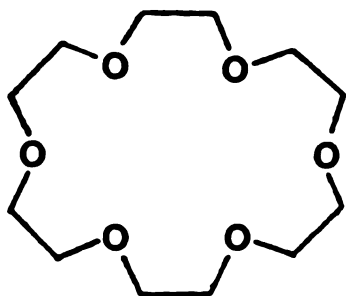
I INTRODUCTION

Alkalides and electrides are a novel class of compounds first synthesized in 1974.^{1,2} An alkalide is an ionic solid in which the cation is an alkali metal encased in 1 or 2 organic macrocyclic or macrobicyclic ligand(s). The anion is then an alkali metal in the -1 oxidation state. An electride is also an ionic solid with the same or a similar cation, but the anion is a solvent-free "trapped" electron. Electrides may be thought of as "stoichiometric F-centers".

Alkali metal anions in solution have been known since 1969 and solvated electrons since the work of Kraus in 1908. Alkali metal solutions have been studied since Weyl's work with sodium and potassium in ammonia in 1864. The solid state counterparts were not possible until the development of suitable cyclic or bicyclic polyether complexants. The role of the ligand is to stabilize the alkalide or electride by complexing the alkali cation to replace the solvation sheath present in solutions.

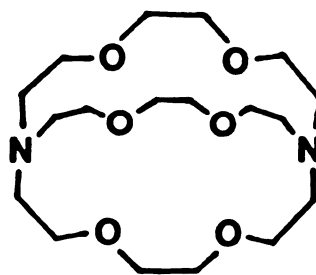
I. A. History of Complexing Agents:

In 1967, Pederson first reported his revolutionary synthesis of 33 cyclic polyethers ["crown ethers", Fig. 1A] and the observation that many of those containing five to ten oxygen atoms formed surprisingly stable complexes with the alkali and alkaline earth metal cations^{3,4}. He also showed that there was a certain amount of selectivity between the crown compounds and the cations



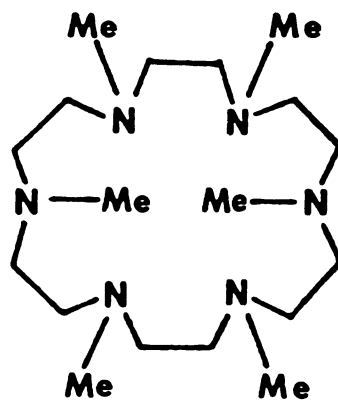
18 Crown-6

A



Cryptand-2,2,2

B



HMHCY

C

Figure 1. A) 1,4,7,10,13,16-Hexaoxacyclooctadecane [18-Crown-6]; B) 1,4,13,16,21,24-Hexaoxa-1,10-Diazabicyclo [8.8.8] Hexacosane [Cryptand 2,2,2]; C) 1,4,7,10,13,16-Hexaaza-1,4,7,10,13,16-Hexamethylcyclooctadecane [HMHCY].

based on the relative sizes of the holes and the cation diameters. It was later observed that when the sizes did not match, 2:1 and even 3:1 complexes of crown to metal could be formed⁵. With the demonstrated success of the macrocyclic polyethers as complexants, Lehn went one step further and synthesized macrobicyclic compounds ["cryptands", Fig. 1B], which contained two bridging $N(CH_2)_3$ groups. These "crypts" formed a cage for the cation; thereby increasing stability and selectivity⁶⁻⁸. Rigid ligands, generally those with small cavities and short nonflexible chains, displayed peak selectivities while the more flexible ligands had plateau selectivities⁷. Cram used the concept of rigid ligands to further improve on the selectivity by introducing additional binding sites or steric barriers at strategic positions on the crown ethers ["spherands"]⁹⁻¹¹. These compounds are macrocyclic or macrobicyclic systems that contain preformed cavities fully organized for complexation during synthesis, rather than during the complexation process.

Since the initial work by Pederson, many researchers have studied the synthesis, complexation, kinetics, reactivity and interactions of macrocyclic ligands with alkali and alkaline earth metal cations. The interest from the synthetic community has broadened the range of available macrocyclic and macrobicyclic compounds. Whereas the first complexants had only oxygen donors, there have since been synthesized materials with nitrogen, sulfur and phosphorous substituted for some or all of the oxygen atoms.

The revelation that crown ethers and related compounds form stable complexes with many different cations, and also demonstrate

selectivity, has prompted researchers to explore the possible applications of these new materials. Some of the processes investigated include: the transport of ions through membranes^{12,13}, the construction of ion selective electrodes^{14,15}, isotope separation^{16,17}, and the increase in solubility of alkali metals in a wide variety of solvents^{18,19}.

I. B. Alkalides & Electrides:

It was while working with the concentrated solutions (~0.4 M) of sodium and the cryptand C222 in ethylamine, that Dye and coworkers were able to form a solid gold-colored precipitate by cooling the solution to Dry Ice temperatures^{1,2}. Based on stoichiometric analysis, the crystalline material was identified as having the formula $\text{Na}^+\text{L}\cdot\text{Na}^-$, where Na^+L refers to the sodium-cryptand complex. This identification was verified by X-ray crystallography giving the first structure of a salt of an alkali metal anion; called an Alkalide.

Ellaboudy and Dye further surprised the scientific community in 1983 by reporting the first crystalline salt with the formula $\text{M}^+\text{L}_2\text{e}^- [\text{Cs}^+(\text{18-crown-6})_2\text{e}^-]$ where all the anionic sites were occupied by solvent-free trapped electrons²⁰. This material was called an Electride. Final conclusive evidence for the assigned stoichiometry was provided by Dawes et al.²¹ who determined the structure of $\text{Cs}^+(\text{18-crown-6})_2\text{e}^-$ by using single crystal x-ray diffraction methods.

Since the first alkalide was prepared in 1974, there have been about 30 alkalides and 7 electrides synthesized and thoroughly

characterized by various methods in these laboratories. The optical and magnetic properties as well as a number of crystal structures of these materials have provided a great deal of insight into the nature of trapped electrons and alkali metal anions.^{22,23}

The applicability of solutions that contain these species to organic reduction processes²⁴⁻²⁹ and to the doping of organic semiconductors³⁰ has already been demonstrated. The utility of alkalides and electrides has been limited, however, by their tendency to decompose thermally. Their inherently strong reducing character requires that they be handled under an inert atmosphere or in vacuo, problems that can readily be overcome. The irreversible decomposition of these compounds at room temperature (in times ranging from a few seconds to several days, depending on the system) poses far more severe handling problems. Prior to the present work, all reported alkalides and electrides have utilized either of two classes of complexing agents, crown ethers or cryptands. The thermal instability of ionic alkalides and electrides results from reductive attack on the ether complexant by the unbound or weakly bound electrons. The cleavage of ethers by alkali metals is a complex but much-studied phenomenon³¹. Two possible mechanisms of crown ether decomposition are shown in Figure 2. With scheme B, the radical formed can cause further decomposition of the ether and formation of a variety of products.

With alkalides and electrides, it is believed that proton abstraction (scheme B) is the prevalent form of decomposition. This belief is based on the fact that when divalent cations such

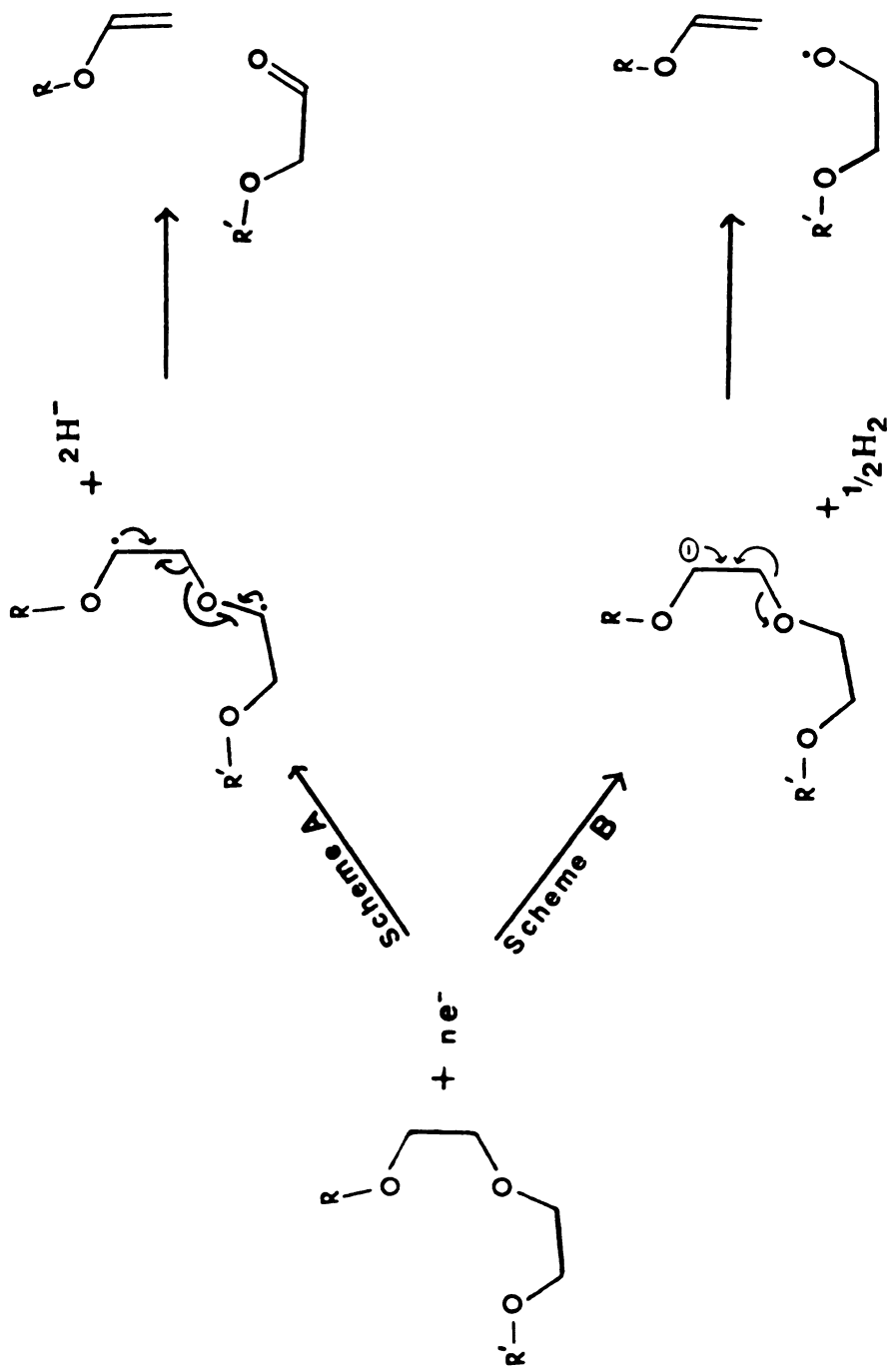


Figure 2. Mechanisms for Crown Ether Decomposition.

A) By hydrogen atom removal.

B) By proton removal.

as Ba^{++} or Ca^{++} are used in conjunction with crowns or crypts, even thin films and solutions at $-60^{\circ}C$ are extremely susceptible to decomposition as a result of the even greater C-H dipoles induced in the molecule by the divalent cations.³² The fact that decomposition is autocatalytic, also favors a radical mechanism.

The thermal instability of the crown ethers and cryptands led us to search for more robust complexing agents that would permit crystallization of alkalides and electrides, yet not be as easily destroyed by reduction. As mentioned earlier, ligands have been synthesized with nitrogen, sulfur and phosphorous replacing some or all of the oxygen donors, as well as various combinations of nitrogen, sulfur, and phosphorous. Substituting only a fraction of the oxygens would not be of any benefit as the ether decomposition would still be present. Therefore, one must consider only the fully aza, thia or phospho ligands. The thia crowns have been studied, and there are indications that they are good complexing agents for alkali and alkaline earth metals;^{33,34,35} however, the high reactivity of the sulfur would make them unlikely candidates for alkalides and electrides. The phospho ligands have not been extensively investigated, but most of the reported work has been with transition metals.^{36,37} Work with the alkali and alkaline earth metals is sparse,³⁸ but they do offer some promise for the future. The aza-crowns, on the other hand, have been studied to some extent and have been shown to complex alkali and alkaline earth metal cations.^{34,39,40} Further, Barrett et al.^{25,26} and Pez et al.²⁸ have shown that mixtures of potassium, sodium and hexamethyl hexacyclen (HMHCY, the fully

methylated nitrogen analog of 18-crown-6: Figure 1C) form stable dark blue solutions [the color one would expect with a solvated electron]. With the alkalides and electrides, the fully methylated compounds are needed as the amino protons would be reduced in the environment of the weakly bound or unbound electrons.

I. C. Current Work:

It was the success of Barrett and Pez that prompted us to use the aza-crown HMHCY to synthesize the alkalide $[K^+(HMHCY) \cdot Na^-]^{41}$. The unprecedented thermal stability of this compound led to the investigation of other metals with this complexant, and to the exploration of the possibilities of using other amine-based ligands.

Several new alkalides and one new electride which employ aza-crowns have been synthesized and characterized. The Differential Scanning Calorimetry (DSC) spectra show that some of these new materials melt and decomplex before any signs of ligand decomposition occur. Other compounds appear to be stable to melting and decomplexation during a DSC scan, yet decomplex if left at room temperature for an extended period of time (over two weeks). The structures of three of these compounds with HMHCY imply a near overlap of the cation and anion electron densities; yet the optical, NMR and EPR spectra verify the retention of cationic and anionic characters respectively. An electride with pentamethyl pentacyclen [PMPCY, the fully methylated nitrogen analog of 15-crown-5], $Li^+(PMPCY) \cdot e^-$, is extremely resistant to

decomposition. Magnetic studies show it to have localized electrons that display antiferromagnetic behavior. These studies, along with others, will be presented for the new amine-based alkalides and electrides synthesized, and the steps taken towards the synthesis of alkalides and electrides with true thermal stability will be described.

II. SYNTHESIS AND ANALYSIS

II. A. Vacuum Lines and Inert Atmosphere Techniques:

As a result of the highly reductive nature of alkalides and electrides, high vacuum or an inert atmosphere was required for the synthesis and all manipulations of the alkalides and electrides. The vacuum lines consisted of an all-glass manifold with a low vacuum and a high vacuum port. On the high vacuum side a liquid nitrogen trap was installed just before the diffusion pump to prevent contamination of the pump oil. A more complete description of the construction of the lines is presented by Van Eck⁴². Manifold pressures (the pressure measured at the manifold and reported as the working pressure throughout this dissertation, although the actual pressure of the system might be greater) of less than 2×10^{-5} Torr are routinely achieved.

A majority of the inert atmosphere work was performed with the sample in a helium-filled glove box [Vac Atmospheres Co.; Model DLX-001-S.G Dri lab] with an added nitrogen scrubbing system [Vac Atmospheres Co. Model NI-20-3]. The contamination of the atmosphere was maintained at less than 0.5 ppm O₂ and less than 0.01 ppm H₂O and was continuously monitored by both moisture and oxygen analyzers [Vac Atmospheres Co. AM-2032 and AO-316-H respectively]. In order to introduce samples and materials into the glove box, an evacuable port was used. The time this required (~25 minutes to prevent contamination of the glove box atmosphere) could allow some samples to decompose. As a result, most samples

were loaded for physical measurements, such as optical studies, thermal analysis and magnetic studies, by use of a polyethylene glove bag (I²R Co.) with a liquid nitrogen bath. The atmosphere in the glove bag was maintained by a constant flow of boil-off nitrogen gas.

II. B. Reagents:

II. B. 1. Complexing Agents:

The complexing agents obtained from Professor Farnum and his group members needed to be further purified. Vacuum distillation or vacuum sublimation (depending on the melting point of the compound) was used to extract the compound from the crude mixture. All purifications were performed at less than 2×10^{-5} Torr with the conditions listed in Table 1. The first distillation usually yielded a slightly yellow material. Further purification was obtained by washing the compound over a film of sodium metal with dimethyl ether, then redistilling or resubliming the resulting mixture. After the initial distillation or sublimation, all handling of the compound was done in the glove box to prevent absorption of water or oxygen.

Table 1. Summary of Purification Conditions For the Various Aza-Crowns.

Complexant	Formula	Temperature (°C)	Method
Hexamethyl Hexacyclen (HMHCY)	$C_{18}H_{42}N_6$	125	dist.
Pentamethyl Pentacyclen (PMPCY)	$C_{15}H_{35}N_5$	75	dist.
Tetramethyl Cyclen (TEIMCN)	$C_{12}H_{28}N_4$	130'	dist.
Tetramethyl Cyclam (TEIMCM)	$C_{14}H_{32}N_4$	85	subl.
Trimethyl Tricyclen (TRIMCY)	$C_9H_{21}N_3$	25*	dist.

'It was later discovered that this compound was extremely impure.

*Could not obtain 2×10^{-5} Torr due to its high vapor pressure.

II. B. 2. Metals

The metals sodium, potassium, and rubidium (Alfa-Ventron Products, 99.95% purity) were obtained under argon in sealed glass ampoules with breakseals on one end. Cesium (a gift from the Dow Chemical Co.) was in 50 gram ampoules and had to be distributed to 10 gram ampoules with breakseals⁴¹. The contents of each tube could then be redistributed into smaller tubes following a procedure described elsewhere⁴³. The required quantities of metal were obtained by premeasuring the inner diameter of the tube and isolating lengths to give the appropriate volumes. Lithium, on the other hand, was cut from a large piece stored in the glove box and weighed on an analytical balance.

II. C. Synthesis

All of the alkalides and electrides were prepared in an apparatus called a K-Cell [Figure 3]. Glass ampoules of the appropriate metals were broken and loaded through side arm A while under the helium atmosphere of the glove box. The stoichiometric amount of complexant was then added through side arm B. Both side arms were then capped with Cajon Ultra-Torr couplings and a sealed glass tube to create a vacuum tight system. The K-Cell could then be removed from the glove box and evacuated to 2×10^{-5} Torr. Both of the Ultra-Torr couplings were removed by flame seal off, the metal was distilled, and the remaining part of side arm A was also sealed off. The apparatus was then cooled to below -20°C (care must be taken not to let the stopcock get cold) and the appropriate solvent, either dimethyl ether or methylamine, was

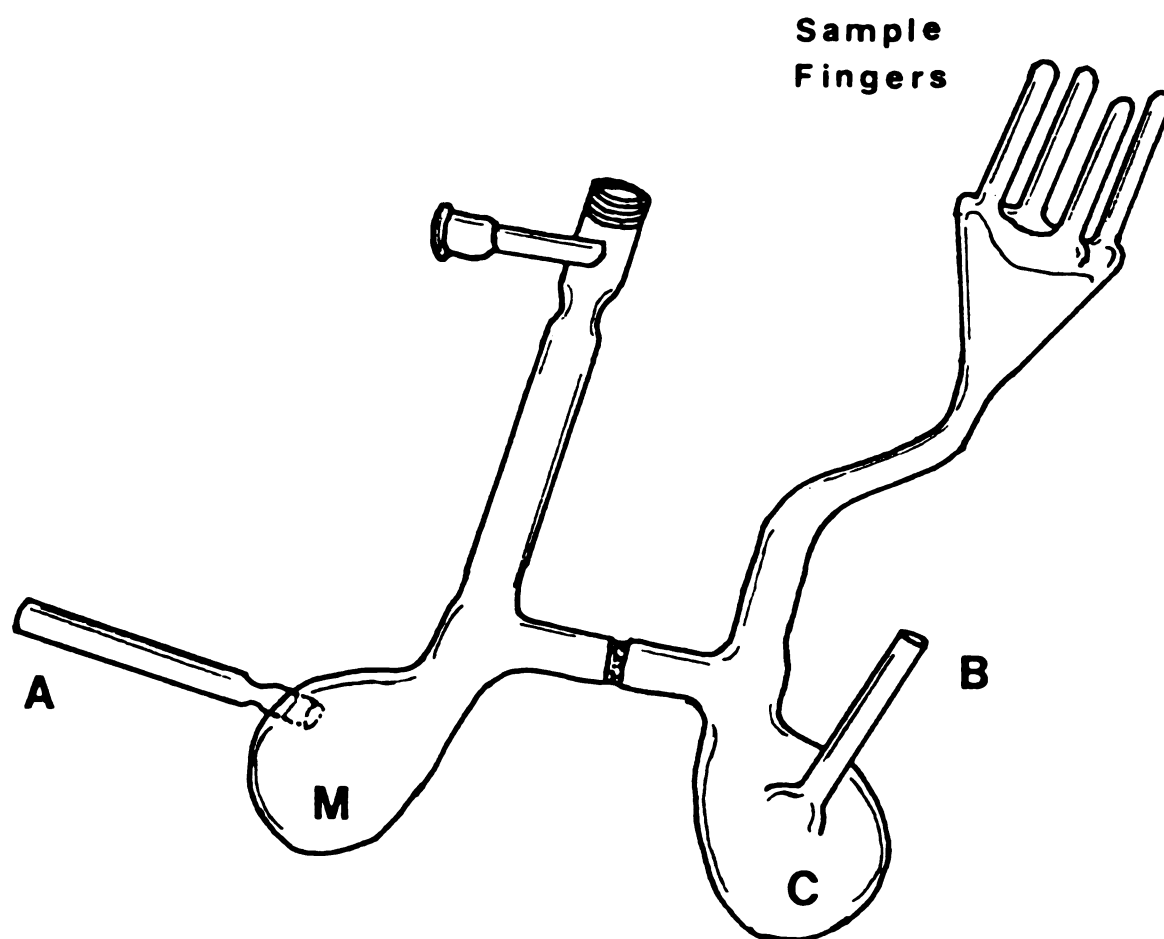


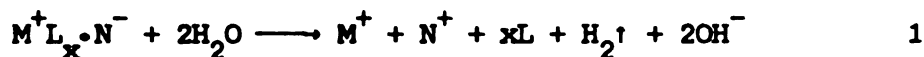
Figure 3. Vacuum apparatus used in the synthesis of alkalis and electrides [K-Cell].

introduced as the vapor through the stopcock and condensed in chamber C. The complexant was dissolved and poured onto the metal in chamber M. Once all the metal had dissolved, the solution was poured through the sintered glass frit back into chamber C. A co-solvent, either dimethyl ether or trimethylamine, was then added and the solution allowed to stand at ~ -78 °C for 3-4 hours to promote crystal growth. To enhance the yield, solvent could then be removed by vacuum distillation until only a very small amount of solvent was left. The remaining solvent was poured back through the glass frit and also distilled off. A washing solvent was then added to rinse the crystals that now were in chamber C. Once the crystals appeared clean, the washing solvent was also removed. The crystals were dried on the vacuum line overnight, then poured into the glass fingers and sealed off for future use. When lithium was used, it was dropped through the stopcock into chamber M. Methylamine was then required as the initial solvent to promote the solubility of the lithium so that it might complex. Once all the metal had dissolved, the solution was allowed to stand at ~ -40 °C for 3-4 hours to insure complete complexation. The methylamine was then completely removed and dimethyl ether was added. The procedure was then the same as with the other metals.

II. D. Analysis:

When an alkali or electride is first synthesized, a specific end product is always expected, but not always realized. So, after making a new compound, a stoichiometric analysis must be completed to help determine the identity of the end product. As

an example of the need for analysis, an attempted synthesis of a "sandwiched" compound of $\text{Cs}^+[\text{HMHCY}\cdot 12\text{-crown-4}]\cdot\text{Na}^-$ resulted in the first successful synthesis of $\text{Cs}^+\text{HMHCY}\cdot\text{Na}^-$. This result would not have been recognized by optical studies or MAS-NMR, and could have caused errors in interpretation at a later time. The analysis of the alkalides is based on Equation 1⁴⁴.



M = metal 1 L = complexant
N = metal 2 x = 1 or 2

In the case of an electricle, the appropriate balancing is employed. The products of the reaction are then evaluated by hydrogen evolution ($\text{H}_2\uparrow$), pH titration (OH^- and $x\text{L}$ in the case of amines), plasma emission (M^+ and N^+), and proton NMR ($x\text{L}$).

II. D. 1. Hydrogen Evolution:

Reaction 1 was carried out using a vacuum system that had been specially designed for hydrogen evolution⁴². The sample was kept at liquid nitrogen temperature and evacuated to $\sim 2 \times 10^{-5}$ Torr. Water that had been previously degassed by repeated freeze-pump-thaw cycles was then distilled into the sample vessel. The liquid nitrogen was removed and as the water melted, it would begin to decompose the material. Once the reaction was complete, a Toepler pump was used to collect the hydrogen gas in a capillary tube of known volume. All the hydrogen had been collected when successive pumpings no longer changed the pressure in the capillary. By measuring the total pressure change and temperature of the

capillary, the ideal gas law could be used to calculate the moles of H_2 evolved. Care must be taken when analyzing samples that contain ligands with high vapor pressures such as TRIMCY not to lose all or part of the ligand to the liquid nitrogen trap. In this situation, the hydrogen was not collected.

II. D. 2. pH Titration:

A pH titration of the residue from the hydrogen evolution offers a second check on the total amount of metal in the sample. When the complexants are amines, which are also bases, information on the amount of complexant present can also be obtained. Using the information from hydrogen evolution to estimate the number of equivalents of base present, the residue was dissolved in a known amount of HCl and conductance water to give a solution of pH~2.75. This solution was then divided into five parts, one for plasma emission, one for 1H NMR, and three for pH titration. A fresh solution of NaOH was standardized with potassium hydrogen phthalate, then used to titrate the residue. A digital pH meter (ORIEN Research, Model 701A) and a Corning electrode were used to determine the endpoints for all titrations. To prevent CO_2 absorption by the base, the titration was done in a sheathed buret with a constant flow of dry nitrogen.

It was observed that the titration curves of the solutions were identical to the curves of the free acidified amines, but shifted to the left by an amount proportional to the number of equivalents of OH^- present. The titration curve for PMPCY is similar to that of HMHCY⁴¹, with endpoints at a pH of ~3.5, 6.5,

and 10.0. The first endpoint is due to a neutralization of the excess acid while the remaining two are due to one and two equivalents of ligand respectively, for a total of three equivalents. The curve for TRIMCY has only two endpoints, one at ~3.5 for the excess acid, and one at ~8.0 for one equivalent of the ligand. By accurately measuring these endpoints, the quantity of ligand in the residue can be determined.

II. D. 3. Plasma Emission:

The metal content of the solution could be determined directly by using atomic emission on a Beckman Spectraspan IV Emission Spectrometer. Solutions of ~30 ppm for each of the metals present (solutions of >100 ppm were needed for Rb^+ and Cs^+) were made from a portion of the residue and analyzed by comparison with a curve obtained from standard solutions.

II. D. 4. 1H NMR:

The remaining amount of residue was analyzed by proton NMR for the complexant content. The solution was first neutralized by adding an equimolar amount of NaOH, as determined by the titration curve, then allowed to dry by slow evaporation. Caution must also be taken at this point to prevent the loss of ligand when it has a high vapor pressure. A weighed amount of sodium acetate was added to the remaining solid and diluted to ~4 ml with D_2O . The integrated intensities of the resulting spectrum could then be compared to determine the number of moles of complexant present.

II. E. Results:

A summary of the compounds synthesized and analyzed are given below with the determined stoichiometry. Also included are compounds that were attempted but could not be synthesized.

II. E. 1. HMHCY Compounds:

With HMHCY as the complexing agent, three sodides were synthesized and fully characterized; $K^+(HMHCY) \cdot Na^-$ (I)⁴¹, $Rb^+(HMHCY) \cdot Na^-$ (II), and $Cs^+(HMHCY) \cdot Na^-$ (III). The crystal structures have been determined and they verify the identifications. A fourth compound with barium has also been synthesized, but is not completely understood at this time. The initial analyses indicate $Ba^{2+}(HMHCY) \cdot (Na_{1.5}e_{0.5})^{2-}$. However, an excess amount of barium metal in the product could account for the apparent electride, or an excess amount of sodium metal in the product could account for the excess sodide. A more careful study of this system is necessary to accurately determine the stoichiometry of the material [more will be said about this compound in later chapters]. From the success with the above compounds, The syntheses of two electrides were attempted, $K^+(HMHCY) \cdot e^-$ and $Cs^+(HMHCY) \cdot e^-$. It was possible to form stable solutions in dimethyl ether, but all attempts to crystallize led to decomplexation to the metal and HMHCY. A synthesis of $Rb^+(HMHCY) \cdot Rb^-$ was also attempted with similar results. With the rubidide, films could be obtained, but not harvested. These results will also be discussed in more detail later.

II. E. 2. FMPCY Compounds:

With FMPCY, two compounds have been synthesized and characterized, $\text{Li}^+(\text{FMPCY})\cdot\text{Na}^-$ (IV) and $\text{Li}^+(\text{FMPCY})\cdot\text{e}^-$ (V). An attempt to synthesize $\text{Na}^+(\text{FMPCY})\cdot\text{Na}^-$ was made, but there was no evidence that the FMPCY complexes sodium.

II. E. 3. TRIMCY Compounds:

The complexant TRIMCY has so far enabled us to synthesize only one compound, $\text{Li}^+(\text{TRIMCY})_2\cdot\text{Na}^-$. The crystal structure has not been determined, but we believe that the lithium cation is "sandwiched" between the two TRIMCY molecules. An attempt to synthesize the corresponding electride was unsuccessful. The material decomposed back to the metal and complexant during the crystallization stage. $\text{Rb}^+(\text{TRIMCY})_x\cdot\text{Na}^-$ was also sought, but there was only a slight indication of complexation in dimethyl ether. At this time, the lithium sodide is the only salt synthesized with TRIMCY as the complexing agent. Complexes of TRIMCY with the other alkali metals may still be possible, and warrant further investigation.

II. E. 4. TETMCM Compounds:

In order to test the stability of compounds that contain β -hydrogens in the presence of the solvated electron, the synthesis of $\text{Li}^+(\text{TETMCM})_x \cdot \text{Na}^-$ was investigated. Dark blue solutions (the color expected for the solvated electron) could be obtained in dimethyl ether after first dissolving the materials in methylamine and pumping dry. However, the solution was found to be temperature dependent. At $\sim -20^\circ\text{C}$, the color would fade and metal flakes could be seen in the solution. If the temperature was then lowered back to below -50°C , the metal redissolved and the solution would again appear dark blue. Even with the dark blue solution at -78°C , attempts to crystallize resulted in decomplexation. The conclusions are that this compound with β -hydrogens is stable to decomposition, but that the complexation constant of TETMCM and lithium, and probably the other alkali metals, is too low for the synthesis of alkalides and electrides.

II. F. Summary:

A list of the alkalides and electrides synthesized to date with the aza-crowns is given in Table 2. The physical properties of these compounds will be discussed in the pages to follow.

Table 2. Summary of Alkalides and Electrides Synthesized and Characterized in This Study.

Compound	Stoichiometric Analysis M:L:N
$K^+(HMICY) \cdot Na^-$	1:1:1
$Rb^+(HMICY) \cdot Na^-$	1:1:1
$Cs^+(HMICY) \cdot Na^-$	1:1:1
$Ba^{2+}(HMICY) \cdot Na^-$	1:1:1.5 [#]
$Li^+(FMPCY) \cdot Na^-$	1:1:1
$Li^+(FMPCY) \cdot e^-$	1:1:0
$Li^+(TRIMCY)_2 \cdot Na^-$	1:2:1 [#]

[#]Structures known. [#]Not positively identified.

III. OPTICAL SPECTROSCOPY

III. A. Introduction:

The optical spectra of alkalides and electrides offer clues about the interaction of the most weakly bound electron with its surroundings and about how tightly it is held. In general, absorption bands occur at 620-760 nm for Na^- , ~800 nm for K^- , ~900 nm for Rb^- , ~1000 nm for Cs^- , and 1100-1700 nm for e^- (trapped)⁴⁵⁻⁴⁸. Thus, the optical spectrum also offers a convenient method of identifying the the anionic species in an alkalide or an electride. Care must be taken, however, in using such an assignment for new materials, since the absorption band has been shown to be dependent on the nature of the complexing agent, the metals involved, and the ratio of metal to complexant. As an example of the variation in the position of the absorption maximum, a list of the wavelengths of maximum absorption is given in Table 3 for various sodide films.

For the alkalides, the major absorption peak is believed to result of an n_s to n_p transition of M^- (where M can be Na, K, Rb, or Cs). A shoulder, which is quite distinct in most sodides and slightly apparent in some potassides, could be due to a bound to continuum transition. Since a pronounced shoulder was present in films of $\text{Na}^+\text{C}_{222}\cdot\text{Na}^-$, but not in some other sodides such as $\text{Rb}^+\text{18C6}\cdot\text{Na}^-$, it was suggested that a charge transfer from Na^- to Na^+ was involved²². Since the shoulder has since been observed in sodides where the cation is not Na^+ , the bound to continuum

Table 3. Absorption Maxima Position for Na^- in Various
Sodide Films. (a)

Film	Peak Position (nm)
$\text{Cs}^+ \text{C}_{222} \cdot \text{Na}^-$	685
$\text{Rb}^+ \text{C}_{222} \cdot \text{Na}^-$	715
$\text{K}^+ \text{C}_{222} \cdot \text{Na}^-$	660
$\text{Na}^+ \text{C}_{222} \cdot \text{Na}^-$	650
$\text{K}^+ \text{18C6} \cdot \text{Na}^-$	715
$\text{Rb}^+ \text{18C6} \cdot \text{Na}^-$	725
$\text{Cs}^+ (\text{18C6})_2 \cdot \text{Na}^-$	715
$\text{Cs}^+ (\text{15C5})_2 \cdot \text{Na}^-$	720
$\text{Rb}^+ (\text{15C5})_2 \cdot \text{Na}^-$	720
$\text{K}^+ (\text{15C5})_2 \cdot \text{Na}^-$	700

a) Reference 5.

transition seems to offer the better explanation. Fluorescence studies are currently underway in these laboratories and others to better identify the origin of these transitions.

The observed spectra for electride films fall in the near infrared as would be expected for a solvent-free trapped electron. These spectra can be divided into two categories, those resulting from localized electrons (trapped in a cavity) and those that appear to involve more delocalized electrons (which can move through the lattice more freely). We refer to the latter systems as those with "metallic" behavior although it now appears that they are not true metals. Localized electriles have electrons trapped in cavities with absorption maxima that correspond to trap depths of 0.5-0.9 eV. These electriles tend to give broad bands that "tail" into the visible. This may result from either electron-electron interactions or a delocalized excited state. The "metallic" electriles have either free or much more shallowly trapped electrons and have absorption spectra that continue to rise from the blue end of the visible spectrum into the infrared. The spectra are remarkably similar to those observed for concentrated (metallic) metal-ammonia solutions⁵⁰.

III. B. Experimental:

Although there are many ways to determine the optical properties of materials, all of the compounds prepared in this work were studied by absorption spectroscopy of thin dry films, prepared by solvent evaporation in a specially designed optical cell [Figure 4]. A previously synthesized sample was loaded into

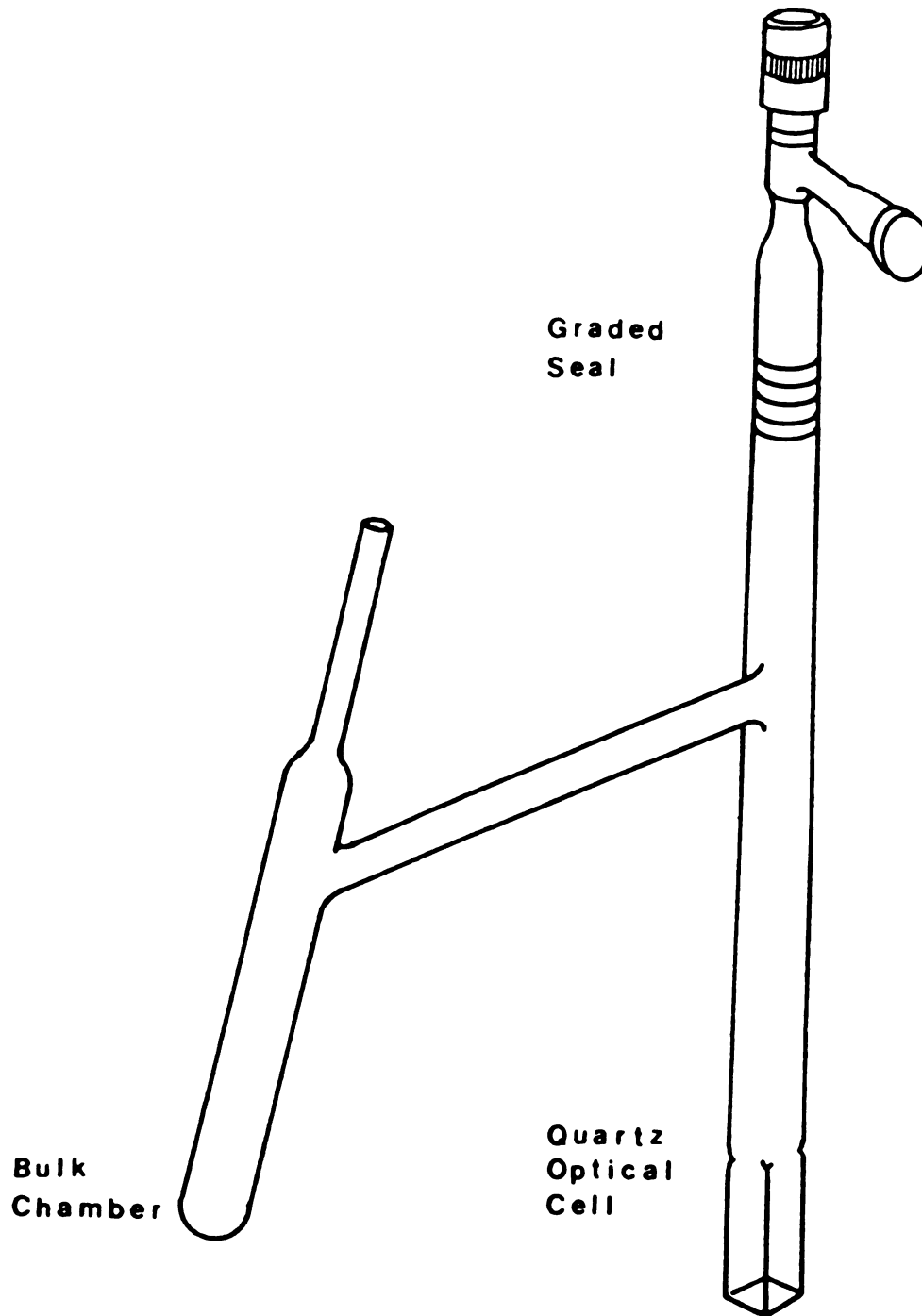


Figure 4. Apparatus used to obtain optical spectra.

the bulk chamber under an inert atmosphere at liquid nitrogen temperature to prevent decomposition. The opening was capped with a Cajon Ultra-Torr coupling, the cell was removed from the glove bag, evacuated to less than 2×10^{-5} Torr, and the arm was flame sealed off. The sample was kept at or below -40 °C during this process and throughout the experiment. A solvent, either dimethyl ether or methylamine, was added and a portion of the solution was poured into the quartz optical cell. Then, while splashing the solution onto the sides of the cell, the solvent was removed by immersing the bulk chamber in liquid nitrogen. The dry polycrystalline film was then placed in the optical path of a Beckman DK-2 spectrophotometer. The temperature of the sample, controlled by a cold dry nitrogen stream that impinged on the cell, was measured with a thermocouple. To prevent solvent from distilling back onto the film, the bulk chamber was kept in a liquid nitrogen bath. A lead sulfide detector with a range of 400-2850 nm, was then used to obtain the absorption spectra. Efforts to study the region below 400 nm were not made, as light scattering by the polycrystalline films, which increases as ν^4 , would tend to mask any absorption bands present.

III. B. 1. Compounds with HMHCY:

The absorption spectra for the three alkalides with HMHCY, $K^+(HMHCY) \cdot Na^-$ (I), $Rb^+(HMHCY) \cdot Na^-$ (II), and $Cs^+(HMHCY) \cdot Na^-$ (III), shown in Figures 5, 6, and 7 respectively, were all obtained from dimethyl ether. In each case an intense peak can be observed, at 660 nm ($\sim 15,100 \text{ cm}^{-1}$) for I, 670 nm ($\sim 14,900 \text{ cm}^{-1}$) for II, and 710

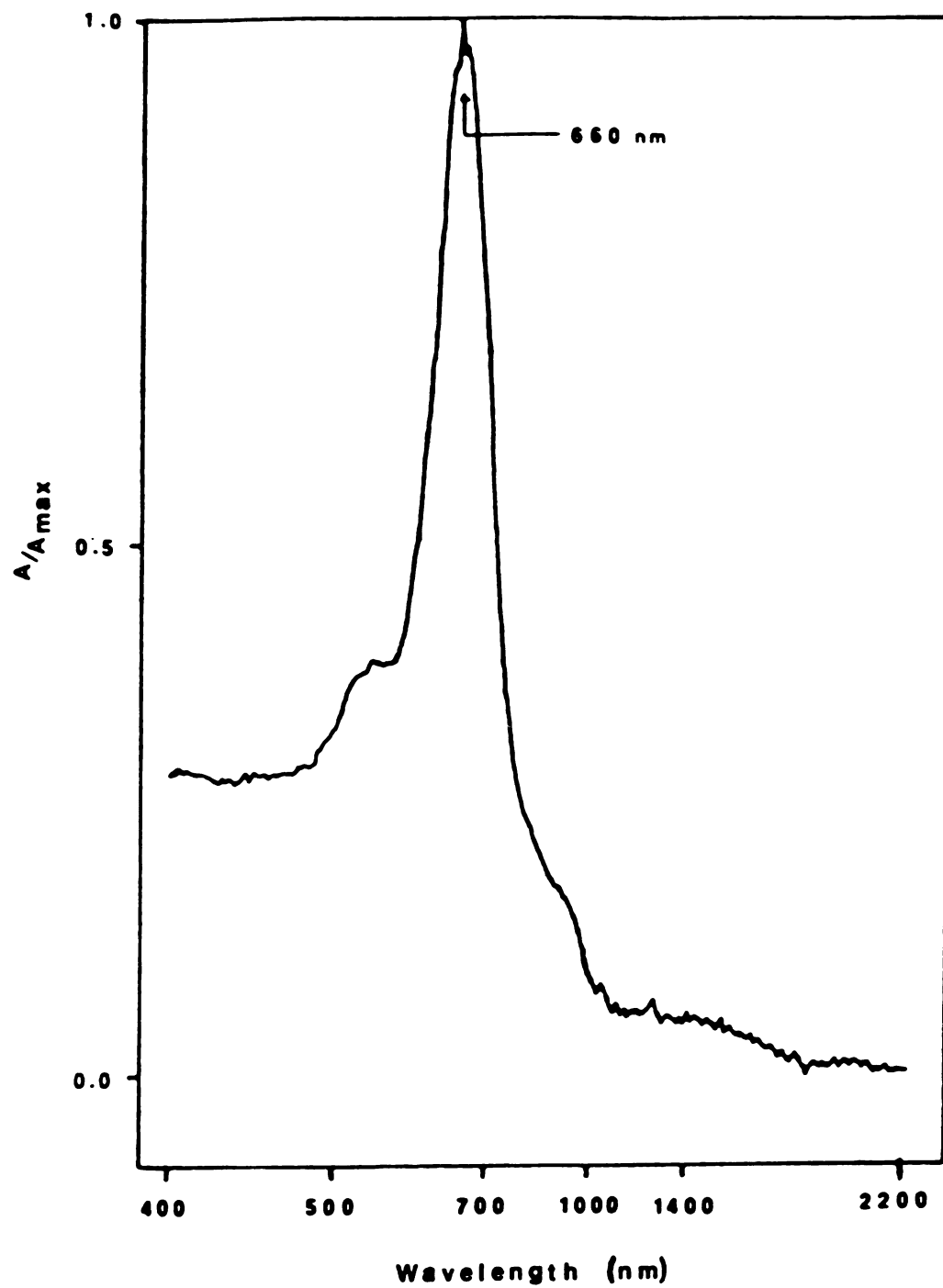


Figure 5. Absorption spectrum of $K^+(HMHCY) \cdot Na^-$ at $-120^\circ C$.

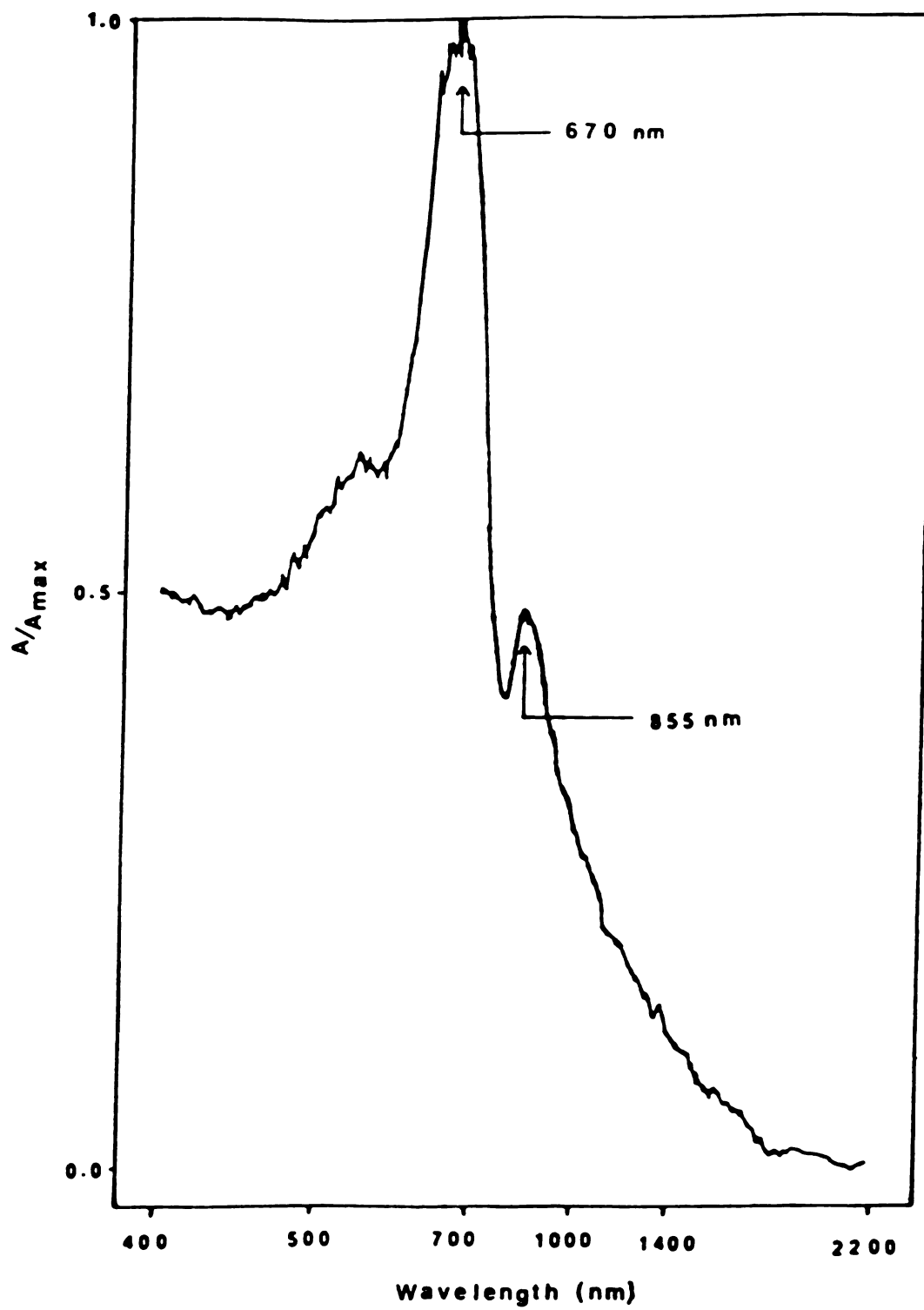


Figure 6. Absorption spectrum of $\text{Rb}^+(\text{HMHCY})\cdot\text{Na}^-$ at $-100\text{ }^\circ\text{C}$.

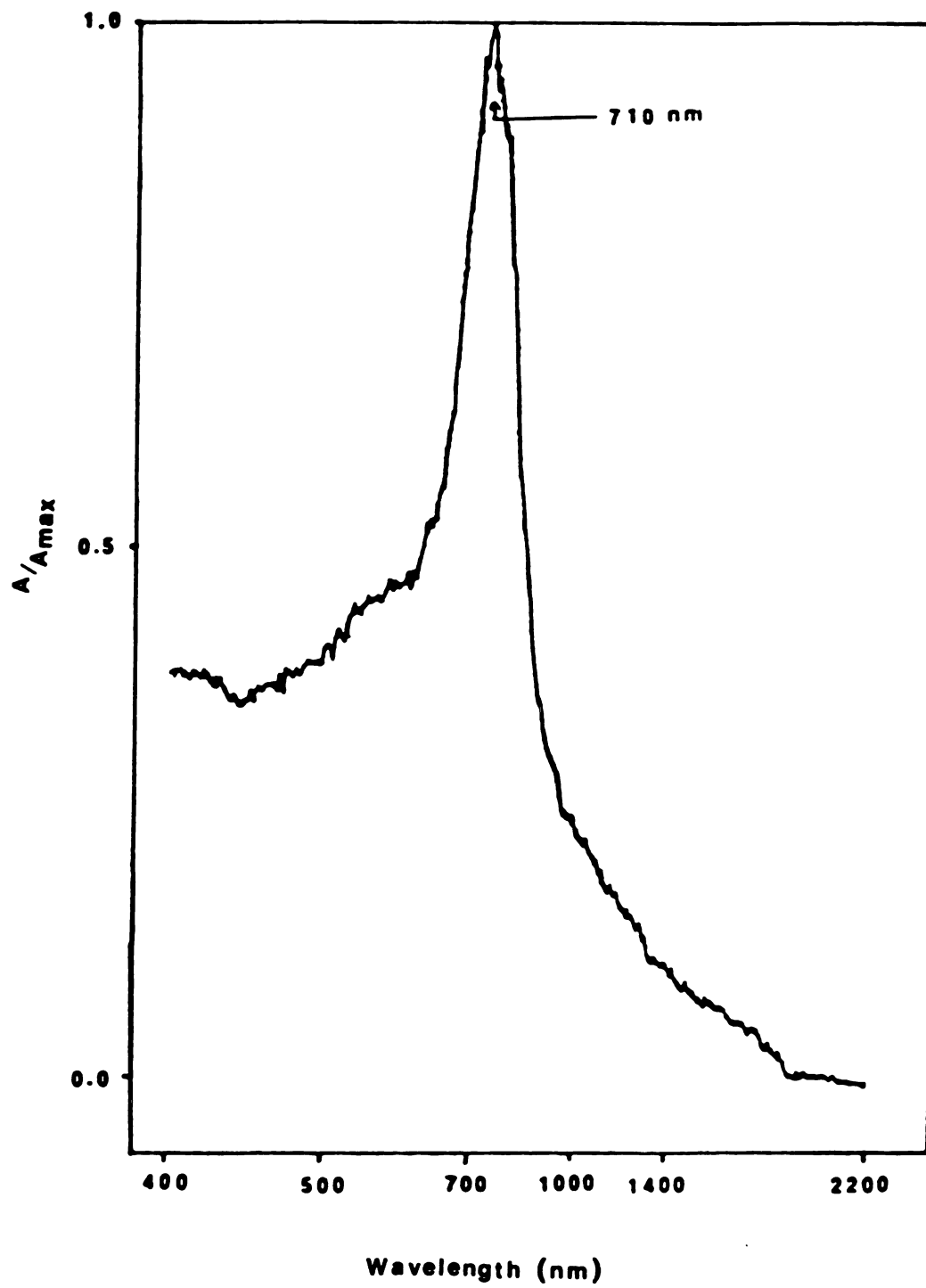


Figure 7. Absorption spectrum of $\text{Cs}^+(\text{HMHCY})\cdot\text{Na}^-$ at $-107\text{ }^\circ\text{C}$.

nm ($\sim 14,100 \text{ cm}^{-1}$) for III. Each compound also had a broad higher energy shoulder centered at about 530 nm. These absorption profiles are characteristic of other sodide films and the maximum positions of the more intense peaks fall within the range of acceptable values for the sodide anion. The red shift with increasing cation size is also expected as the transition energy depends on the environment of Na^- , and as can be seen from the structures [see chapter 5 of this Dissertation], the larger cations have a greater overlap of densities with the sodium anion. In the spectrum for II, there is also a distinct lower energy band at 855 nm ($\sim 11,700 \text{ cm}^{-1}$). It is believed that this absorption is due to a small amount of contamination from $\text{Rb}^+(\text{HMHCY})\cdot\text{Rb}^-$. The "normal" position for the rubidide peak is ~ 900 nm, but as stated earlier, this depends on the compound involved. For example, $\text{Rb}^+(\text{C222})\cdot\text{Rb}^-$ shows an absorption peak at 860 nm ($\sim 11,600 \text{ cm}^{-1}$)²². The contamination could either result from nonstoichiometric ratios in the initial synthesis, or from the method used to produce the film. The salt $\text{Rb}^+(\text{HMHCY})\cdot\text{Na}^-$ is the least stable to decomplexation of the three discussed here (see chapter 4 of this Dissertation), and part of the sample may have decomplexed to form rubidium, HMHCY and sodium in the local environment. $\text{Rb}^+(\text{HMHCY})\cdot\text{Rb}^-$ might then form, leaving excess HMHCY and sodium metal behind. A similar effect has been observed with other compounds in vapor deposition experiments in this lab⁴⁹. The absence of any lower energy peaks and the sharpness of the sodide peak in the spectra for $\text{K}^+(\text{HMHCY})\cdot\text{Na}^-$ and $\text{Cs}^+(\text{HMHCY})\cdot\text{Na}^-$ indicates that there was no similar contamination by K^- or Cs^- in

I or III respectively. Although it is possible that a small peak of K^- might be hidden beneath the Na^- peak, it is not likely. That would probably broaden the Na^- peak or appear as a shoulder. Based on the above observations, the compounds were identified as sodides, with the understanding that II had some contamination from rubidide.

The compound synthesized with barium, sodium, and HMCY was also studied by optical absorption to help determine the nature of the species present. The absorption spectrum is shown in Figure 8. Although the analysis indicates that there is a mixture of sodide and electride present, the optical spectrum shows only the presence of sodide with a maximum absorption at 700 nm ($14,300\text{ cm}^{-1}$). The small apparent peak at ~ 1400 nm is a result of light scattering by the optical cell, and is also present in blank runs.

III. B. 2. Compounds with PMPCY:

The absorption profiles of $Li^+(PMPCY)\cdot Na^-$ (IV), and $Li^+(PMPCY)\cdot e^-$ (V) were also studied by the optical absorption technique, with dimethyl ether as the working solvent. Their spectra are shown in Figure 9. $Li^+(PMPCY)\cdot Na^-$ has the characteristic spectrum of other sodides with the major absorption peak at 680 nm ($14,700\text{ cm}^{-1}$) and a slightly apparent shoulder centered at about 535 nm. $Li^+(PMPCY)\cdot e^-$, on the other hand, has a broad absorption band centered at about 1400 nm ($7,100\text{ cm}^{-1}$) with a profile similar to that of a localized electride^{48,23,50} [the apparent shoulder at ~ 2200 nm is an artifact of the optical cell].

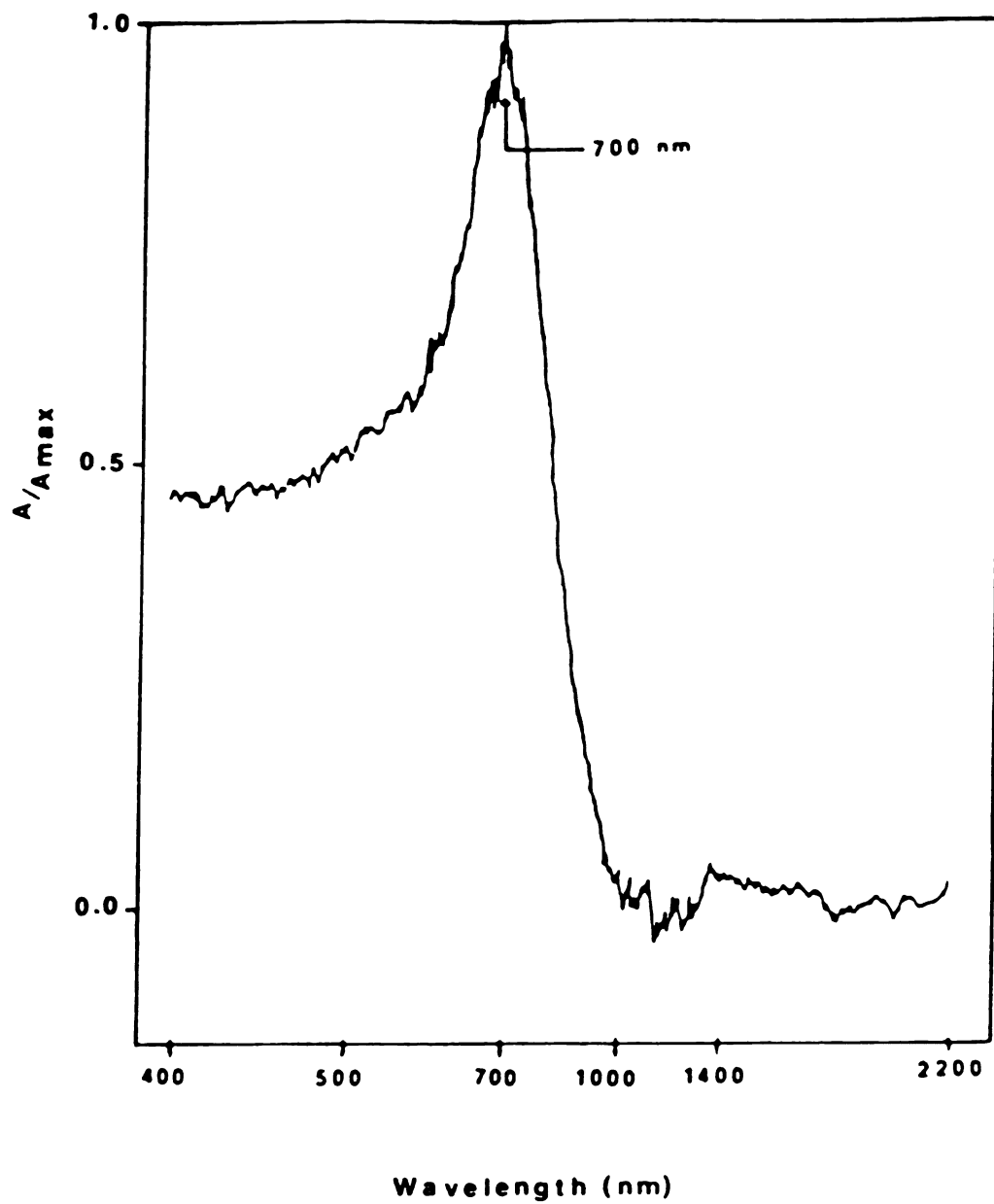


Figure 8. Absorption spectrum of $\text{Ba}^{2+}(\text{HMHCY}) \cdot (\text{Na}_x\text{e}_{2-x})^{2-}$
at -117°C .

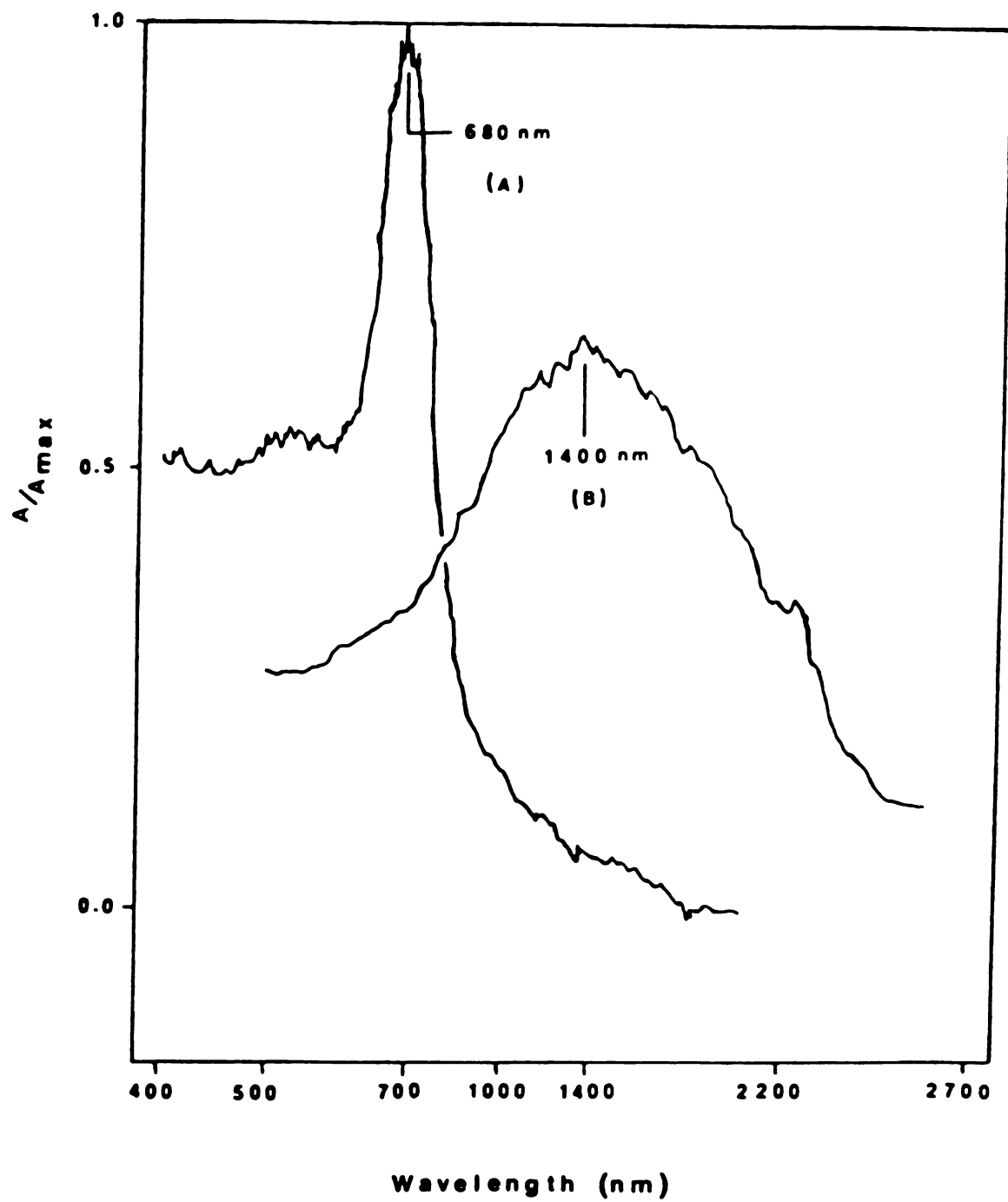


Figure 9. Absorption spectrum of A) $\text{Li}^+(\text{PMPCY}) \text{Na}^-$ at -80°C ; and B) $\text{Li}^+(\text{PMPCY})\cdot\text{e}^-$ at -90°C .

The low background for IV in the lower energy region and a similar low background for V in the higher energy region verify that these materials are the sodide and electride for IV and V respectively.

An important observation illustrated by this Figure is that there are two distinct spectra for the two very similar compounds. The only difference in the preparation of these two materials was the presence of sodium in the synthesis of IV, which gives rise to a Na^- absorption in thin films of the resulting compound. Since one would expect lithium and PMPCY to behave consistently under similar conditions, any material formed in the absence of sodium should still contain $\text{Li}^+(\text{PMPCY})$ as the cation. As can be seen in Figure 9, a material with an optical absorption is obtained, even when there is no sodium present. This leaves only e^- as a possible counter ion since Li^- has yet to be seen in an alkalide, and in any event would absorb at higher energies. These results provide added confirmation for the formation of the electride, $\text{Li}^+(\text{PMPCY}) \cdot e^-$.

III. B. 3. $\text{Li}^+(\text{TRIMCY})_2 \cdot \text{Na}^-$:

The optical spectrum of $\text{Li}^+(\text{TRIMCY})_2 \cdot \text{Na}^-$ was similar to that observed with other sodides. The major absorption peak was at 700 nm ($14,300 \text{ cm}^{-1}$) (Figure 10). In the higher wavelength (lower energy) region out to 2200 nm, there were no significant features that might indicate a mixture of sodide and electride. It is interesting that the higher energy shoulder ascribed to the bound-to-continuum transition is not apparent. It could be hidden under the high energy "tail" of the main peak, but comparison with Figure 5, for example, suggests that it is qualitatively different in this case.

III. C. Summary:

A summary of the electronic absorption maxima for the compounds studied is given in Table 4. Based on the optical spectra and the results of the stoichiometric analyses, it is believed that six new sodides and one new electride have been synthesized.

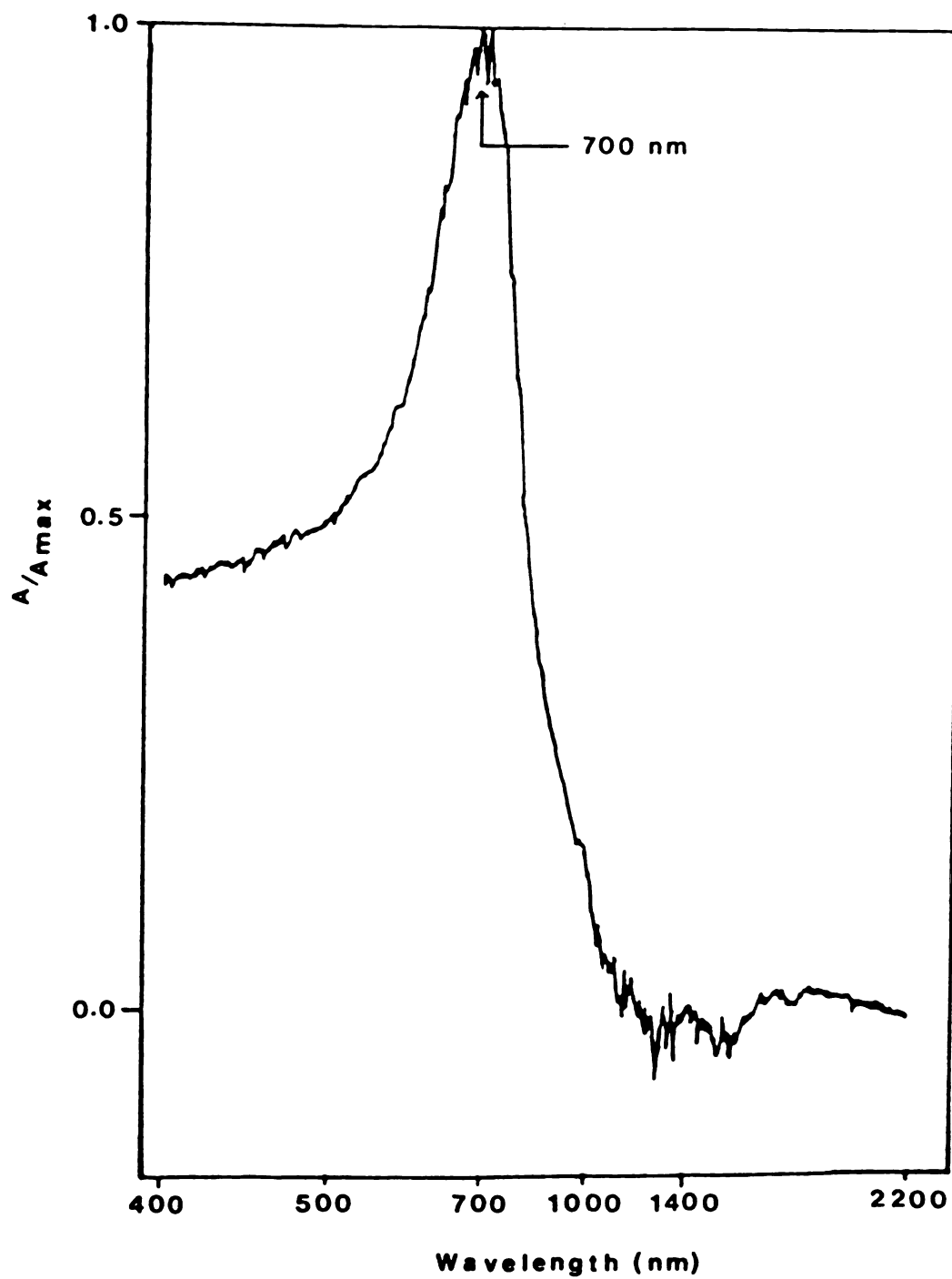


Figure 10. Absorption spectrum of $\text{Li}^+(\text{TRIMCY})_2 \cdot \text{Na}^-$ at -114°C .

Table 4. Summary of Optical Absorption Peak Positions.

Compound	Wavelength of the Maximum (nm)
$K^+(HMICY) \cdot Na^-$	660
$Rb^+(HMICY) \cdot Na^-$	670 [†]
$Cs^+(HMICY) \cdot Na^-$	710
$Ba^+(HMICY) \cdot Na^-$	700
$Li^+(PMPCY) \cdot Na^-$	680
$Li^+(PMPCY) \cdot e^-$	1400
$Li^+(TRIMCY) \cdot Na^-$	700

[†]The Rb^- absorption has been omitted.

IV THERMODYNAMIC PROPERTIES

IV. A. Introduction:

The primary reason for expanding the research on alkalides and electriles into the area of aza-crowns was to find materials that were thermally stable. One method of testing the thermal stability is by heating a sample at a constant rate and measuring the enthalpy changes that occur. This method does not take kinetic effects into consideration, as most of the compounds decomplex or decompose with time at temperatures much lower than indicated by heating at a constant rate. This results from processes that are kinetically slow at the lower temperature although thermodynamically favored. However, this method does provide an accurate measure of the heat of reaction for a transition and offers a means of comparing the relative stabilities of various alkalides and electriles. The enthalpy (ΔH) is determined by converting the temperature axis to a time axis, then measuring the area under the curve of heat flow (W/g) vs. time and dividing by the mass of the sample. The transition temperature is then obtained by extrapolating the steepest part of the onset curve to the baseline. The temperature at this intersection is the reported temperature of the transition.

Many of the alkalides (especially sodides) and a few electriles are relatively stable up to their melting point, above which they decompose rapidly and irreversibly, presumably as a

result of attack on the ligand by the strongly reductive environment. The unique property obtained by the use of amine based complexants such as the aza-crowns, is that they tend to decomplex rather than decompose. In some cases, the free amine is then stable in the presence of the highly reducing alkali metals (even the alkali metal alloys) to temperatures above 120 °C.

IV. B. Experimental Methods:

The thermal behavior of these compounds was explored by differential scanning calorimetry (DSC) using an E.I. duPont de Nemours 9900 Series thermal analysis system. Microcrystalline samples were loaded into anodized aluminum DSC sample pans under nitrogen atmosphere at liquid nitrogen temperatures. The pans were then hermetically sealed to permit handling outside of the glove bag. The studies were made by introducing the samples to the instrument at between -50 and -80 °C and scanning at between 2 and 10 deg/min until decomposition occurred. As previously mentioned, the peak temperature is dependent on the heating rate.^{51,52} A relationship between the heating rate and peak temperature for an nth order reaction is given by Equation 2⁵³;

$$\frac{E \phi}{RT_m} = A e^{-E/RT_m} \quad 2$$

where R is the gas constant, T_m is the peak temperature, E is the activation energy for the transition, A is the pre-exponential factor, and φ is the heating rate. By determining the peak temperature at various heating rates, the activation energy and

frequency factor may be determined.⁵¹ In this study, only one heating rate was employed to determine only the enthalpy of reaction (ΔH) and the approximate temperature of the endothermic and exothermic transitions of various compounds. The rate of 5 deg/min was chosen to give the best results on determining the enthalpy for most compounds. A slower rate would provide a better estimate of the transition temperature; however, the slower rates resulted in a baseline drift which made enthalpy determination more difficult.

When the observed transitions in the DSC trace could not be unequivocally assigned, a visual observation of the heating was also obtained by using a Thomas Hoover capillary melting point apparatus. In this case, capillary tubes were loaded at room temperature under a helium atmosphere, then evacuated and flame sealed while keeping the sample in liquid nitrogen. The observations were started at at ~ 0 °C, by allowing the temperature to come to equilibrium first, then heating at ~ 20 deg/min until the sample noticeably decomposed.

IV. C. Thermodynamic Properties

IV. C. 1. HMHCY Compounds:⁵⁴

As mentioned before, the most noteworthy feature of these materials is their resistance to thermal decomposition. When a microcrystalline sample of $K^+(HMHCY) \cdot Na^-$ (I) is heated, as monitored by DSC (Figure 11), it begins to melt at ~ 42 °C and decomplexes into the alkali metals (presumably NaK^{55}) and free amine at ~ 74 °C. Further heating yields no sign of decomposition of the complexant at temperatures up to 120 °C at which point the HMHCY decomposes and evolves a gas. To verify that the transitions indicated by DSC were melting and decomplexation respectively, a visual observation of the heating process was also made. At ~ 40 °C, the red-orange metallic-appearing crystals melted to form a deep blue liquid. At this point, if the sample was removed from the hot bath and immersed in liquid nitrogen, a red-orange film could be obtained. The melting and freezing were repeatable over more than one cycle. Continued heating of the sample to ~ 60 °C resulted in the appearance of a silvery metallic substance and a light blue liquid which eventually became clear. The metal and complexant remained stable until the temperature reached ~ 140 °C, at which point the solution became dark and a gas was evolved (decomposition of the HMHCY; see Figure 2). In a separate experiment, the crystals were heated until they decomplexed to give a slightly pale blue solution, then cooled to -78 °C. Upon addition of dimethyl ether, the solution became dark blue, the color expected for a solvated alkali metal anion, and

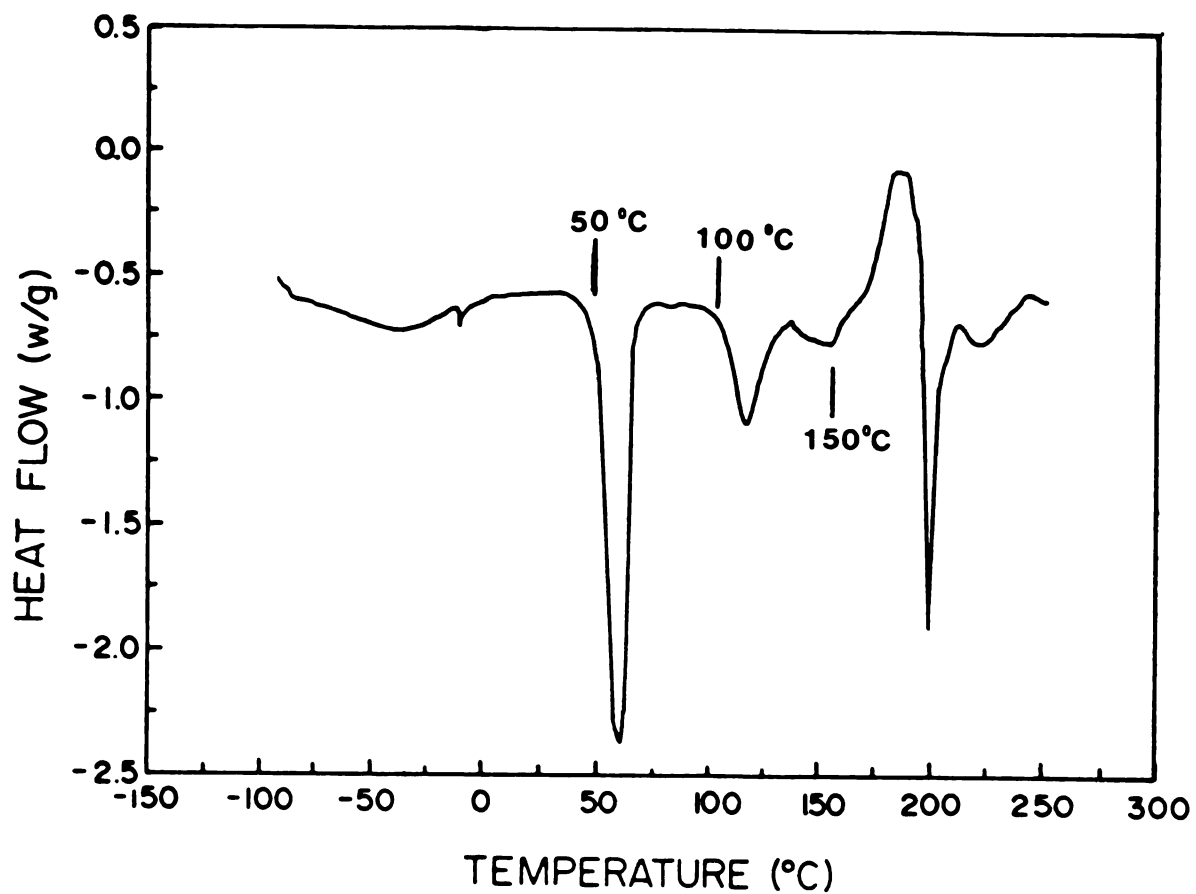


Figure 11. Differential scanning calorimetry trace for a 3.3 mg sample of $K^+(HMCY) \cdot Na^-$ at 10 deg/min.

Endothermic values are negative.

The peaks are shifted to higher temperatures than reported; possibly as a result of the faster scan rate.

red-orange films could be seen on the walls of the glass cell. These observations indicate that the endothermic process that occurs at ~ 74 °C in the DSC pattern is decomplexation. Further, since the exothermic decomposition does not occur until the temperature is above 120 °C, HMHCY is resistant to reductive attack in the presence of alkali metals at temperatures well above 100 °C

After measuring the melting point in the DSC, the sample was cooled to below -20 °C and reheated to check the reproducibility of the melting. This was repeated several times, but the endothermic transition at the melting point was absent except for a small dip in the baseline. If, however, on the second heating the temperature was allowed to continue to increase, decomplexation occurred at the normal temperature of 74 °C. If the sample was held just above the melting point for several hours, it would remain stable until the temperature was increased to the decomplexation point. It is our belief that the crystalline compound melts at 42 °C to give a liquid, but when it is recooled it remains in a glassy state so that no melting transition can be detected. Crystals of $K^+(HMHCY)\cdot Na^-$ that are left at room temperature decomplex after about 4 days. This indicates that the solid compound is thermodynamically unstable to decomplexation at room temperature, even though it must be stable at the temperature of formation (-50 °C). The remarkable stability of the melt below 74 °C suggests that the decomplexation process must be very slow, even in the liquid state.

Polycrystalline samples of $Cs^+(HMHCY)\cdot Na^-$ (III) had a behavior

similar to those of $\text{K}^+(\text{HMHCY})\cdot\text{Na}^-$. The former compound appeared to melt at $\sim 8^\circ\text{C}$ and decomplex into alkali metals [presumably $\text{Na}(\text{s})+\text{Cs}(\text{l})$] and free amine at $\sim 37^\circ\text{C}$, (Figure 12). NaCs forms a liquid alloy at $\sim 45^\circ\text{C}$,⁵⁵ near the end of the decomplexation process. As with compound I, a visual melting point was obtained for this sodide which agreed with these assignments. This compound also decomplexes if left at room temperature after about 4 days. Thus, decomplexation of the melt is slow in this case also.

The third compound in this series, $\text{Rb}^+(\text{HMHCY})\cdot\text{Na}^-$ (II), has a thermal profile similar to the other two (Figure 13). This compound has an apparent melting transition at $\sim 7^\circ\text{C}$ and decomplexation into the alkali metals [presumably $\text{Na}(\text{s})+\text{Rb}(\text{s})$] and free amine at $\sim 30^\circ\text{C}$. Rb would melt at 39°C under the decomplexation curve and RbNa would then form at $\sim 53^\circ\text{C}$ ⁵⁵ near the end of the decomplexation process. Due to the similarity in behavior of this compound to $\text{K}^+(\text{HMHCY})\cdot\text{Na}^-$ (I) and $\text{Cs}^+(\text{HMHCY})\cdot\text{Na}^-$ (III) and to the similarity in their structures (chapter 6 of this Dissertation), a visual melting point was not obtained. This compound also decomplexes if left at room temperature as with compounds I and III, but in 1 day or less. This is not very surprising, as the decomplexation temperature is only slightly above room temperature. However, the decomplexation is still slow for the melt as with I and III. The fact that $\text{Rb}^+(\text{HMHCY})\cdot\text{Na}^-$ does decomplex much more readily than either $\text{K}^+(\text{HMHCY})\cdot\text{Na}^-$ or $\text{Cs}^+(\text{HMHCY})\cdot\text{Na}^-$ and that its enthalpy of formation is so much lower, prompted the proposed mechanism of Rb^- formation found in

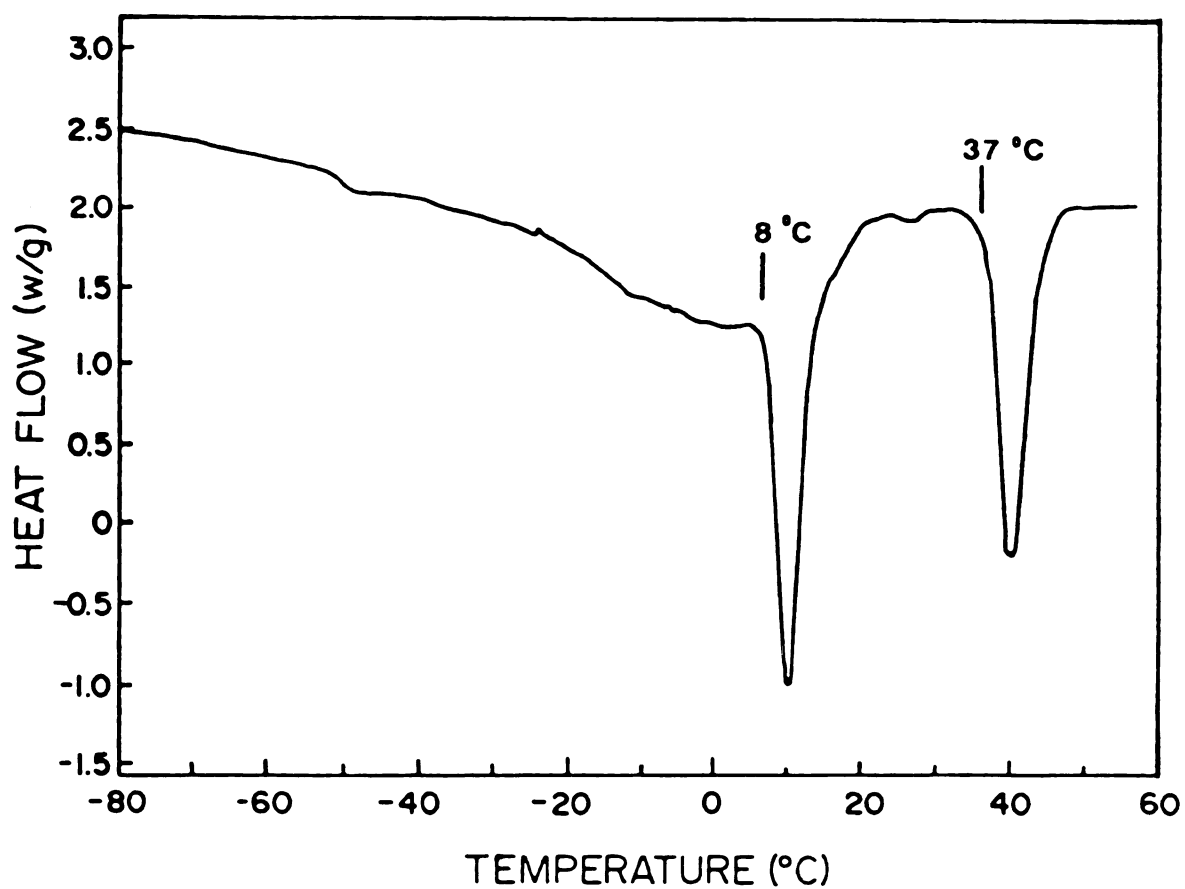


Figure 12. Differential scanning calorimetry trace for a 2.5 mg sample of $\text{Cs}^+(\text{HMICY})\cdot\text{Na}^-$ at 5 deg/min.

Endothermic values are negative.

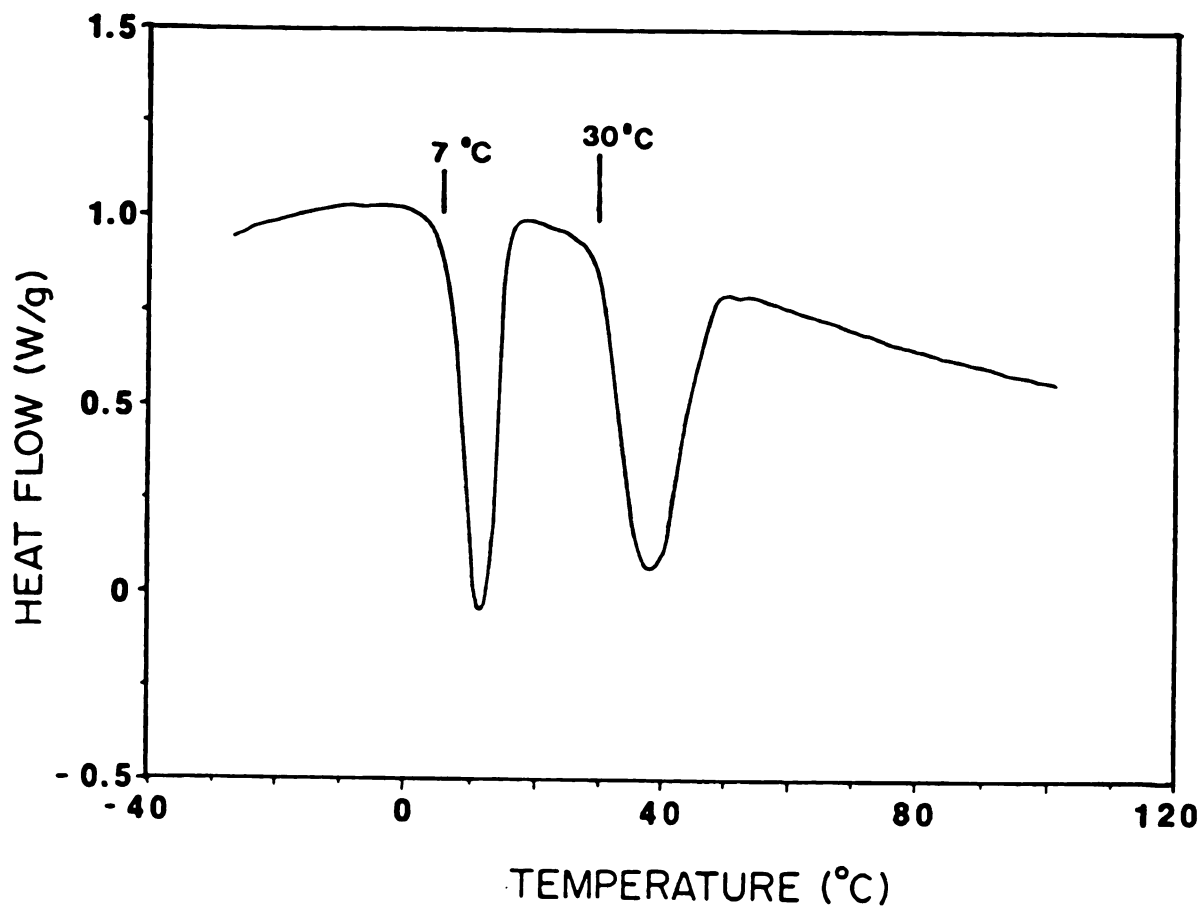


Figure 13. Differential scanning calorimetry trace for a 2.2 mg sample of $\text{Rb}^+(\text{HMTCY})\cdot\text{Na}^-$ at 5 deg/min.

Endothermic values are negative.

the studies of the optical spectra.

To estimate the enthalpy of formation of these three alkalides from the DSC information, the thermodynamic cycle shown in Figure 14 was used. The enthalpy of formation of the liquid alloy was obtained by summing the enthalpy of mixing of the liquid metal⁵⁶ and the enthalpy of fusion⁵⁷ of the metals involved (ie. $\Delta H_f^{\text{Na}} + \Delta H_f^{\text{K}} + \Delta H_{\text{mixing}} = \Delta H_{\text{formation}}^{\text{NaK}}$; Table 5). The value obtained for NaK in this way was comparable to the value reported by McKisson and Bromley (5.8 to 6.3 kJ mol⁻¹).⁵⁸ The enthalpy of fusion of HMHCY was also obtained from DSC measurements. The heat capacities for the various components were not included, as terms that contain them should nearly cancel out in the cycle. The results are given in Table 6.

By examining the measured enthalpy of decomplexation at various temperatures and the entropies of melting of $\text{K}^+(\text{HMHCY})\cdot\text{Na}^-$, HMHCY, and NaK, we can understand why the compound is stable to decomplexation at 225 K but decomplexes (slowly) at 300 K and above. Since the sodide is stable at the temperature of formation (225 K) and the value for the enthalpy of decomplexation of the sodide at 225 K, directly from Figure 12, is $\Delta H = 52.5 \text{ kJ mol}^{-1}$, it would imply $\Delta S < 233 \text{ J mol}^{-1} \text{ K}^{-1}$ at this temperature. At 300 K, the sodide decomplexes slowly with time. This indicates that, at this temperature, the compound is not stable, or $\Delta G \geq 0$. By calculating the enthalpy of decomplexation at 300 K, we can obtain a lower limit to the enthalpy of stabilization. Since the products of decomplexation at 300 K are $\text{NaK}_{(1)}$ and $\text{HMHCY}_{(1)}$, the

Table 5. Values Used to Obtain the Enthalpy of Formation of the Metal Alloys.

Metal	ΔH_{fusion} (kJ mol ⁻¹)	$\Delta H'_{\text{mixing}}$ (kJ mol ⁻¹)
Na	2.7	—
K	2.3	0.8
Rb	2.2	1.2
Cs	2.1	0.9

*for the reaction $M(l) + Na(l) \rightarrow MNa(l)$

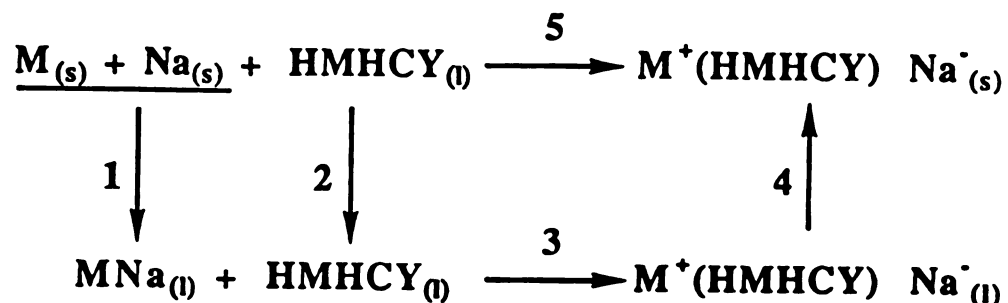


Figure 14. Thermodynamic cycle used to calculate enthalpy of formation of $K^+(HMHCY) \cdot Na^-$, $Rb^+(HMHCY) \cdot Na^-$, and $Cs^+(HMHCY) \cdot Na^-$ from the metals and complexant at 225 K from the DSC measurements.

Table 6. Summary of Enthalpy Changes for Various Steps in the Thermodynamic Cycle Shown in Figure 14.

Step	$K^+(HMHCY) \cdot Na^-$ kJ/mol	$Rb^+(HMHCY) \cdot Na^-$ kJ/mol	$Cs^+(HMHCY) \cdot Na^-$ kJ/mol
1*	5.8	6.0	5.6
2**	5.9	5.9	5.9
3**	-29.0	-28.0	-31.0
4**	-35.2	-12.2	-35.1
5	-52.5	-28.4	-54.6

*The value for steps 3 and 4 are suspect: see text.

**Calculated values. *From DSC measurements.

enthalpy change is a sum of the values for the melting and decomplexation steps [steps 3 and 4 in Figure 14 and Table 6] for the sodide. This yields $\Delta H = 64 \text{ kJ mol}^{-1}$ and implies that $\Delta S > 213 \text{ J mol}^{-1} \text{ K}^{-1}$. In order to determine a lower limit to ΔS at 225 K, the entropies of crystallization for NaK and HMHCY ($\Delta H/T_m$; -22.6 and -21.8 $\text{J mol}^{-1} \text{ K}^{-1}$ respectively) must be added to the entropy calculated for decomplexation at 300 K. This correction is necessary as NaK and HMHCY are solid at 225 K. This requires that the lower limit be $\Delta S > 170 \text{ J mol}^{-1} \text{ K}^{-1}$ for the decomplexation process at 225 K. Thus, at the temperature of formation of the crystalline compound, $170 \text{ J mol}^{-1} \text{ K}^{-1} < \Delta S < 233 \text{ J mol}^{-1} \text{ K}^{-1}$. Decomplexation above the melting points of the products would occur for any value of ΔS between these limits.

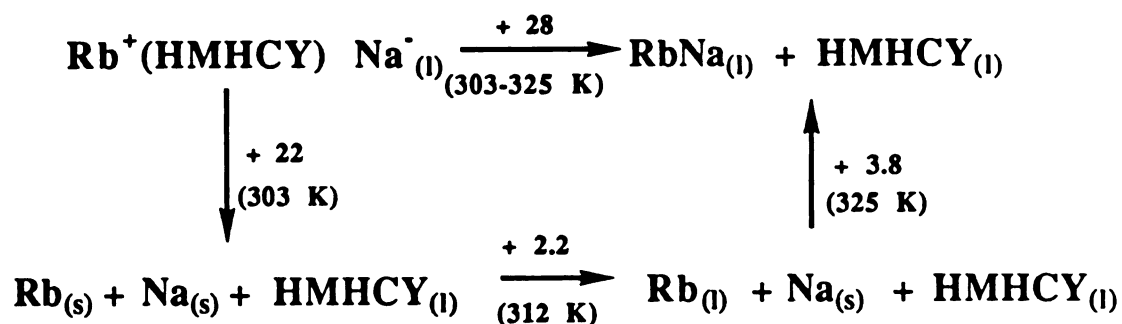
Application of the same analogy to $\text{Rb}^+(\text{HMHCY})\cdot\text{Na}^-$ (II) and $\text{Cs}^+(\text{HMHCY})\cdot\text{Na}^-$ (III), which are stable at 225 K with $\Delta H = +28.4$ and $\Delta H = +54.6$ for decomplexation, respectively [calculated from Figure 14 and Table 6], implies that $\Delta S < 126 \text{ J mol}^{-1} \text{ K}^{-1}$ for II and $\Delta S < 243 \text{ J mol}^{-1} \text{ K}^{-1}$ for III at 225 K. In order to calculate the lower limit for ΔS , there need to be some changes in the thermodynamic cycles used.

At 300 K, both compounds II and III as well as HMHCY are in the liquid state. Also, in an ideal case the solid metals precipitate without formation of the alloy when the alkalides decomplex. However, since the enthalpic values reported are under a large temperature envelope (Figures 12 & 13), alloy formation must be taken into account in the calculations. From the thermodynamic cycles shown in Figure 15 A and 16 A for

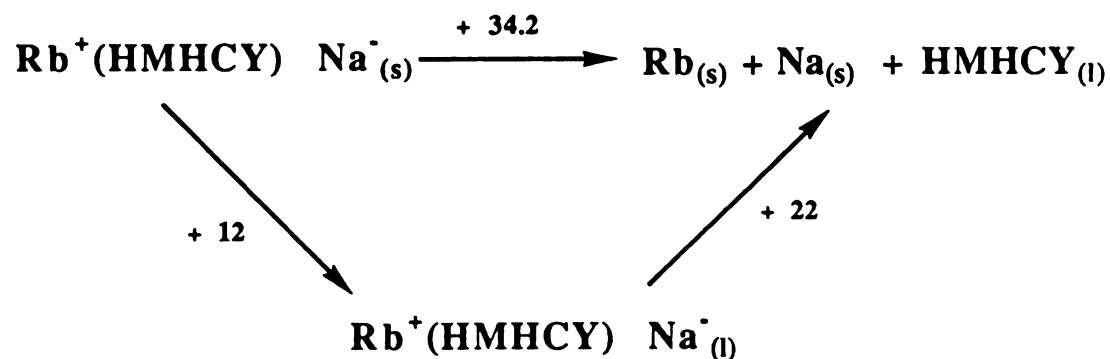
$\text{Rb}^+(\text{HMHCY})\cdot\text{Na}^-$ and $\text{Cs}^+(\text{HMHCY})\cdot\text{Na}^-$ respectively, the energy required to decomplex the liquid alkalides into $\text{M}_{(s)}$, $\text{Na}_{(s)}$, and $\text{HMHCY}_{(l)}$ can be calculated (22.0 and 27.2 $\text{kJ mol}^{-1} \text{K}^{-1}$ for II and III respectively). Then, Figures 15 B and 16 B allow one to calculate the energy required for the solid alkalides to decomplex into $\text{M}_{(s)}$, $\text{Na}_{(s)}$, and $\text{HMHCY}_{(l)}$ at 300 K. The enthalpy of decomplexation would then be $\Delta H = 34.2 \text{ kJ mol}^{-1}$ and $\Delta H = 60.2 \text{ kJ mol}^{-1}$ for II and III respectively. This implies that $\Delta S > 114 \text{ kJ mol}^{-1} \text{K}^{-1}$ for II and $\Delta S > 200 \text{ J mol}^{-1} \text{K}^{-1}$ for III.

In order to determine the lower limit for the entropy change at the temperature of formation, 225 K, we must add the entropy of crystallization for the HMHCY, $-21.8 \text{ J mol}^{-1} \text{K}^{-1}$, for both II and III (since both M and Na are already in the solid state, their crystallization entropies need not be added). This requires $\Delta S > +92 \text{ J mol}^{-1} \text{K}^{-1}$ for II and $\Delta S > 178 \text{ J mol}^{-1} \text{K}^{-1}$ for III. Thus, at the temperature of formation, 225 K, for $\text{Rb}^+(\text{HMHCY})\cdot\text{Na}^-$ $+92 < \Delta S < 126 \text{ J mol}^{-1} \text{K}^{-1}$ and for $\text{Cs}^+(\text{HMHCY})\cdot\text{Na}^-$ $178 < \Delta S < 243 \text{ J mol}^{-1} \text{K}^{-1}$. Decomplexation above the melting points of the two alkalides would occur for any value of ΔS between the respective limits.

It is inconsistent that $\text{Rb}^+(\text{HMHCY})\cdot\text{Na}^-$ has such a different thermal behavior than the other two alkalides, when their structures and other physical properties are so similar. By examining Figures 15 and 16, it can be seen that the major difference is in the enthalpy of melting of the two compounds. $\text{Cs}^+(\text{HMHCY})\cdot\text{Na}^-$ has an enthalpy of melting similar to that of $\text{K}^+(\text{HMHCY})\cdot\text{Na}^-$, while that of $\text{Rb}^+(\text{HMHCY})\cdot\text{Na}^-$ is much lower. All other values, including the enthalpy of decomplexation, are

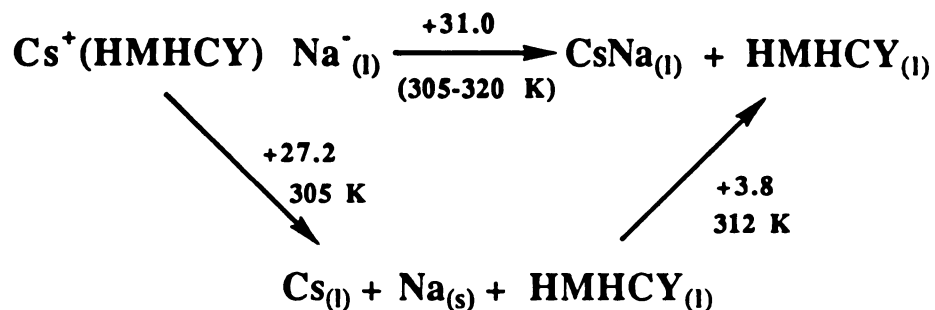


A

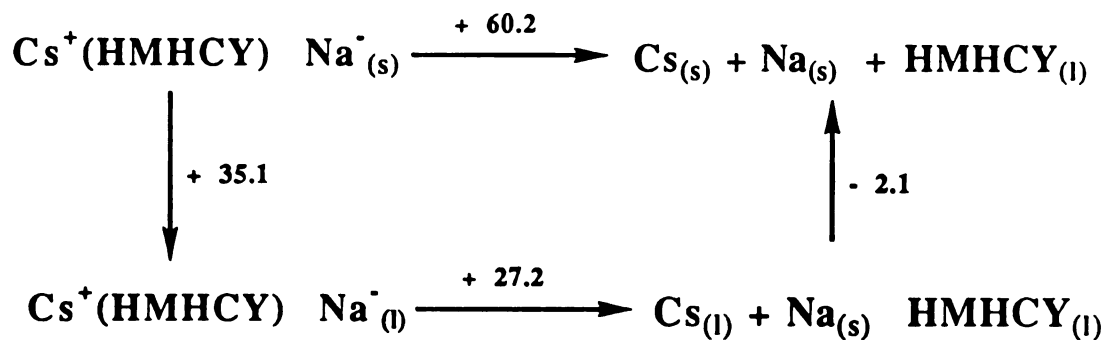


B

Figure 15. Thermodynamic cycles for $\text{Rb}^+(\text{HMHCY})\cdot\text{Na}^-$; A) Processes occurring during decomplexation over a large temperature range. B) Decomplexation process at 300 K. Enthalpy values are in kJ mol^{-1} .



A



B

Figure 16. Thermodynamic cycles for $\text{Cs}^+(\text{HMHCY})\cdot\text{Na}^-$; A) Processes occurring during decomplexation over a large temperature range. B) Decomplexation process at 300 K. Enthalpy values are in kJ mol^{-1} .

similar for the three alkalides. We believe that the enthalpy of melting for II is inaccurate. As mentioned earlier, these compounds glassify if melted and recooled. In the process of either loading the sample into the DSC pan or collecting the sample from the initial synthesis, the sample may have partially melted and then glassified upon recooling. Since the glassy product does not contribute to the enthalpy of melting, the associated value would be lower. However, the molten compound would decomplex at the expected temperature. This would account for the low values for the enthalpy of melting yet "normal" values for decomplexation. The thermodynamic calculations for $\text{Rb}^+(\text{HMICY})\cdot\text{Na}^-$ should be repeated on a sample which has been treated more carefully and not allowed to melt, in order to more accurately determine the enthalpy of melting.

The thermodynamic properties of the barium compound with HMICY were not obtained. However, thermodynamic measurements might provide a useful method of determining whether a mixture of two compounds exists, or if it is one material with a unique stoichiometry.

IV. C. 2. FMPCY Compounds

When microcrystalline samples of $\text{Li}^+(\text{FMPCY})\cdot\text{Na}^-$ (IV) and $\text{Li}^+(\text{FMPCY})\cdot\text{e}^-$ (V) are heated at 5 deg/min, as monitored by DSC (Figure 17 A & B), there are no melting or decomplexation transitions seen. The spectrum for $\text{Li}^+(\text{FMPCY})\cdot\text{Na}^-$ does have a small ($\sim 1.1 \text{ kJ mol}^{-1}$) endothermic transitions at $\sim -54^\circ\text{C}$ and a larger ($\sim 40 \text{ kJ mol}^{-1}$) exothermic transition at $\sim 120^\circ\text{C}$. The spectrum for $\text{Li}^+(\text{FMPCY})\cdot\text{e}^-$ has a similar behavior with a small ($\sim 2.3 \text{ kJ mol}^{-1}$) endothermic transition at $\sim -74^\circ\text{C}$ with a corresponding larger ($\sim 32 \text{ kJ mol}^{-1}$) exothermic transition at $\sim 80^\circ\text{C}$. The exothermic peaks are a result of sample decomposition for each compound. This assignment is based on the behavior of V under visual observation of the heating process. When this sample was heated at $\sim 20 \text{ deg/min}$, it appeared to remain stable until the temperature reached $\sim 85^\circ\text{C}$. At that point, the sample started to melt then immediately turned yellow and evolved a gas. The similar DSC pattern of compound IV would lead one to believe that it is undergoing a similar process at the higher temperature.

The lower temperature endotherm is more difficult to explain. Unlike the melting and decomplexation steps in the study of the three sodides with HMFCY, this transition was reversible (Figure 18) and reproducible. By alternately raising and lowering the temperature through this range (but remaining well below the decomposition temperature), the transition was repeated several times, and the position and intensity were consistent. Since there is no visually noticeable change in the materials and the process is present in both the sodide and the electride, there

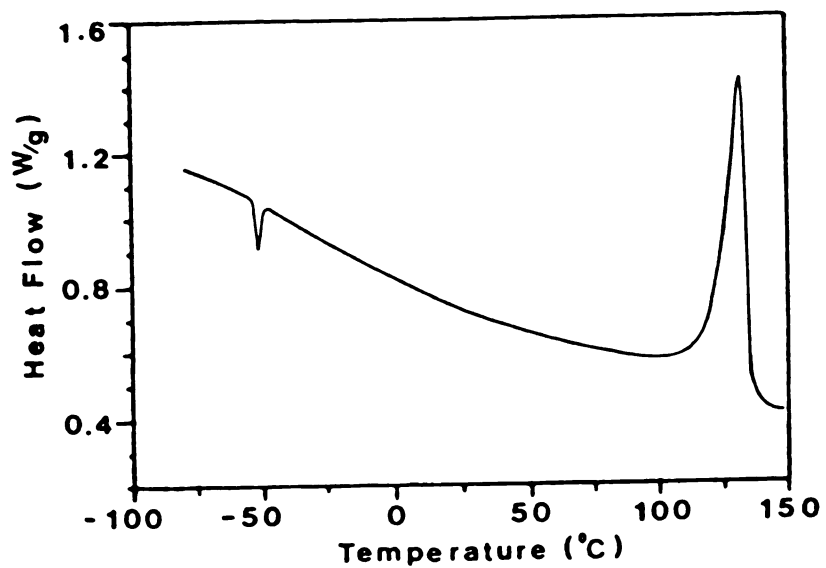
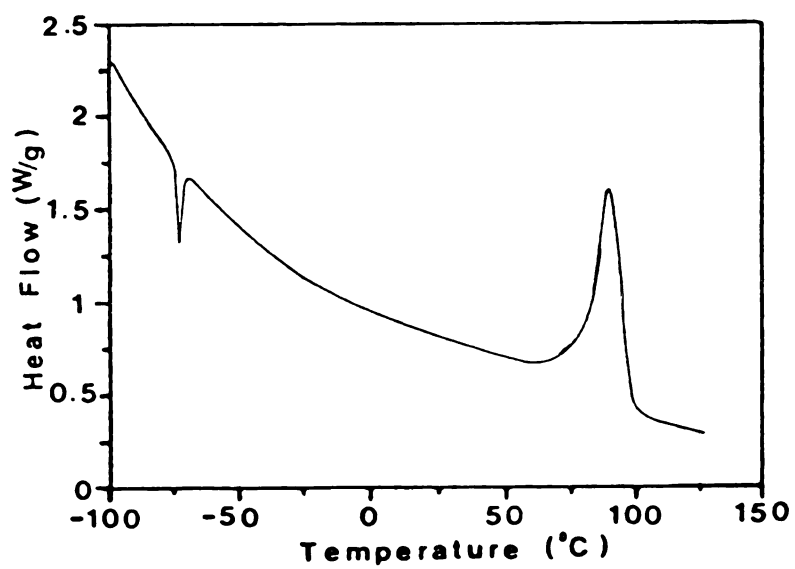
**A****B**

Figure 17. DSC spectrum for A) $\text{Li}^+(\text{PMPCY})\cdot\text{Na}^-$; and B) $\text{Li}^+(\text{PMPCY})\cdot\text{e}^-$; at 5 deg/min.

Endothermic values are negative.

must be some internal change in the molecule, possibly the orientation of the PMPCY ring around the Li^+ , or a partial melting of the material. This transition will be discussed in more detail later, as it was also detected in the electride by magnetic susceptibility measurements and conductivity.⁵⁹ It would be an interesting experiment to test whether it is present or not in model salts of $\text{Li}^+(\text{PMPCY})$ with conventional anions such as I^- or SCN^- .

Notwithstanding their novel properties, these two compounds do behave in a similar fashion to the alkalides synthesized with HMPCY in one respect. They decomplex if left at room temperature for an extended period of time (over 60 days and over 10 days for IV and V respectively). In order to verify that the compounds did truly decomplex, samples of each compound, $\text{Li}^+(\text{PMPCY})\cdot\text{Na}^-$ and $\text{Li}^+(\text{PMPCY})\cdot\text{e}^-$, were left at room temperature, under vacuum, until they noticeably "died" (they lost their color and crystallinity so all that remained were a clear liquid and metallic flakes). In the case of the sodide, dimethyl-ether was then added to produce a dark blue solution, the color expected with alkalide and electride solutions, and orange metallic films. With the electride, methylamine was added to give a dark blue solution [$\text{Li}^+(\text{CH}_3\text{NH})_4 + \text{e}(\text{s})^-$; this is proof that the metal had not been destroyed], then removed to give a black mass of material which appeared to be the electride. If either sample had decomposed rather than decomplexed, the dark blue solutions would not have been seen.

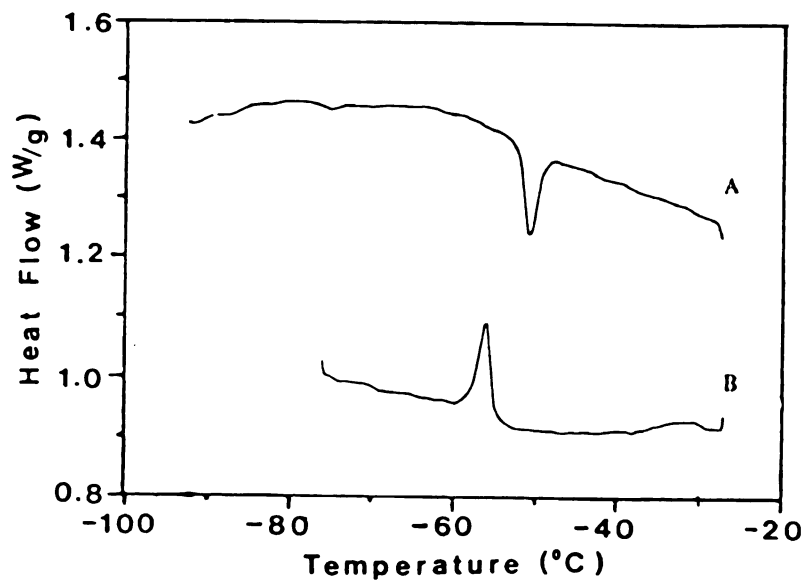


Figure 18. DSC trace over the phase transition in $\text{Li}^+(\text{PMPCY})\cdot\text{Na}^-$.
A) Heating; B) Cooling.

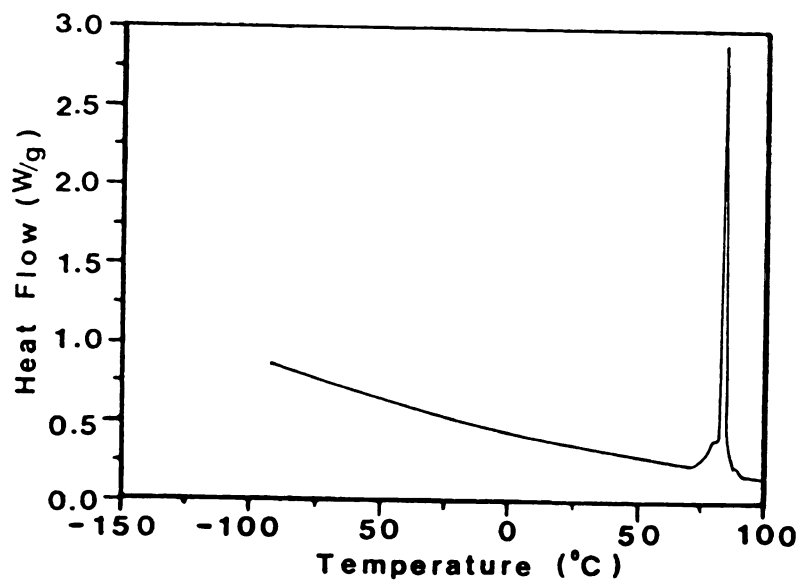


Figure 19. DSC spectrum of $\text{Li}^+(\text{TRIMCY})_2\cdot\text{Na}^-$ at 5 deg/min.
Endothermic values are negative.

IV. C. 3. $\text{Li}^+(\text{TRIMCY})_2 \cdot \text{Na}^-$:

The final compound in this study, $\text{Li}^+(\text{TRIMCY})_2 \cdot \text{Na}^-$, was also investigated by DSC (Figure 19). This material presented no indication of melting, decomplexation, or any other type of transition other than a sharp exothermic process at $\sim 80^\circ\text{C}$ which has been identified as a decomposition. Preliminary studies have indicated that this compound is stable at room temperature for up to three months. Although there is no quantitative proof, it appeared that decomplexation rather than decomposition was the governing process in its "death". This compound should be studied in greater detail to determine the extent of its thermal stability.

IV. F. Summary:

A summary of the thermal processes that occur in the 5 sodides and 1 electride are given in Table 7. It seems that these compounds have provided a solution to the problem of autocatalytic decomposition at room temperature, but they now suffer from low complexation strength. The fact that some of them decompose at temperatures near or above 100°C is not a major concern to the goal of finding alkalides and electrides that are stable at room temperature. The neat complexants also tend to decompose if heated ($\sim 140^\circ\text{C}$ for HMCY). However, the problem of decomplexation when the materials are left at room temperature for periods ranging from 1 to 60 days remains; one must try to find ligands with a greater affinity for the alkali metals.

Table 7. Summary of the Thermal Processes That Occur in the DSC Traces With a Heating Rate of 5 deg/min in °C.

Compound	M.P.	Decomplexation Temperature	Decomposition Temperature	Phase Change
$K^+(HMHCY) \cdot Na^-$	42'	74	140**	----
$Rb^+(HMHCY) \cdot Na^-$	7	30	140**	----
$Cs^+(HMHCY) \cdot Na^-$	8	37	140**	----
$Li^+(PMPCY) \cdot Na^-$	---	---	120	-54
$Li^+(PMPCY) \cdot e^-$	---	---	80	-74
$Li^+(TRIMCY)_2 \cdot Na^-$	---	---	80	----

*Heating rate at 10 deg/min.

**Decomposition of the HMHCY ligand.

V MAGNETIC PROPERTIES

The magnetic properties of alkalides and electrides offer a method of identifying the cationic and anionic species in these unusual solid state materials as well as a means of understanding the nature of the cation-anion interactions. Magic Angle Spinning Nuclear Magnetic Resonance (MAS-NMR) spectroscopy is a powerful technique for probing the local structure around the nucleus, while Electron Paramagnetic Resonance (EPR) spectroscopy can reveal information about the trapping sites of the electron, the electron-electron interactions, and electron-nuclear interactions for electrides and contaminant electrons in alkalides. The magnetic susceptibility is another technique used to probe the interactions between the unpaired electrons in the electrides. All these techniques are employed, when possible, to help understand the behavior and properties of these unusual materials.

V. A. MAS-NMR

The chemical shift in the MAS-NMR spectrum of alkalides and electrides can be used as a "fingerprint" to identify the anionic or cationic species present.²³ Also, there are several on-going projects in this laboratory to better understand the interactions of the complexed cations and the solvent-free anions with their surroundings. However, in this study, MAS-NMR was used only as a means of identifying the anionic and cationic species. All samples were studied with a Bruker 180 MHz (proton frequency) spectrometer using polycrystalline samples.⁶⁰

V. A. 1. HMHCY Compounds:

The regions of both ^{39}K and ^{23}Na were examined for $\text{K}^+(\text{HMHCY})\cdot\text{Na}^-$ (I). Sodium-23 MAS-NMR gave a single sharp resonance at -60.8 ppm [relative to Na^+ (aq.)], a chemical shift that is characteristic of all sodide salts.^{61,62} No peaks of Na^+ or K^- were observed. As expected on the basis of its large quadrupolar broadening,⁶³ the signal of K^+ was not seen.

For $\text{Cs}^+(\text{HMHCY})\cdot\text{Na}^-$ (III), the regions of ^{133}Cs and ^{23}Na were examined. Again, sodium-23 MAS-NMR gave a single resonance at -60 ppm [relative to Na^+ (aq.)]. Surprisingly, MAS-NMR gave no discernible peaks of ^{133}Cs even though Cs^+ is normally detectable in other crystalline alkalides and electrides.^{61,64} No peaks were observed for Na^+ or Cs^- .

The MAS-NMR spectrum of $\text{Rb}^+(\text{HMHCY})\cdot\text{Na}^-$ has not yet been determined. It is expected that the ^{23}Na spectrum will have a peak at ~ -60 ppm [relative to Na^+ (aq.)] as with the two similar compounds. The ^{87}Rb spectrum would probably not be observed for Rb^+ as a result of its large quadrupolar broadening.⁶⁵ However, there might be a peak due to Rb^- if the contamination observed with the optical sample is present. An interesting study would be to carefully load a sample (not allow it to warm up to decomplexation temperatures), and then study the possible formation of Rb^- upon temperature cycling.

V. A. 2. PMPCY Compounds

The regions of both ${}^7\text{Li}$ and ${}^{23}\text{Na}$ were examined for samples of $\text{Li}^+(\text{PMPCY})\cdot\text{Na}^-$ (IV). As with the other sodides, sodium-23 MAS-NMR gave a single sharp resonance at -60.7 ppm [relative to Na^+ (aq.)]. Lithium-7 MAS-NMR gave a single sharp resonance at ~ -0.1 ppm [relative to Li^+ (aq.)]. No peaks were observed for either Na^+ or Li^- . For $\text{Li}^+(\text{PMPCY})\cdot\text{e}^-$ (V), only the region of ${}^7\text{Li}$ was examined. This compound gave a single very sharp resonance at $+21.0$ ppm [relative to Li^+ (aq.)]. The sharpness of this peak ($\Delta\nu_{1/2} = 160$ Hz; 3.8 kHz spinning rate) indicates that the ${}^7\text{Li}$ nucleus is surrounded by a very symmetric environment. Also, it can be seen that the Li^+ signal is paramagnetically shifted in this compound, as would be expected for an electride. For both compounds, the temperature dependence of the peak position and line shape was examined. The MAS-NMR signal was not noticeably affected by the transitions that occur at -54 °C for IV and -74 °C for V. This indicates that the transition found by DSC and, for compound V, by conductivity and susceptibility measurements (vide infra) is probably due to lattice changes rather than changes in the local structure around the lithium cation.

V. B. EPR:

The electron has a spin angular momentum with two degenerate energy levels. In the presence of a magnetic field, the degeneracy is removed causing the levels to split into two states characterized by the spin quantum numbers $m = \pm 1/2$. Each level has an energy $E_m = g\beta H m$, where g is the electronic g -value

(similar to the chemical shift in NMR), β is the Bohr magneton ($\beta = 9.2741 \times 10^{-21}$ erg gauss⁻¹),⁶⁶ and H is the applied magnetic field. The separation between these energy levels (Zeeman levels) is $\Delta E = h\nu = g\beta H$. In this equation, h is Planck's constant and ν is the frequency. The latter is determined by the type of EPR spectrometer used. The most common spectrometer is called an X-band spectrometer with $\nu = 9$ GHz.

For a free noninteracting electron, the EPR spectrum would have a single sharp resonance at $g = 2.0023$.⁶⁶ In practice, the electron interacts with its surroundings causing a shift in the parameter g , and hence the resonance field H_0 , as well as a change in the line shape. Electron-electron interactions can produce either a strong g -shift or the appearance of a triplet state. If the electron couples (for times long compared with the EPR time scale) to a nucleus of spin I , the signal will split into $(2I + 1)$ lines. As an example, an electron coupled to a potassium nucleus ($I = 3/2$) will produce 4 lines in the EPR spectrum. This results from a nonvanishing electron density at the nucleus because of an overlap of electronic wavefunctions. Qualitatively, the species formed would be the monomeric pair $K^+ \cdot e_{(x)}^-$; where (x) is a number less than one and is directly related to the hyperfine coupling constant (A) . By measuring the separation between the resonance lines, the hyperfine coupling constant (A) may be determined, where A is defined by Equation 3.⁶⁶

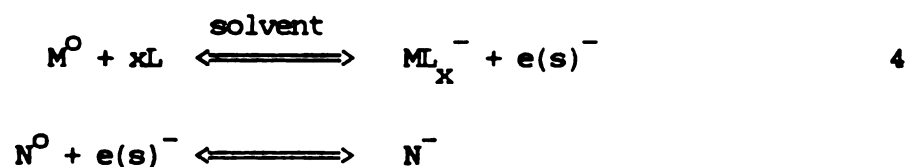
$$A = \frac{8\pi}{3} g_N \beta_N S(S+1) |\psi_0|^2 \quad 3$$

In this equation, g_N and β_N are the nuclear g-factor and the nuclear Bohr magneton. By comparing the measured value of A to that for the atomic species, the percent atomic character of the nucleus can be determined. This is a measure of the amount of electron density at the nucleus, and can be thought of as the value of x in the monomeric pair. An atomic species would have the value $x = 1$.

With polycrystalline solids, anisotropic interactions are also detected in the EPR spectrum. These interactions can reveal valuable information about the local structure of the species in the vicinity of the resonant electron. Such information is lost in liquid samples due to molecular and ionic motion.

V. B. 1. Alkalides and Electrudes:

In a pure polycrystalline alkalide, all of the electrons are spin paired (ns^2). As a result, one would not expect to detect an EPR signal. However, as a result of the methods used to synthesize alkalides, there is a low concentration of electron impurities in most alkalides. This results from the equilibria shown in Equation 4.



During the crystallization process, electrons may become trapped in the crystal in a fashion similar to "color centers". As an example, electron doping can be produced in alkali halides by heating in the presence of alkali metal vapors or by irradiation with γ -rays.⁶⁷

The samples used in this study were obtained from a "normal" synthesis. A polycrystalline sample was loaded into a quartz tube (3 or 4 mm diameter) and sealed under vacuum at liquid nitrogen temperature. The spectra were recorded on a Bruker model 200 X-band spectrometer.⁶⁸

V. B. 2. Results:

The EPR spectra for $K^+(HMHCY) \cdot Na^-$ (I), $Rb^+(HMHC) \cdot Na^-$ (II), and $Cs^+(HMHCY) \cdot Na^-$ (III) are shown in Figures 20 A, 20 B, and 20 C respectively.⁶⁸ All three alkalides show a clear hyperfine coupling to the metal cation, where $I = 3/2, 5/2,$ and $7/2$ for K, Rb, and Cs respectively. The measured hyperfine coupling constants are 3.5 G for I, 38 G for II, and 100 G for III. The corresponding hyperfine coupling constants for atomic ^{39}K , ^{85}Rb , and ^{133}Cs are 82.38 G, 361.06 G, and 819.94 G respectively⁶⁹. These values correspond to approximate percent atomic characters of 4.2 for I, 10.5 for II, and 12.2 for III.

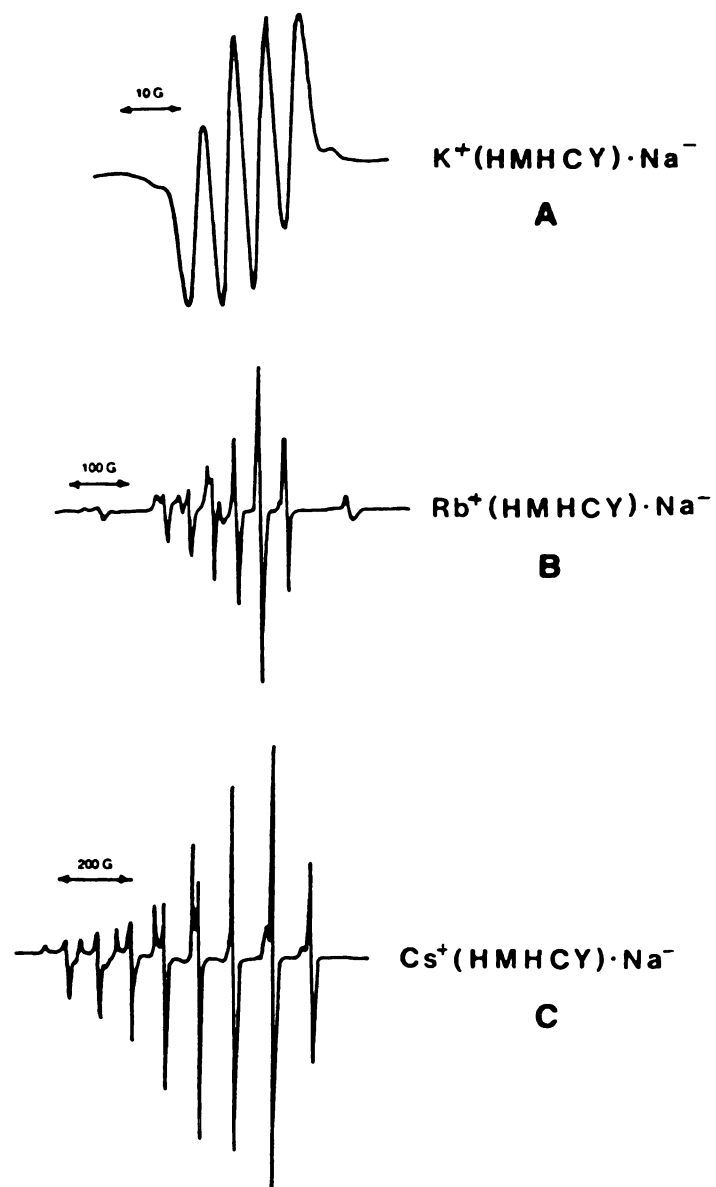


Figure 20. EPR spectra for the three sodides; A) $K^+(HMHCY) \cdot Na^-$; B) $Rb^+(HMHCY) \cdot Na^-$; C) $Cs^+(HMHCY) \cdot Na^-$. Taken with an X-band spectrometer.

From the EPR spectra it is apparent that electrons are trapped in the crystal, but the trapping site is still unknown. The strong hyperfine interaction indicates that the electron is in close proximity to a single alkali metal cation. The crystal structures of these three sodides show a close contact between the sodium anion and the complexed metal cations [Figure 27; Chapter 6 of this Dissertation]. The EPR spectra provide strong evidence for electron trapping at the anionic site. This is also in accord with charge considerations that require e^- to replace Na^- , unless excess cations are present.

The EPR patterns for all three compounds are characteristic of environments with axial symmetry (showing parallel and perpendicular components). For compound I, the anisotropy is not obvious because of the small overall breadth of the spectrum. However, the line shapes for all three were fitted by assuming that g and A have parallel and perpendicular components⁷⁰, and the crystal structures shows that there is axial symmetry around the sodium anions in the three compounds (chapter 6 of this Dissertation). The most surprising result is the absence of any apparent interactions with the protons on the HMHCY ring. A power study (the line intensity as a function of microwave power) shows a completely homogeneous hyperfine coupling. This indicates that the electron is not strongly coupled with all the protons on the "walls" of the cavity. Also, since the protons from the methyl groups are protruding into the cavity between the anionic site and the cation [Figure 27], it would seem that the electronic wavefunction is "bending" itself around the protons to interact

with the cation. A similar behavior has been noted for solvated electrons in amines, where there is a positive electron density at the nitrogen atom and a "negative" density at the protons.⁸⁵ However, it is still possible that the electrons may interact through space (via dipolar coupling) to nearby protons as well as to other nuclei. This behavior can be investigated by Electron Nuclear Double Resonance spectroscopy (ENDOR). These studies are currently under investigation in our laboratory in cooperation with Professor Babcock and his group.⁷¹

V. C. Magnetic Susceptibility:

The magnetic susceptibility (χ) of a sample is an important piece of information in understanding the interactions between unpaired electrons. Since the alkalides all have an ns^2 electronic ground state, they would be expected to have a diamagnetic behavior⁷². The small doping of electrons seen by EPR methods would probably give rise to a small Curie tail, but not much information could be gained. Therefore, only the electride, $Li^+(PMPCY) \cdot e^-$, has been investigated by using magnetic susceptibility. In order to obtain the susceptibility of the "pure" electride, the contributions from the bucket and other impurities (possibly from partial decomposition) must be removed. Landers et al.⁷³ devised a method to subtract the bulk diamagnetic contributions by allowing the sample to decompose after the susceptibility measurements on the "live" sample had been made. The susceptibility of the decomposition products could then be measured and subtracted from the original data. This removes all

contributions to the susceptibility except those due to the unpaired electrons.

The susceptibility of a pure paramagnetic material has been found to be inversely proportional to the temperature and can be related by a proportionality constant [C; the Curie constant]. When the material has 100 % of its spins unpaired in the state $S = 1/2$ and in the absence of orbital angular momentum of the electrons, $C = 0.3760$. This "law" was modified to include mean field effects generated by ferromagnetic and antiferromagnetic materials above their transition temperatures. The resultant relationship is given by Equation 5;

$$\chi = \frac{C}{T - \theta} \quad 5$$

where C is the Curie constant and θ is the Weiss constant. To reflect the possibility that a mole of compound may not contain a mole of unpaired electrons, C in equation 5 should be replaced by fC in which f is the fraction of electrons that are unpaired. This law is then called the Curie-Weiss law. The high temperature susceptibility may then be used to predict whether a material has a tendency to be ferromagnetic ($\theta > 0$), paramagnetic ($\theta = 0$), or antiferromagnetic ($\theta < 0$). In a true antiferromagnetic sample, a characteristic feature of a plot of χ vs T is a cusp at a temperature $T = T_N$, where T_N is called the Néel or ordering

temperature. Below the Néel temperature, the electronic spins tend to be aligned in an antiparallel arrangement and are completely ordered at $T = 0$. This ordering temperature may be approximated by $T_N = -\theta$. Below the Néel temperature, the components of the spin axis which are parallel and perpendicular to the applied magnetic field will be different. The perpendicular component (in the limit $T \rightarrow 0$) $\chi_{\perp} = 1/\mu$, where μ is the magnetic moment, and the parallel component $\chi_{\parallel} = 0$. The susceptibility of a random powder will therefore level off at $2/3$ of the maximum value at T_N .

V. C.1. Li⁺(PMPCY).e⁻:

The temperature dependent susceptibility was measured for Li⁺(PMPCY).e⁻ up to 300 K with an applied magnetic field of 3 kG (Figure 21). This compound exhibits antiferromagnetic behavior with a Néel temperature of 35 K. The susceptibility levels off at about 75 % of the maximum value rather than 67 %; however, this could be due to the rounding of χ at the maximum. One interesting feature of the spectrum is a sharp drop in susceptibility at ~ 190 K. This is the same temperature region as the unusual endothermic transition observed in the DSC trace (195 K). As with the DSC spectrum, this transition is reversible and reproducible.

In order that we might understand the interactions more clearly, we will examine the spectrum from a different perspective. If we invert and rearrange Equation 5, we obtain Equation 6.

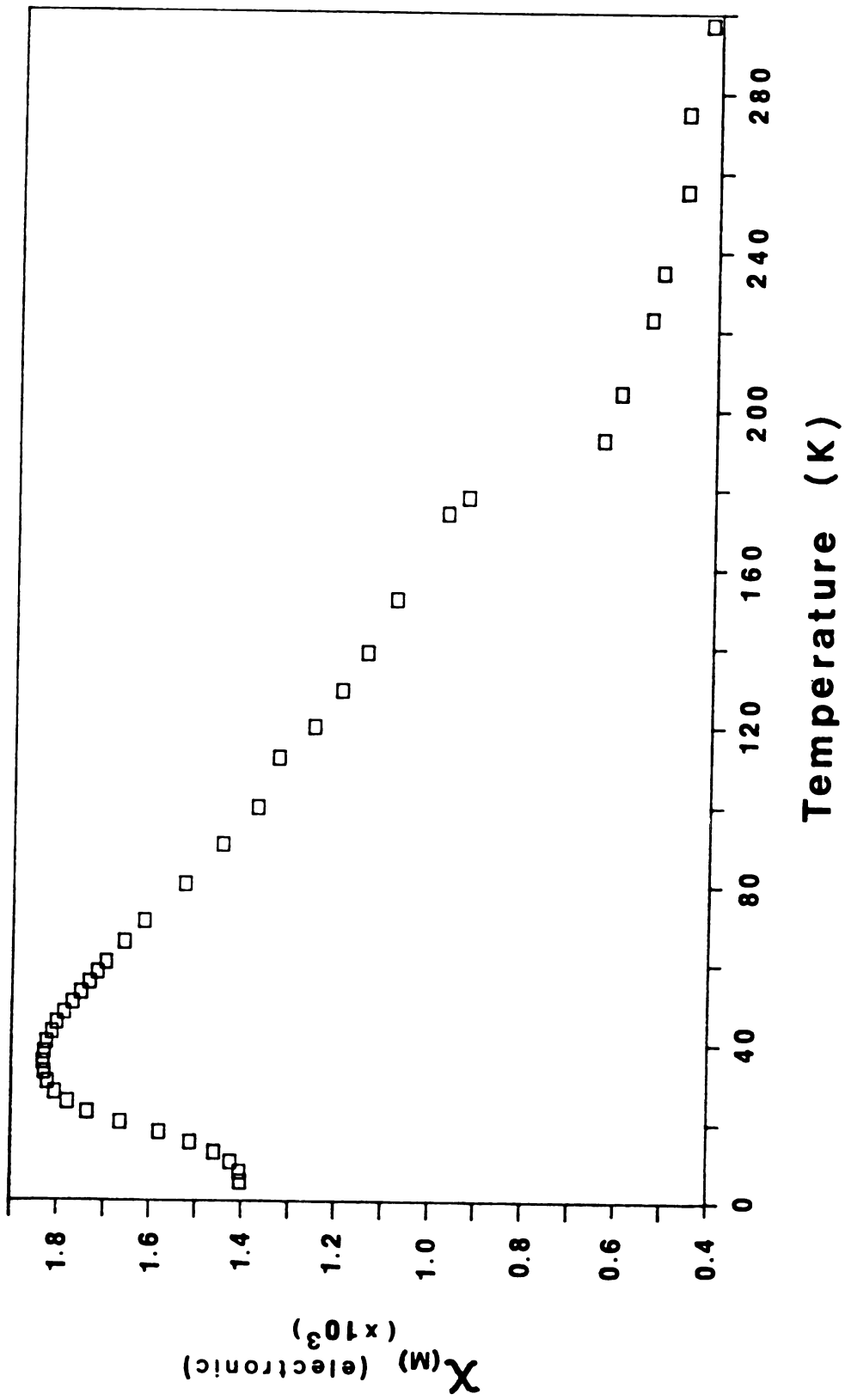


Figure 21. Plot of the molar susceptibility of $\text{Li}^+(\text{PMPCY})\cdot\text{e}^-$ as a function of temperature in a 3 kG magnetic field.

$$\frac{1}{\chi} = \frac{1}{fC} T - \frac{\theta}{fC} \quad 6$$

By plotting $1/\chi$ vs T , the value of f can be obtained from the slope and the Weiss constant can be obtained from the intercept of the line. This plot is shown in Figure 22. An interesting feature of this curve is that 2 separate straight line regions are obtained, one between the Néel temperature and the transition temperature, R_1 , and a second above the transition temperature, R_2 . Clearly, these two regions must be treated individually. From Equation 6, values of $fC = 0.237$ and $fC = 0.120$ are obtained for R_1 and R_2 respectively. These correspond to a value of ~65 % unpaired spins for R_1 and ~32 % unpaired spins for R_2 . Similarly, the Weiss constant may be obtained from the intercept of each line. Region 1 has an intercept on the y-axis of 290 giving a Weiss constant of $\theta = -68$. Region 2 has an intercept on the y-axis of ~ 0 to give a corresponding Weiss constant of 0.

The values obtained for both regions have some uncertainty since there were few points to fit with each line. For Region 1, Curie law behavior is not generally considered valid until the temperature reaches about $4 T_N$ or 140 K, and would cease at the transition. Region 2 was limited by the upper limit in temperature. A more careful temperature study should be performed with a larger number of points taken, which might change the values slightly. However, using the values obtained as rough

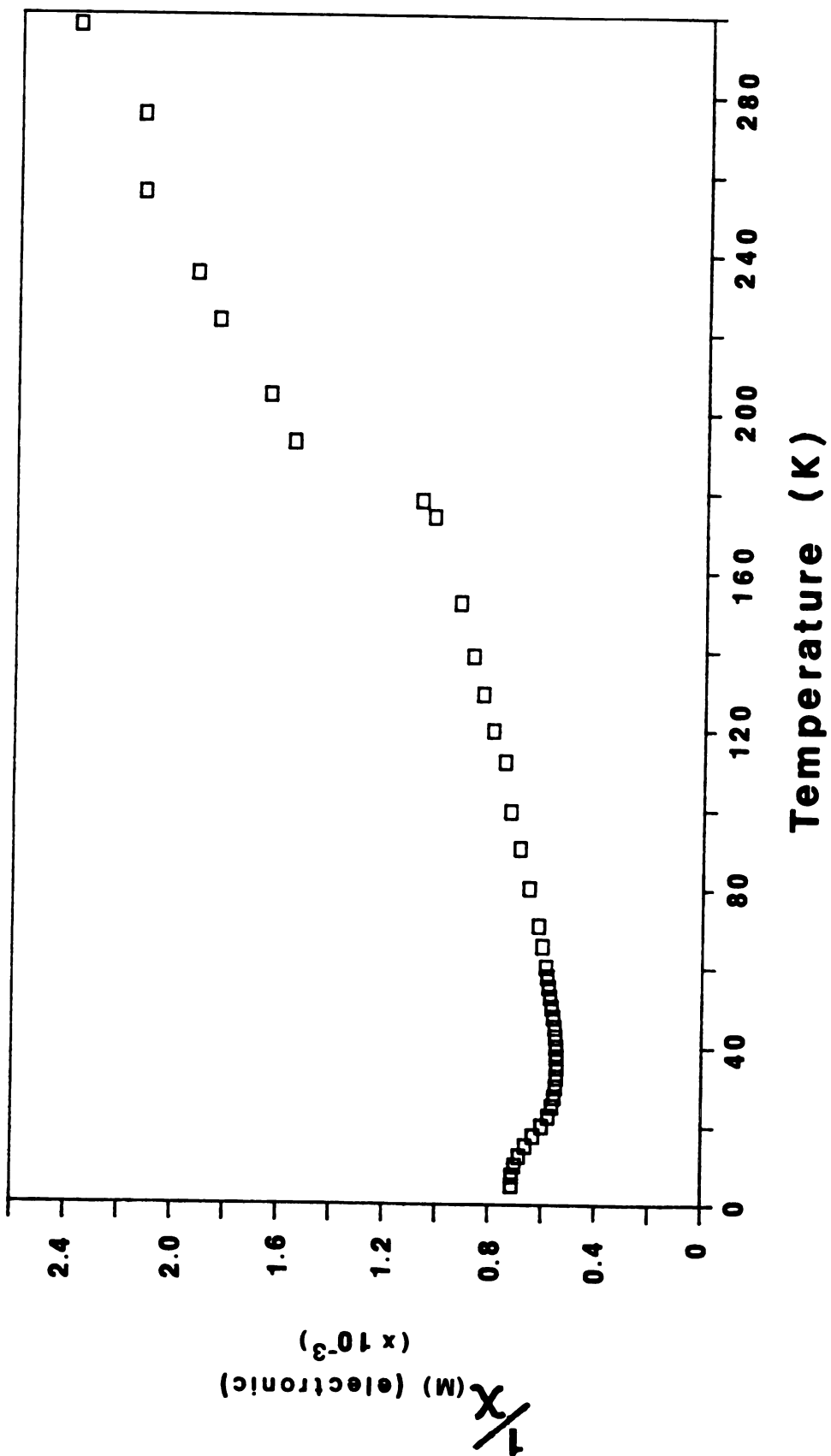


Figure 22. Plot of $1/\chi$ as a function of temperature. There are two noticeably different behaviors above and below the transition at ~ 190 K.

estimates, some general conclusions can be reached. Recalling the previous "rules" relating θ to the expected magnetic behavior, in region 1 the sample behaves as an antiferromagnet while in region 2 it behaves as a paramagnet. From the observed change in the "Curie constant" and the Weiss constant, there appears to be an interesting reorganization of the crystal lattice at the transition temperature which allows a greater pairing of the electrons. Interestingly, pressed powder conductivity measurements indicate an increased conductivity and a smaller band gap above the transition temperature.⁵⁹ This shows that the electrons can move more freely through the lattice. The structure of $\text{Li}^+(\text{PMPCY})\cdot\text{e}^-$ has not yet been determined, so the exact nature of the lattice transformation is not known. A remaining puzzle is the low value of f in each region and its constancy at various temperatures. Clearly, more work needs to be done to understand this system.

V. D. Summary:

The magnetic properties have helped to confirm the identities of the species present in the compounds studied. Further, the MAS-NMR and magnetic susceptibility studies on $\text{Li}^+(\text{PMPCY})\cdot\text{e}^-$ indicate that the transition occurring at ~ 190 K is a result of a lattice transformation. The interactions of the unbound electrons appear to be affected, rather than the environment of the lithium with respect to the PMPCY. The initial assumption that the PMPCY ring was somehow "twisting" around the lithium cation is not valid.

The MAS-NMR results for the three HMCY sodides show that the cations and anions retain their respective characters, even though they appear to be in contact. The EPR spectra give us some clues as to the location of the trapped electrons. The evidence suggests that e^- replaces Na^- in an anionic site, coupling to the cation but not directly to the protons surrounding the cavity.

VI STRUCTURE DETERMINATION

VI. A. Introduction:

Single crystal X-ray diffraction is the ultimate method of determining the identity and stoichiometry of a compound. As an example, a compound thought to be the electride $\text{Cs}^+(\text{C}_{222})\cdot\text{e}^-$,⁷⁵ was proven to be a ceside, $\text{Cs}^+(\text{C}_{222})\cdot\text{Cs}^-$,⁷⁴ by single crystal structure determination. Although the electron density due to the electrons in the electride is so diffuse that it is hidden in the background, the absence of significant electron density in some regions can be informative. It is believed that these "holes" are sites at which the electron is "trapped". With alkalides and electrides, the structure also helps one understand the electronic, magnetic, optical, and thermal properties of these unique solid state materials. It may also help to predict certain properties, such as how to increase thermal stability, by understanding the nature of the complexation of new ligand types. From an understanding of cation-ligand and cation-anion interactions, we may be able to "modify" the ligand to increase complexation of the cation. This might then overcome the decomplexation problems which currently plague the amine-based alkalides.

VI. B. Experimental:

The factor that limits crystal structure determinations of alkalides and electrides is the difficulty of growing suitable single crystals. Single crystals can sometimes be obtained from the initial synthesis, but usually the sample must be recrystallized. The two most successful recrystallization methods used in the study of alkalides and electrides are slow temperature scanning and slow solvent evaporation. The crystals used in this study were all grown by the second method. Polycrystalline samples, synthesized by the methods described in Chapter 2, were loaded into one chamber of a two-chamber apparatus used for crystal growing. Dimethyl ether was then added to dissolve the material and the solution was filtered through a sintered glass frit, after which the less polar solvent, trimethylamine, was added. The solution was then cooled to $-78\text{ }^{\circ}\text{C}$ and all the solvent was removed by slow evaporation (~ 6 hrs.).

In order to select a good single crystal, the solvent-free sample was transferred onto a cold copper block kept at $-45\text{ }^{\circ}\text{C}$ in a nitrogen-filled glove bag. The crystals were then covered with cold, purified n-octane to protect them from the atmosphere of the glove bag long enough for a well formed crystal to be selected by microscopic examination. Once a suitable crystal had been found, it was mounted on the end of a glass fiber with Celvacene (medium) high vacuum grease and transferred under a stream of cold nitrogen gas ($-60\text{ }^{\circ}\text{C}$) to a Nicolet P3F computer-controlled 4-circle diffractometer that used graphite-monochromatized $\text{MoK}\alpha$ radiation ($\lambda = 0.71073\text{ \AA}$). The crystal was kept under a cold nitrogen

stream throughout the entire data collection with a locally modified Nicolet LT-1 low temperature system to prevent thermal decomposition or oxidation. A more complete description of the procedure used to select and mount a crystal is given by Dawes.⁷⁶

VI. C. X-Ray Data Collection

VI. C. 1. $K^+(HMHCY) \cdot Na^-$: 41,54,77

Preliminary examination of the bronze, irregularly-shaped crystal as well as the subsequent data collection were performed with the crystal kept at or below -67°C . Due to its irregular shape, the dimensions of the crystal were not obtained.

The unit cell constants and an orientation matrix for the data collection were obtained by least squares refinement from the setting angles of 16 reflections in the range $7.5 < \theta < 10^\circ$. The orthorhombic primitive cell constants are $a = 11.091(3)$, $b = 11.172(4)$, and $c = 22.531(7)$ for a calculated cell volume of $2791.8(14) \text{ \AA}^3$. With a formula weight of 404.67 and $Z = 4$, the calculated density is then 0.96 g/cm^3 . From the systematic absences of reflections and from least squares refinement, the space group was determined to be $P2_12_12_1$ (#19 in the International Tables⁷⁸).

The intensity data were collected by using the θ - 2θ scanning technique at $4^\circ/\text{min}$ (in 2θ) up to $\sin\theta/\lambda = 0.5385 \text{ \AA}^{-1}$, ($2\theta = 45^\circ$). A total of 6405 reflections (2094 unique) were recorded. Three monitor reflections (measured every 93 reflections) indicated that there was negligible decay of the crystal during the data

collection. Therefore, a decay correction was not employed. With a data cut-off of $I > 3\sigma(I)$, there were 1222 observed and 872 unobserved (unmeasurably weak but not systematic absences) data points. The structure was solved by using the Patterson method. Full-matrix least squares refinement was on $F(I^{1/2})$. The non-H-atoms were refined anisotropically while the H-atoms were constrained to ride on their bonded C-atoms with fixed isotropic thermal parameters.

After the final cycle of refinement, the maximum shift/error ratio [the shift in a parameter divided by the standard deviation in the measurement] $(\delta/\sigma) = 0.03$, and $R = 0.045$; where R is defined by Equation 7.⁷⁹

$$R = \frac{\sum | |F_o| - |F_c| |}{\sum |F_o|} \quad 7$$

F_o is the observed structure factor and F_c is the structure factor calculated from the refined structure. R then compares how well the calculated model fits the measured data. The final difference map peak heights ranged from $-0.20(4)$ to $0.22(4) \text{ e \AA}^{-3}$. The molecular structure and numbering of the atoms are shown in Figure 23 A; and the stereopacking diagram is shown in Figure 23 B. The positional parameters, bond distances, and bond angles are given in Appendix A; Tables A1, A4, and A5 respectively.

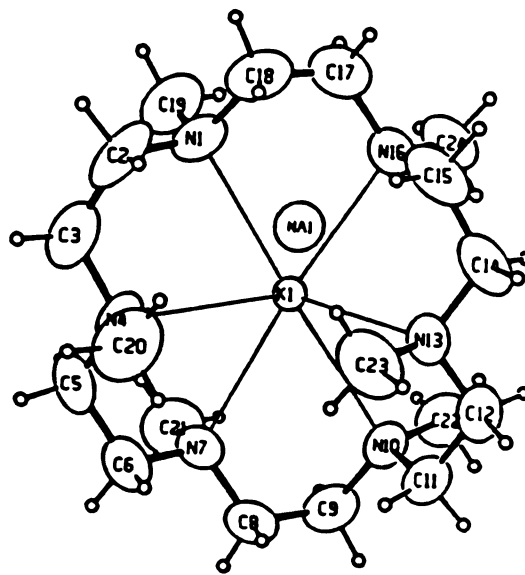
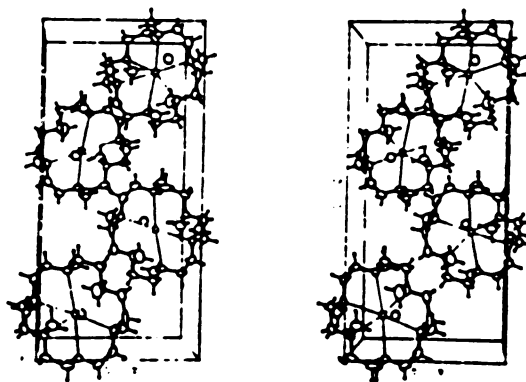
**A****B**

Figure 23. A) The molecular structure and the numbering of the atoms; and B) stereographic packing diagram of $K^+(HMHCY) \cdot Na^-$.

VI. C. 2. $\text{Cs}^+(\text{HMICY})\cdot\text{Na}^-$: 54,77

Preliminary examination of the copper colored crystal and data collection were performed with the sample kept at ~ -75 °C. This crystal appeared to be prism shaped and had approximate dimensions of $0.20 \times 0.28 \times 0.45$ mm.

The unit cell and an orientation matrix for the data collection were determined by least squares refinement from the setting angles of 12 reflections in the range $7.5 < \theta < 10^\circ$. The orthorhombic primitive cell constants are $a = 11.021(4)$, $b = 11.411(4)$, and $c = 22.886(6)$ Å. These yield a calculated cell volume of $2878.2(14)$ Å³. With a formula weight of 498.47 g/mole and $Z = 4$, the calculated density of this sodide is 1.15 g/cm³. From the systematic absences of reflections and least squares refinement, the space group was determined to be $P2_12_12_1$, isostructural with $\text{K}^+(\text{HMICY})\cdot\text{Na}^-$.

The intensity data were also collected by using θ - 2θ scanning techniques at $4^\circ/\text{min}$ (in 2θ), to $\sin\theta/\lambda = 0.7035 \text{ \AA}^{-1}$, ($2\theta = 60^\circ$). A total of 4726 reflections (4696 unique) were recorded. In this case, the three monitor reflections decreased by an average of 0.6% in intensity. It was therefore necessary to employ a linear decay correction. With a data cut-off of $I > 3\sigma(I)$, there were 2996 observed and 1700 unobserved data points. This structure was solved by using the coordinates of the $\text{K}^+(\text{HMICY})\cdot\text{Na}^-$ structure as initial values for full-matrix least squares refinement on F. The non-H-atoms were refined anisotropically while the H-atoms were constrained to ride on their bonded C-atoms with fixed isotropic thermal parameters.

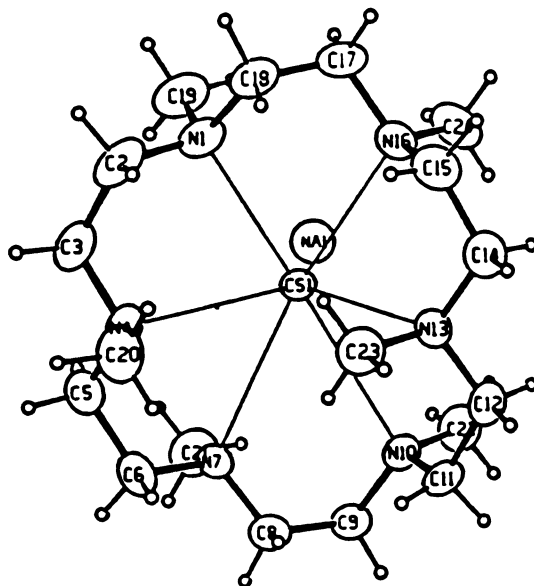
After the final cycle of refinement, the maximum shift/error ratio $(\delta/\sigma) = 0.07$ and $R = 0.033$. The final difference map peak heights ranged from $-0.37(7)$ to $0.61(7)$ $e \text{ \AA}^{-3}$. The molecular structure and numbering of the atoms are shown in Figure 24 A; the stereo-graphic packing diagram is shown in Figure 24 B. The positional parameters, bond distances, and bond angles are given in Appendix A in Tables A3, A4, and A5 respectively.

VI. C. 3. $\text{Rb}^+(\text{HMHCY})\cdot\text{Na}^-$:⁷⁷

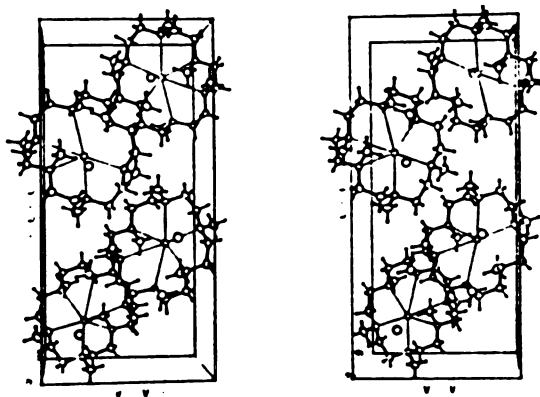
Preliminary examination of the bronze colored crystal and data collection were performed with the sample kept at ~ -87 °C. This crystal appeared rod-shaped and had approximate dimensions of $0.18 \times 0.25 \times 0.40$ mm.

The unit cell and orientation matrix for the data collection were determined by least squares refinement from the setting angles of 13 reflections in the range of $6.5 < \theta < 10^\circ$. The orthorhombic primitive cell constants are $a = 11.075(4)$, $b = 11.227(6)$, and $c = 22.781(10)$ Å for a calculated cell volume of $2832.6(3.8)$ Å³. With a formula weight of 451.12 g/mole and $Z = 4$, the calculated density of this sodide is 1.06 g/cm³. From the systematic absences of reflections and least squares refinement, the space group was determined to be $P2_12_12_1$; isostructural with $\text{K}^+(\text{HMHCY})\cdot\text{Na}^-$ and $\text{Cs}^+(\text{HMHCY})\cdot\text{Na}^-$.

The intensity data were collected by using an Omega scanning technique at $4^\circ/\text{min}$ (in 2θ), to $\sin\theta/\lambda = 0.5385 \text{ \AA}^{-1}$, ($2\theta = 45^\circ$). The θ - 2θ method could not be used in this case, as the poor quality of the crystal caused a broadening of the scattering



A



B

Figure 24. A) The molecular structure and the numbering of the atoms; and B) Stereographic packing diagram of $\text{Cs}^+(\text{HMHCY})\text{Na}^-$.

profile. A total of 4037 reflections (2121 unique) were recorded. The three monitor reflections indicated that there was negligible decay of the crystal during the data collection. Therefore, it was not necessary to employ a decay correction. With a data cut-off of $I > 3\sigma(I)$, there are only 984 observed and 1137 unobserved data points. An attempt was made to solve the structure by least squares refinement on F using the coordinates from the $K^+(HMHCY)\cdot Na^-$ structure as initial values, but the coordinates did not refine. The Patterson method was then employed to solve the structure. Full-matrix least squares refinement was employed on F with non-H-atoms refined anisotropically, while the H-atoms were constrained to ride on their bonded C-atoms with fixed isotropic thermal parameters.

After the final cycle of refinement, the maximum shift/error ratio (δ/σ) = 0.09 and $R = 0.037$. The final difference map peak heights ranged from $-0.27(6)$ to $0.2(1)$ e A.⁻³ The molecular structure and numbering of the atoms are shown in Figure 25 A; and the stereo-packing diagram is shown in Figure 25 B. The positional parameters, bond distances, and bond angles are given in Appendix A; Tables A2, A4, and A5 respectively.

VI. D. Discussion:

The cell constants for the three sodides are summarized in Table 8. Qualitatively, the HMHCY ring [1,4,7,10,13,16-hexaaza-1,4,7,10,13,16-hexamethyl-cyclooctadecane] forms a "cup" around the alkali cation. Nitrogens 1,7,10,16 are in the ring, coplanar within ± 0.09 Å for $K^+(HMHCY)\cdot Na^-$ (I), ± 0.06 Å for $Rb^+(HMHCY)\cdot Na^-$

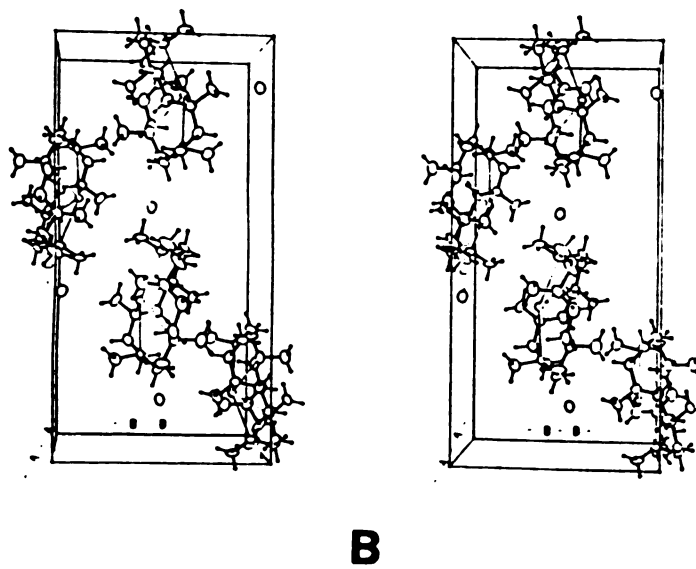
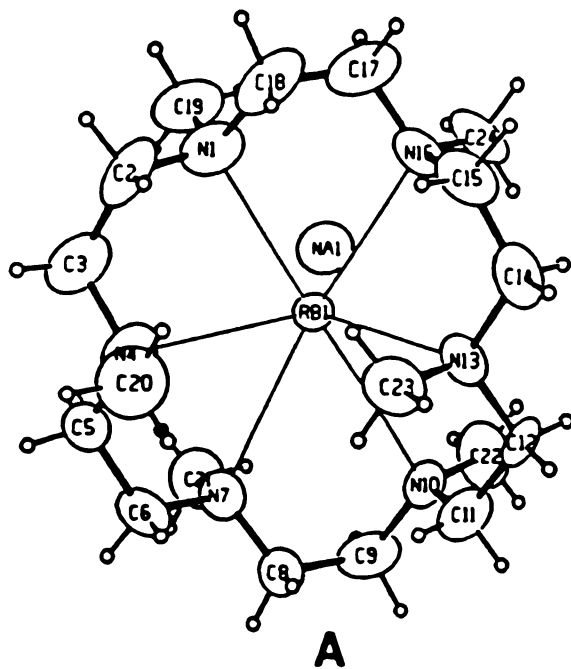


Figure 25. A) The molecular structure and the numbering of the atoms; and B) Stereographic packing diagram of $\text{Rb}^+(\text{HMHCY}) \text{Na}^-$.

Table 8. Summary of Cell Constants For $K^+(HMICY) \cdot Na^-$ (I),
 $Rb^+(HMICY) \cdot Na^-$ (II), and $Cs^+(HMICY) \cdot Na^-$ (III).

	$K^+(HMICY) \cdot Na^-$ (I)	$Rb^+(HMICY) \cdot Na^-$ (II)	$Cs^+(HMICY) \cdot Na^-$ (III)
a =	11.091(3) Å	11.075(4) Å	11.021(4) Å
b =	11.172(4) Å	11.227(6) Å	11.411(4) Å
c =	22.531(7) Å	22.781(10) Å	22.886(6) Å
V =	2791.8(14) Å ³	2832.6(38) Å ³	2878.2(14) Å ³
d =	0.96 g/cm ³	1.06 g/cm ³	1.15 g/cm ³
R =	4.5 %	3.7 %	3.3 %

(II), and ± 0.03 Å for $\text{Cs}^+(\text{HMHCY})\cdot\text{Na}^-$ (III) with the corresponding methyl groups forming a cage around the cation. Nitrogens 4 and 13 are below the plane 1.27 and 1.63 Å for I, 1.12 and 1.51 Å for II, and 1.14 and 1.43 Å for III, with the methyl groups effectively closing off the bottom of the ring. The cation is located 0.29 Å, 0.59 Å, and 0.91 Å above the center of the plane for I, II, and III respectively. The cations are coordinated to all six nitrogens with K-N distances ranging from 2.903(6) to 3.014(6) Å for I, Rb-N distances ranging from 3.014(10) to 3.170(11) Å for II, and Cs-N distances ranging from 3.157(6) to 3.333(6) Å for III. The sodide anion is 4.280(3) Å from the potassium cation in I, 4.202(10) Å from the rubidium cation in II, and 4.254(3) Å from the cesium cation in III. The planar arrangement is shown in Figure 26 with the associated values given in Table 9. The example of a "molecule" shown in Figure 27, which was obtained from a computer generation of the structure of $\text{Cs}^+(\text{HMHCY})\cdot\text{Na}^-$ shows the nature of the $\text{Cs}^+\text{-Na}^-$ ion pair. The structures of $\text{K}^+(\text{HMHCY})\cdot\text{Na}^-$ and $\text{Rb}^+(\text{HMHCY})\cdot\text{Na}^-$ would be similar. At first glance, it might seem unusual that the a cell edge gets smaller with increasing cation size. However, the concept of the plane with its associated atomic distances allows one to understand the slight collapse. The larger cation must be farther above the center of the HMHCY molecule as a result of size constraints. This requires N4 and N13 to move closer to the plane in order that they might still interact strongly with the cation. As they move up, the ring is pinched in one direction (the a - axis) and thereby expanded along the perpendicular axis (the c -

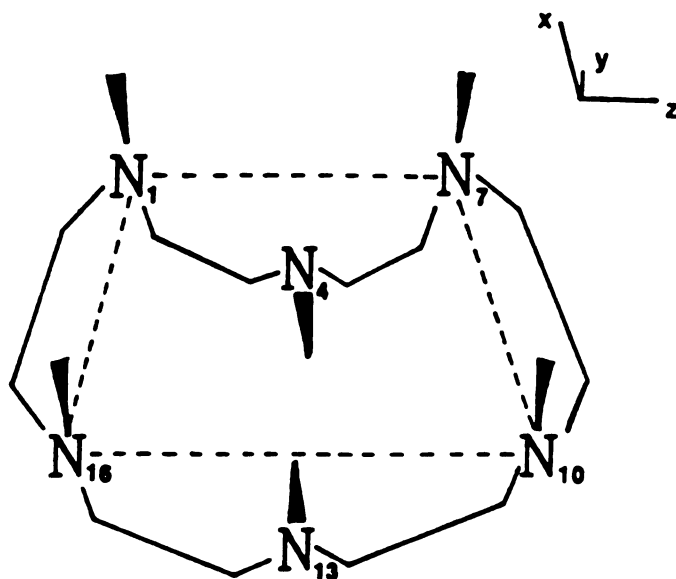


Figure 26. Diagram of plane through the nitrogens 1,7,10,16.

The axes are only approximate.

Table 9. Summary of Atomic Distances With Respect to the Plane in Figure 26.

	$K^+(HMICY) \cdot Na^-$	$Rb^+(HMICY) \cdot Na^-$	$Cs^+(HMICY) \cdot Na^-$
N-1,7,10,16 planar	$\pm 0.09 \text{ \AA}$	$\pm 0.06 \text{ \AA}$	$\pm 0.03 \text{ \AA}$
N-4 below plane	1.27 \AA	1.12 \AA	1.14 \AA
N-13 below plane	1.63 \AA	1.51 \AA	1.43 \AA
cation above plane	0.29 \AA	0.59 \AA	0.91 \AA
sodide from cation	4.28 \AA	4.20 \AA	4.25 \AA

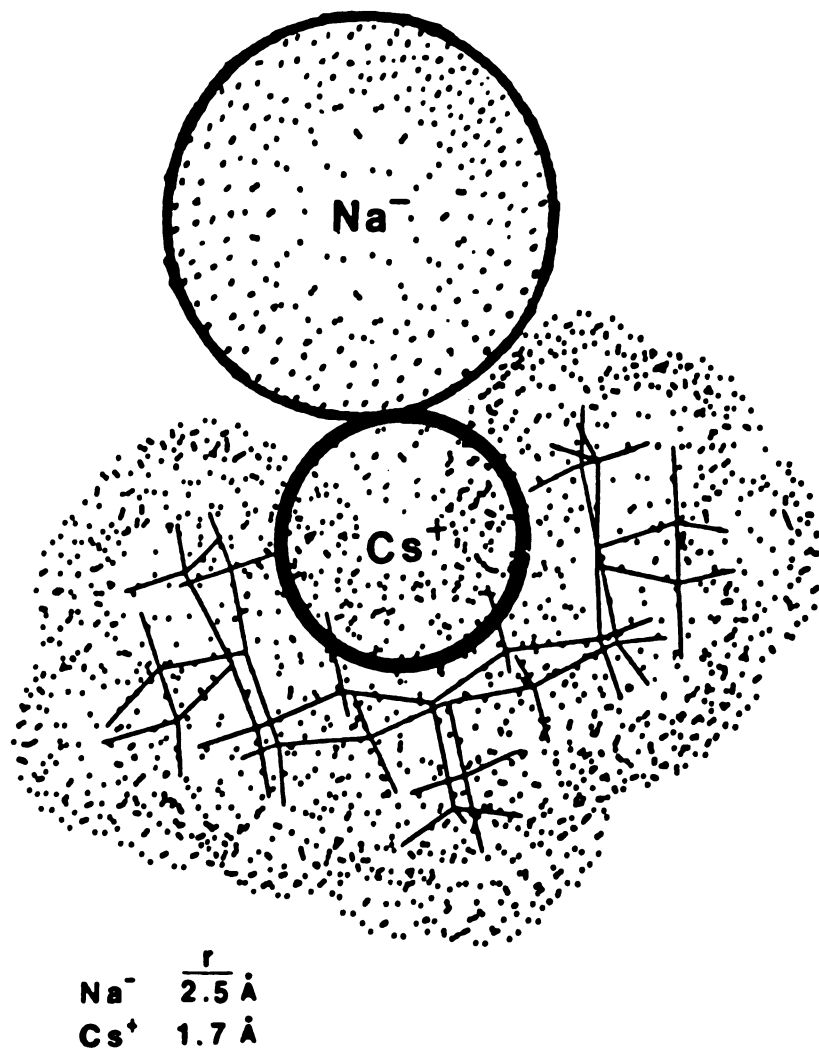


Figure 27. Computer simulation of one "Molecule" of $\text{Cs}^+(\text{HMICY})\cdot\text{Na}^-$. Generated on an Evens & Sutherland PS350 system with the program FRODO. [$\text{K}^+(\text{HMICY})\cdot\text{Na}^-$ and $\text{Rb}^+(\text{HMICY})\cdot\text{Na}^-$ appear similar].

axis).

The most unusual feature of these molecular structures is the close cation-anion distances, especially in $\text{Cs}^+(\text{HMHCY})\cdot\text{Na}^-$. Taking the effective radii of K^+ , Rb^+ , and Cs^+ to be 1.33 Å, 1.49 Å, and 1.69 Å respectively,⁸⁰ and the effective radius of Na^- to be between 2.50 and 2.70 Å (determined from the anionic cavity size in other sodides^{2,81}) the separation between the van der Waals surfaces of the cation and anion is between 0.25 and 0.45 Å for I, between 0.02 and 0.22 Å for II, and between -0.13 and 0.07 Å for III. This is the first evidence for contact ion pairs between alkali metal cations and alkali metal anions in alkalides. It is interesting that similar close contacts are observed in the rubidide $\text{Rb}^+(\text{18C6})\cdot\text{Rb}^-$.⁸²

It is remarkable that, in spite of the close proximity of the oppositely charged ions, the optical and NMR properties of Na^- show no evidence of appreciable charge transfer to the cation; that is, the properties are the same as for other sodides in which Na^- is well isolated from the cation. The absence of an NMR signal for ^{133}Cs , however, may be due to a strong perturbation of the p-electrons in Cs^+ as a result of this close proximity to Na^- .

In the unit cell, the molecules are ordered in a staggered arrangement to give a distorted octahedral coordination between the complexed cation and the sodium anions. The distances between K^+ and the six nearest Na^- neighbors are 4.28 Å for the "ion-pair" and from 6.99 to 8.31 Å for the next five closest neighbors in I. The distances between Rb^+ and the nearest six Na^- neighbors are 4.21 Å for the "ion-pair" and from 7.12 to 8.49 Å for the next

five closest neighbors in II. The distances between Cs^+ and the nearest six Na^- neighbors are 4.26 Å for the "ion-pair" and from 7.23 to 8.63 Å for the next five closest neighbors in III. Also, the sodium anions are effectively shielded from one another by the large complexed cations. The distances between Na^- and the six nearest neighboring anions range from 8.66 to 9.94 Å for I, from 8.88 to 9.88 Å for II, and from 9.94 to 10.00 Å for III. Two views of the packing are shown in Figure 28 [these views are for $\text{K}^+(\text{HMHCY})\cdot\text{Na}^-$; however, $\text{Rb}^+(\text{HMHCY})\cdot\text{Na}^-$ and $\text{Cs}^+(\text{HMHCY})\cdot\text{Na}^-$ would appear the same except for small dimensional changes].

VI. E. FMPCY Compounds:

We also wished to obtain the crystal structures of $\text{Li}^+(\text{FMPCY})\cdot\text{Na}^-$ (IV) and $\text{Li}^+(\text{FMPCY})\cdot\text{e}^-$ (V) in order that we might better understand the peculiar magnetic properties of the electride and the nature of the apparent phase change which occurs in each species. However; several attempts to grow single crystals of each compound, by both slow solvent evaporation and slow cooling, were unsuccessful. Compound IV tended to form golden flakes similar to metal filings, while compound V always ended up as a black powder. It is possible that the use of different solvents or a combination of solvents might yield suitable crystals, and this should be explored in the future.

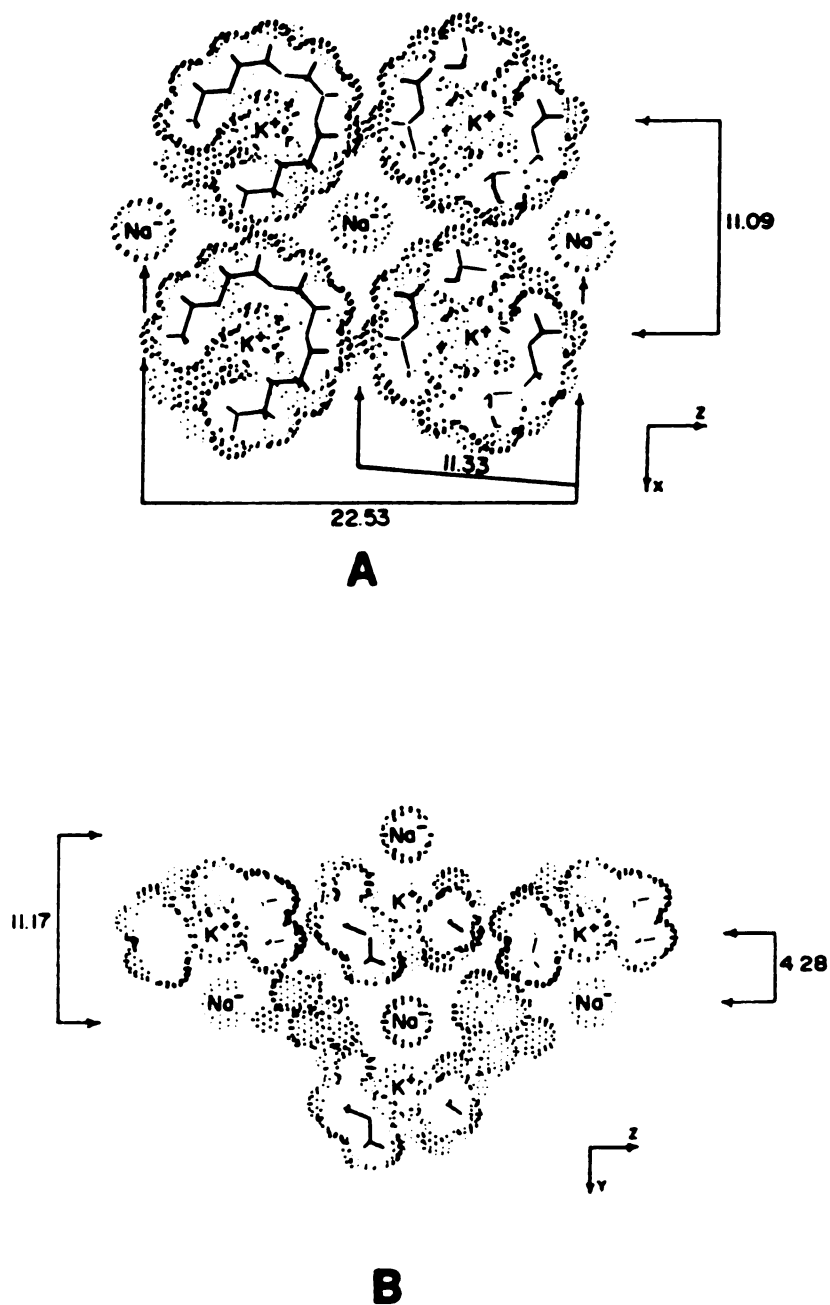


Figure 28. Two cutaway views of the cation-anion packing in $K^+(HMHCY) Na^-$. A) View down the y -axis; B) View down the x -axis. Distances are in Angstroms. The Na^- is not drawn to scale. The structures of $Rb^+(HMHCY) Na^-$ and $Cs^+(HMHCY) Na^-$ are similar.

VII CONCLUSIONS

The pursuit of thermally stable alkalides and electrides via the aza-crown complexants has not only yielded promise of success, but has also provided some interesting new compounds. The study of these new alkalides and electrides has provided new insights into the nature and properties of solvent-free trapped electrons and alkali metal anions. These compounds have shown that the complexed cation can be in contact with an alkali metal anion yet not destroy the essential character of either species. Through EPR and ENDOR we have also been able to better understand the nature of the electron trapping as well as how the electron interacts with its surroundings. Probably the most important result of this work is that we have proven that aza-crowns are stable to decomposition in the strong reducing environment of alkalides and electrides. The only drawback to the current aza-complexants is their weak affinity for the alkali metal cations, which causes decomplexation to occur slowly when the temperature is raised. In many cases, decomplexation occurs at room temperatures.

The fact that these compounds are less stable to decomplexation than their oxo-analogs is not too surprising. Studies have shown that the effect of substituting N-CH₃ for O in crown ethers decreases the stability of the complex by a factor of 10 for each substitution.⁸³ This results from the lower dipole moment or donicity of the amine group. Some good does come out of

this "problem" however. This is probably what enables us to synthesize a compound with barium when all other attempts that used ethers had failed. We must now try to find amine-based complexants which can compensate for the lower affinity, yet still form stable alkalides and electrides. Studies are currently in progress in our laboratories, in cooperation with Professor Farnum, to acquire "hinged" sandwich complexes or fully methylated aza-cryptands. This should yield a more stable complex by encapsulating the cation. It has been shown that macrobicyclic ligands (cryptands) increase the stability of metal complexes by enthalpic stabilization³⁴. This process is designated as the cryptate effect. The same stability considerations should apply to the "hinged" complexants.

VII. A. Designing New Complexants:

In the design of new complexing agents, certain factors which influence the stability and selectivity must be considered. The first consideration is the donor atom type or types. There is a limitation in this respect when working with alkalides and electrides. For the alkali and alkaline earth metals, the oxygen donors are the most favorable, while the amine donors are better suited for metals such as Cu^{2+} , Co^{2+} , Ni^{2+} , etc.⁸³. However, as mentioned in Chapter One of this Dissertation, the ether links are more susceptible to reduction. Therefore, we must settle for the less favorable amine compounds and try to maximize the other variables. A second consideration is the length of the bridging groups. Izatt et.al.⁸⁴ have shown that by alternating ethano and

propano or by using only propano groups, strong stability losses occur compared with the ethano-crowns. This is presumably a result of partial diversion of the dipole ends away from the center of the cavity. As an example, replacing one ethano group in 18-Crown-6 with a propano group (19-Crown-6) reduces the complexation constant by 50 %.⁸⁴ The failure of all attempts to synthesize alkalides with tetramethyl cyclam (N4-14-Crown-4) is probably due to this effect. A third consideration is the overall size of the ligand. The most stable complexes are formed when the ligand cavity closely matches the cation size. This effect is not as critical, since macrocycles are not completely rigid. Most of them are quite flexible and capable of orienting their donor groups in space. Larger macrocycles are free to fold, resulting in variable 3-dimensional cavities. However, this factor should not be ignored since we already have "one strike" against us in using the amines.

In conclusion, the ability to synthesize thermally stable alkalides and, more importantly, electriles is just around the corner. The limiting factor is in maximizing the complexation strength of the ligand by adjusting several parameters. We require a complexant that will complex and stabilize the cation, yet not be easily reduced by the strongest known reducing agents. The wide variety of optical, magnetic, and electron emission properties of electriles might make them useful in device applications if the problem of stability can be overcome. This work appears to be a step in the right direction.

APPENDIX

APPENDIX A

Positional parameters, bond distances, and bond angles
for $K^+(HMHCY) \cdot Na^-$ (I), $Rb^+(HMHCY) \cdot Na^-$ (II), and $Cs^+(HMHCY) \cdot Na^-$

Table

- A1. Positional parameters and their estimated standard deviations for $K^+(HMHCY) \cdot Na^-$ (I).
- A2. Positional parameters and their estimated standard deviations for $Rb^+(HMHCY) \cdot Na^-$ (II).
- A3. Positional parameters and their estimated standard deviations for $Cs^+(HMHCY) \cdot Na^-$ (III).
- A4. Bond distances for $K^+(HMHCY) \cdot Na^-$ (I), $Rb^+(HMHCY) \cdot Na^-$ (II), and $Cs^+(HMHCY) \cdot Na^-$ (III).
- A5. Bond angles for $K^+(HMHCY) \cdot Na^-$ (I), $Rb^+(HMHCY) \cdot Na^-$ (II), and $Cs^+(HMHCY) \cdot Na^-$ (III).

The parameters for the hydrogen atoms have not been included, as they were constrained to ride on their C-bonded hosts in all three cases.

Table A1. Positional Parameters and Their Estimated Standard
Deviations for $K^+(HMICY) \cdot Na^- (I)$.

Atom	x	y	z	B(A ²)
K1	0.7677(1)	0.5798(1)	0.87093(6)	2.93(3)
Na1	0.7203(3)	0.9527(3)	0.8917(1)	6.90(9)
N1	0.5287(6)	0.5065(6)	0.9129(3)	6.8(2)
N4	0.6097(5)	0.4297(6)	0.7892(3)	5.8(2)
N7	0.8190(5)	0.5798(6)	0.7444(2)	5.3(2)
N10	1.0219(5)	0.6063(5)	0.8335(3)	4.7(2)
N13	0.9497(5)	0.4166(6)	0.9208(2)	5.1(1)
N16	0.7444(7)	0.5057(7)	0.9946(2)	6.5(2)
C2	0.4665(7)	0.4186(8)	0.8736(4)	8.6(3)
C3	0.4859(7)	0.4447(8)	0.8098(4)	8.0(3)
C5	0.6214(8)	0.4774(9)	0.7292(3)	8.2(3)
C6	0.7529(9)	0.4907(8)	0.7099(3)	7.5(2)
C8	0.9458(7)	0.5672(8)	0.7307(3)	6.4(2)
C9	1.0260(8)	0.6402(7)	0.7702(3)	7.1(2)
C11	1.0877(7)	0.4952(7)	0.8431(4)	6.4(2)
C12	1.0741(7)	0.4406(8)	0.9051(3)	6.9(2)
C14	0.9390(8)	0.3963(8)	0.9849(3)	7.4(3)
C15	0.8104(9)	0.3947(8)	1.0068(3)	8.1(3)
C17	0.6179(9)	0.498(1)	1.0109(4)	12.3(4)
C18	0.5380(8)	0.453(1)	0.9734(4)	12.0(4)
C19	0.4632(8)	0.6206(8)	0.9119(4)	9.6(3)
C20	0.6425(9)	0.3025(8)	0.7906(5)	10.1(3)
C21	0.7734(9)	0.7009(7)	0.7304(4)	8.7(3)
C22	1.0722(8)	0.7015(7)	0.8699(4)	7.7(3)
C23	0.9044(9)	0.3155(8)	0.8872(4)	8.8(3)
C24	0.8010(8)	0.6076(8)	1.0245(3)	8.0(3)

Table A2. Positional Parameters and Their Estimated Standard Deviations for $\text{Rb}^+(\text{HMHCY})\cdot\text{Na}^-$ (II).

Atom	x	y	z	B(A ²)
Rb1	0.7621(1)	0.6028(1)	0.87207(5)	3.31(2)
Na1	0.7174(6)	0.9721(5)	0.8939(3)	6.6(2)
N1	0.525(1)	0.498(1)	0.9132(6)	7.1(4)
N4	0.607(1)	0.443(1)	0.7857(6)	6.3(4)
N7	0.8214(9)	0.594(1)	0.7421(5)	4.3(3)
N10	1.0269(9)	0.615(1)	0.8314(5)	4.7(3)
N13	0.952(1)	0.4319(9)	0.9174(4)	4.6(3)
N16	0.740(2)	0.504(1)	0.9945(4)	5.7(3)
C2	0.464(1)	0.420(1)	0.8714(8)	7.6(5)
C3	0.482(1)	0.456(1)	0.8072(7)	6.6(5)
C5	0.621(1)	0.497(2)	0.7281(6)	7.0(5)
C6	0.751(2)	0.510(1)	0.7079(6)	6.2(4)
C8	0.950(1)	0.576(1)	0.7299(6)	5.4(4)
C9	1.031(1)	0.648(1)	0.7689(6)	6.5(5)
C11	1.086(1)	0.503(1)	0.8401(7)	6.3(4)
C12	1.080(1)	0.453(1)	0.9013(6)	5.4(4)
C14	0.939(1)	0.401(2)	0.9797(6)	6.1(4)
C15	0.809(1)	0.390(1)	1.0038(6)	6.5(4)
C17	0.617(2)	0.483(2)	1.0112(8)	10.0(6)
C18	0.536(1)	0.436(2)	0.9698(7)	9.3(5)
C19	0.457(1)	0.609(2)	0.9195(7)	8.1(5)
C20	0.637(2)	0.314(1)	0.7831(8)	8.9(6)
C21	0.781(2)	0.717(1)	0.7295(7)	7.6(5)
C22	1.075(2)	0.712(1)	0.8666(8)	8.2(5)
C23	0.898(1)	0.338(1)	0.8813(7)	6.3(4)
C24	0.793(2)	0.603(2)	1.0262(5)	8.2(5)

Table A3. Positional Parameters and Their Estimated Standard Deviations for $\text{Cs}^+(\text{HMICY})\cdot\text{Na}^-$ (III).

Atom	x	y	z	B(A ²)
Cs1	0.75388(4)	0.63250(3)	0.87396(1)	2.807(4)
Na1	0.7166(3)	1.0010(3)	0.8958(1)	5.40(9)
N1	0.5218(6)	0.4904(6)	0.9134(3)	4.5(1)
N4	0.6059(5)	0.4527(5)	0.7839(3)	3.9(1)
N7	0.8189(5)	0.6101(5)	0.7397(2)	3.3(1)
N10	1.0292(5)	0.6256(5)	0.8277(2)	3.4(1)
N13	0.9470(5)	0.4446(5)	0.9140(2)	3.5(1)
N16	0.7418(8)	0.4993(5)	0.9955(2)	4.2(1)
C2	0.4626(6)	0.4192(7)	0.8687(4)	5.4(2)
C3	0.4798(7)	0.4651(7)	0.8056(4)	4.6(2)
C5	0.6160(8)	0.5144(8)	0.7278(3)	4.8(2)
C6	0.745(1)	0.5284(6)	0.7054(3)	4.7(1)
C8	0.9479(6)	0.5899(7)	0.7272(3)	4.1(2)
C9	1.0352(6)	0.6579(7)	0.7654(3)	4.4(2)
C11	1.0929(7)	0.5146(7)	0.8372(3)	4.1(2)
C12	1.0739(7)	0.4622(7)	0.8973(3)	4.1(2)
C14	0.9395(7)	0.4004(8)	0.9752(3)	4.8(2)
C15	0.8120(7)	0.3908(8)	0.9983(3)	5.2(2)
C17	0.6133(8)	0.4791(9)	1.0132(4)	5.7(2)
C18	0.5369(7)	0.4232(7)	0.9668(3)	4.8(2)
C19	0.4505(8)	0.5975(8)	0.9243(4)	6.0(2)
C20	0.6346(8)	0.3287(6)	0.7761(4)	5.3(2)
C21	0.7845(8)	0.7310(6)	0.7267(3)	5.3(2)
C22	1.0793(7)	0.7184(7)	0.8634(4)	5.4(2)
C23	0.8877(7)	0.3614(6)	0.8745(4)	4.7(1)
C24	0.7938(9)	0.5947(8)	1.0296(3)	6.2(2)

Table A4. Bond Distances (in Angstroms) for $K^+(HMICY) \cdot Na^-$ (I),
 $Rb^+(HMICY) \cdot Na^-$ (II), and $Cs^+(HMICY) \cdot Na^-$ (III).

Atom 1	Atom 2	(I) Distance	(II) Distance	(III) Distance
K,Rb,Cs	Na1	4.280(3)	4.205(10)	4.254(3)
K,Rb,Cs	N1	2.917(6)	3.025(14)	3.160(6)
K,Rb,Cs	N4	3.014(6)	3.170(11)	3.333(6)
K,Rb,Cs	N7	2.907(5)	3.035(10)	3.165(5)
K,Rb,Cs	N10	2.964(6)	3.080(10)	3.215(5)
K,Rb,Cs	N13	2.909(6)	3.026(11)	3.157(6)
K,Rb,Cs	N16	2.903(6)	3.014(10)	3.173(5)
N1	C2	1.491(11)	1.46(2)	1.461(11)
N1	C18	1.493(12)	1.47(2)	1.452(10)
N1	C19	1.468(11)	1.47(2)	1.474(11)
N4	C3	1.459(10)	1.47(2)	1.483(9)
N4	C5	1.459(10)	1.45(2)	1.468(10)
N4	C20	1.466(11)	1.49(2)	1.461(9)
N7	C6	1.460(11)	1.45(2)	1.465(10)
N7	C8	1.447(9)	1.46(2)	1.468(9)
N7	C21	1.479(10)	1.48(2)	1.461(9)
N10	C9	1.478(10)	1.47(2)	1.473(9)
N10	C11	1.456(10)	1.44(2)	1.465(10)
N10	C22	1.454(10)	1.45(2)	1.447(10)
N13	C12	1.450(10)	1.49(2)	1.463(9)
N13	C14	1.466(9)	1.47(2)	1.491(9)
N13	C23	1.451(10)	1.46(2)	1.466(9)
N16	C15	1.466(11)	1.50(2)	1.461(11)
N16	C17	1.452(12)	1.43(2)	1.491(12)
N16	C24	1.465(11)	1.45(2)	1.459(11)

Table A4. Bond distances cont.

Atom 1	Atom 2	(I) Distance	(II) Distance	(III) Distance
C2	C3	1.482(12)	1.53(2)	1.549(12)
C5	C6	1.530(13)	1.52(3)	1.522(14)
C8	C9	1.498(11)	1.51(2)	1.514(10)
C11	C12	1.532(11)	1.50(2)	1.513(11)
C14	C15	1.510(13)	1.55(2)	1.506(11)
C17	C18	1.326(14)	1.41(3)	1.497(12)

Table A5. Bond Angles (in Degrees) for $K^+(HMHCY) \cdot Na^-$ (I),
 $Rb^+(HMHCY) \cdot Na^-$ (II), and $Cs^+(HMHCY) \cdot Na^-$ (III).

<u>Atom1</u>	<u>Atom2</u>	<u>Atom3</u>	(I) <u>Angle</u>	(II) <u>Angle</u>	(III) <u>Angle</u>
Na1	K,Rb,Cs	N1	96.4(2)	104.3()	113.3(1)
Na1	K,Rb,Cs	N4	121.7(1)	124.6()	129.3(1)
Na1	K,Rb,Cs	N7	96.5(1)	100.0()	102.5(1)
Na1	K,Rb,Cs	N10	91.8(1)	95.5()	98.9(1)
Na1	K,Rb,Cs	N13	129.9(1)	131.8()	134.6(1)
Na1	K,Rb,Cs	N16	98.4(2)	104.2()	111.5(1)
N1	K,Rb,Cs	N4	61.9(2)	60.1()	57.7(2)
N1	K,Rb,Cs	N7	120.1(2)	118.5(3)	114.8(2)
N1	K,Rb,Cs	N10	171.1(2)	159.6(4)	147.7(2)
N1	K,Rb,Cs	N13	110.3(2)	104.4(3)	96.6(2)
N1	K,Rb,Cs	N16	62.5(2)	60.0(4)	58.0(2)
N4	K,Rb,Cs	N7	61.7(2)	59.5()	57.4(1)
N4	K,Rb,Cs	N10	116.3(2)	110.9()	104.1(1)
N4	K,Rb,Cs	N13	108.2(2)	103.2()	95.2(1)
N4	K,Rb,Cs	N16	113.0(2)	108.8()	103.1(2)
N7	K,Rb,Cs	N10	62.2(2)	60.1(3)	57.6(1)
N7	K,Rb,Cs	N13	104.8(2)	99.3(3)	94.2(1)
N7	K,Rb,Cs	N16	164.5(2)	155.2(3)	145.3(2)
N10	K,Rb,Cs	N13	61.4(2)	58.1(3)	56.1(2)
N10	K,Rb,Cs	N16	112.9(2)	111.8(4)	108.5(2)
N13	K,Rb,Cs	N16	61.9(2)	60.3(4)	56.5(2)
K,Rb,Cs	N1	C2	113.5(5)	115.5(9)	116.5(5)
K,Rb,Cs	N1	C18	109.8(5)	112.6(9)	114.8(4)
K,Rb,Cs	N1	C19	102.6(5)	98.3(9)	93.1(4)
C2	N1	C18	108.1(7)	109. (1)	110.3(6)
C2	N1	C19	109.5(6)	110. (1)	109.9(6)

Table A5. Bond Angles cont.

<u>Atom1</u>	<u>Atom2</u>	<u>Atom3</u>	(I) <u>Angle</u>	(II) <u>Angle</u>	(III) <u>Angle</u>
C18	N1	C19	113.4(7)	111. (1)	110.9(6)
K,Rb,Cs	N4	C3	106.9(5)	104.2()	101.2(4)
K,Rb,Cs	N4	C5	108.5(5)	105.6()	102.0(4)
K,Rb,Cs	N4	C20	111.4(5)	116.9()	124.5(5)
C3	N4	C5	109.6(6)	111. (1)	108.5(6)
C3	N4	C20	109.8(7)	109. (1)	109.6(6)
C5	N4	C20	110.6(7)	110. (1)	109.9(6)
K,Rb,Cs	N7	C6	114.3(4)	115.3(8)	116.5(4)
K,Rb,Cs	N7	C8	113.4(4)	113.6(7)	114.9(4)
K,Rb,Cs	N7	C21	99.2(4)	95.3(8)	93.6(4)
C6	N7	C8	107.9(6)	110. (1)	109.4(6)
C6	N7	C21	109.8(6)	110. (1)	110.4(6)
C8	N7	C21	112.1(7)	113. (1)	111.1(6)
K,Rb,Cs	N10	C9	109.5(4)	109.6(8)	110.8(4)
K,Rb,Cs	N10	C11	109.5(4)	110.6(9)	115.1(4)
K,Rb,Cs	N10	C22	107.0(4)	102.5(8)	99.0(4)
C9	N10	C11	110.2(6)	110. (1)	109.8(6)
C9	N10	C22	110.2(6)	110. (1)	110.3(6)
C11	N10	C22	110.4(6)	114. (1)	111.5(5)
K,Rb,Cs	N13	C12	117.0(5)	118.5(8)	118.4(4)
K,Rb,Cs	N13	C14	114.8(5)	114.3(8)	117.7(4)
K,Rb,Cs	N13	C23	91.8(5)	88.8(8)	87.7(4)
C12	N13	C14	110.3(6)	112. (1)	110.2(6)
C12	N13	C23	110.2(6)	112. (1)	110.7(6)
C14	N13	C23	111.4(6)	110. (1)	109.6(6)
K,Rb,Cs	N16	C15	111.1(4)	114.0(8)	115.0(4)
K,Rb,Cs	N16	C17	110.1(5)	112. (1)	110.6(5)
K,Rb,Cs	N16	C24	101.3(4)	98.3(7)	95.4(4)
C15	N16	C17	112.8(8)	108. (1)	111.1(6)

Table A5. Bond Angles cont.

<u>Atom1</u>	<u>Atom2</u>	<u>Atom3</u>	(I) <u>Angle</u>	(II) <u>Angle</u>	(III) <u>Angle</u>
C15	N16	C24	110.9(7)	113. (1)	113.7(7)
C17	N16	C24	110.0(7)	112. (1)	110.1(6)
N1	C2	C3	112.3(7)	114. (1)	114.2(6)
N4	C3	C2	115.0(7)	114.1(1)	113.2(6)
N4	C5	C6	112.5(7)	115.1(1)	114.6(7)
N7	C6	C5	113.1(7)	114. (1)	113.9(6)
N7	C8	C9	113.4(6)	114. (1)	115.0(6)
N10	C9	C8	114.5(7)	114. (1)	113.7(6)
N10	C11	C12	115.1(7)	116. (1)	114.2(6)
N13	C12	C11	113.0(6)	110. (1)	115.1(6)
N13	C14	C15	113.6(7)	117. (1)	114.0(6)
N16	C15	C14	113.6(7)	110. (1)	114.6(7)
N16	C17	C18	120.5(8)	119. (2)	114.1(6)
N1	C18	C17	118. (1)	118. (2)	115.9(7)

LIST OF REFERENCES

REFERENCES

- 1 J.L. Dye, J.M. Ceraso, M.T. Lok, B.L. Barnett, and F.J. Tehan; J. Am. Chem. Soc. 96, 608, (1974).
- 2 F.J. Tehan, B.L. Barnett, and J.L. Dye; J. Am. Chem. Soc. 96, 7203, (1974).
- 3 C.J. Pederson; J. Am. Chem. Soc. 89, 2495, (1967).
- 4 C.J. Pederson; J. Am. Chem. Soc. 89, 7017, (1967).
- 5 C.J. Pederson; J. Am. Chem. Soc. 92, 386, (1970).
- 6 J.M. Lehn; Structure and Bonding, 16, 1, (1973)
- 7 J.M. Lehn and J.P. Sauvage; J. Am. Chem. Soc. 97, 6700, (1975).
- 8 J.M. Lehn and J.P. Sauvage; Chem. Comm. 1971, 440.
- 9 D.J. Cram and J.M. Cram; Science, 183, 803, (1974).
- 10 D.J. Cram and J.M. Cram; Accounts Chem. Res. 11, 8, (1978).
- 11 D.J. Cram; Angew. Chem. Int. Ed. Engl. 25, 1039, (1986).
- 12 D.C. Tosteson; Fed. Proc. 27,1269, (1968).
- 13 R.M. Izatt, G.C. Lindh, R.L. Bruening, J.S. Bradshaw, J.D. Lamb, and J.J. Christensen; Pure Appl. Chem. 58, 1453, (1986).
- 14 O. Ryba and J. Petranek; J. Electroanal. Chem. Interfacial Electrochem. 44, 425, (1973).
- 15 T. Ogata; Kagaku to Seibutsu, 25, 598, (1987).
- 16 B.E. Jepson and R. DeWitt; J. Inorg. Nucl. Chem. 38, 1175, (1976).
- 17 B.E. Jepson and W.F. Evans; Sep. Sci. Technol. 22, 1029, (1987).
- 18 J.L. Dye, M.G. DeBacker, and V.A. Nicely; J. Am. Chem. Soc. 92, 5226, (1970).

- 19 J.L.Dye, M.T. Lok, F.J. Tehan, R.B. Coolen, N. Papadakis, J.M. Ceraso, and M.G. DeBacker; Ber. Bunsenges. Phys. Chem. 75, 659, (1971).
- 20 A. Ellaboudy, J.L. Dye, and P.B. Smith; J. Am. Chem. Soc. 105, 6490, (1983).
- 21 S.B. Dawes, D.L. Ward, R.H. Huang, and J.L. Dye; J. Am. Chem. Soc. 108, 3534, (1986).
- 22 J.L. Dye; Prog. Inorg. Chem. 32, 327, (1984).
- 23 J.L. Dye and M.G. DeBacker; Ann. Rev. Phys. Chem. 38, 271, (1987).
- 24 D.J. Mathre and W.C. Guida; Tetrahedron Lett. 21, 4773, (1980).
- 25 A.G.M. Barrett, C.R.A. Godfrey, D.M. Hollinshead, P.A. Prokopiou, D.H.R. Barton, R.B. Boar, L. Joukhadar, J.F. McGhie, and S.C. Misra; J. C. S. Perkin Trans. I, 1981, 1501.
- 26 A.G.M. Barrett, P.A. Prokopiou, and D.H.R. Barton; J. C. S. Perkin Trans. I, 1981, 1510.
- 27 T. Ohsawa and T. Oishi; J. Incl. Phen. 2, 185, (1984).
- 28 G.P. Pez, I.L. Mador, J.E. Galle, R.K. Crissey, and C.E. Forbes; J. Am. Chem. Soc. 107, 4098, (1985).
- 29 T. Ohsawa, T. Kobayashi, Y. Mizuguchi, T. Saitoh, and T. Oishi; Tetrahedron Lett. 26, 6103, (1985).
- 30 R. Liepins and M. Aldissi; Mol. Cryst. Liq. Cryst. 105, 151, (1984).
- 31 A. Maercker; Angew. Chem. Int. Ed. Engl. 26, 972, (1987).
- 32 R.H. Huang, M.K. Faber, B. VanEck, and J.L. Dye; unpublished results, this laboratory.
- 33 R.M. Izatt, L. Eblerhardt, G.A. Clark, R.L. Bruening, J.S. Bradshaw, M.H. Cho, and J.J. Christensen; Separation Science and Technology, 22, 701, (1987).
- 34 R.M. Izatt, J.S. Bradshaw, S.A. Nielsen, J.D. Lamb, and J.J. Christensen; Chem. Rev. 85, 271, (1985).
- 35 M.N. Bell, A.J. Blake, M. Schroder, and T.A. Stephenson; J. Chem. Soc., Chem. Commun. 1986, 471.
- 36 T.A. Del Donno and W. Rosch; J. Am. Chem. Soc. 99, 8051, (1977).

- 37 B.N. Diel, R.C. Haltowanger, and A.D. Norman; J. Am. Chem. Soc. 104, 4700, (1982).
- 38 E.I. Sinyavskaya; Koord. Khim. 12, 1155, (1986).
- 39 M. Kodama, E. Kimura, and S. Yamaguchi; J. C. S. Dalton, 1980, 2536.
- 40 M. Kodama and E. Kimura; J. C. S. Dalton, 1978, 1081.
- 41 M.E. Kuchermeister; M.S. Thesis, Michigan State University, (1986).
- 42 B. VanEck; Ph.D. Dissertation, Michigan State University, (1981).
- 43 J.L. Dye; J. Phys. Chem. 84, 1084, (1980).
- 44 B. VanEck, L.D. Le, D. Issa, and J.L. Dye; Inorg. Chem. 21, 1966, (1982).
- 45 M.T. Lok, F.S. Tehan, and J.L. Dye; J. Phys. Chem. 76, 2975, (1972).
- 46 J.L. Dye, M.R. Yemen, M.G. Dague, and J.M. Lehn; J. Chem. Phys. 68, 1665, (1978).
- 47 L.D. Le, D. Issa, B. VanEck, and J.L. Dye; J. Phys. Chem. 86, 7, (1982).
- 48 J.L. Dye, M.G. Dague, M.R. Yemen, J.S. Landers, and H.L. Lewis; J. Phys. Chem. 84, 1096, (1980).
- 49 J. Skowrya and J.L. Dye; unpublished results this Laboratory.
- 50 M.G. Dague, J.S. Landers, H.L. Lewis, and J.L. Dye; Chem. Phys. Lett. 66, 169, (1979).
- 51 R.G. Patel and M.M. Chaudhri; Thermochimica Acta. 25, 247, (1978).
- 52 Z. Osawa; Bull. Chem. Soc. Japan, 38, 1881, (1965).
- 53 H.E. Kissinger; Anal. Chem. 29, 1702, (1957).
- 54 M.E. Kuchermeister and J.L. Dye; J. Am. Chem. Soc. in press.

- 55 H.O. Borgstedt and C.K. Mathews; Applied Chemistry of the Alkali Metals, Plenum: New York, p. 166 1987.
- 56 T. Kokokawa and O.J. Kleppa; J. Chem. Phys. 40, 46, (1964).
- 57 Handbook of Chemistry and Physics; Weast, R.C., Ed.; 62 nd. edition, CRC Press Inc. (1981).
- 58 R.L. McKisson and L.A. Bromley; J. Am. Chem. Soc. 73, 314, (1951).
- 59 K. Moeggenborg and J. Papaioannou; unpublished results this laboratory.
- 60 Spectra obtained by L.E. Hill and J. Kim
- 61 A. Ellaboudy, M.L. Tinkham, B. VanEck, J.L. Dye, and P.B. Smith; J. Phys. Chem. 88, 3852, (1984).
- 62 A. Ellaboudy and J.L. Dye; J. Magn. Reson. 66, 491, (1986).
- 63 M.L. Tinkham and J.L. Dye; J. Am. Chem. Soc. 107, 6129, (1985).
- 64 S.B. Dawes, A.S. Ellaboudy, and J.L. Dye; J. Am. Chem. Soc. 109, 3508, (1987).
- 65 M.L. Tinkham, A. Ellaboudy, J.L. Dye, and P.B. Smith; J. Phys. Chem. 90, 14, (1986).
- 66 J.E. Wertz and J.R. Bolton; "Electron Spin Resonance: Elementary Theory and Applications", McGraw Hill (New York) 1972.
- 67 W. Bell Flower, "Physics of Color Centers", Academic Press, (New York) (1986).
- 68 Spectra obtained by A. Ellaboudy and D.H. Shin.
- 69 R. Catterall and P.P. Edwards; Adv. in Molecular Relaxation and Interaction Process, 13, 123, (1978).
- 70 Fitting was done by J. Kim and D.H. Shin.
- 71 A.S. Ellaboudy, C. Bender, G.T. Babcock, M.E. Kuchenmeister, and J.L. Dye; to be published.
- 72 D. Issa, A. Ellaboudy, R. Janakiraman, and J.L. Dye; J. Phys. Chem. 88, 3847, (1984).
- 73 J.S. Landers, J.L. Dye, A. Stacey, and M.J. Sienko; J. Phys. Chem. 85, 1096, (1981).

- 74 A. Ellaboudy; Ph. D. Dissertation, Michigan State University, (1984).
- 75 R.H. Huang, D.L. Ward, M.E. Kuchermeister, and J.L. Dye; J. Am. Chem. Soc. 109, 5561, (1987).
- 76 S.B. Dawes; Ph. D. Dissertation, Michigan State University, (1986).
- 77 D.L. Ward, M.E. Kuchermeister, and J.L. Dye; Submitted for Publication.
- 78 D.T. Cromer and J.T. Waber; International Tables for X-ray Crystallography, Vol IV, (1974), Table 2.2 B, Birmingham: Kynoch Press.
- 79 G.H. Stout and L.H. Jenson; X-ray Structure Determination: A Practical Guide, Macmillan Publishing Co.; New York, (1968).
- 80 R.D. Shannon and C.T. Prewitt; Acta. Crystallogr. 1969, B25, 925.
- 81 R.H. Huang, S.B. Dawes, D.L. Ward, and J.L. Dye; Unpublished results this laboratory.
- 82 R.H. Huang and D.L. Ward; unpublished results this laboratory.
- 83 F. Vogtle and E. Weber, Angew. Chem. Int. Ed. 13, 814, (1974).
- 84 R.M. Izatt and J.J. Christensen; Synthetic Multidentate Compounds (1978).
- 85 J.C. Thomson; Electrons in Liquid Ammonia, Claredon Press, Oxford, (1976).